Sub-micron grinding of a food product

Stéphen Hennart

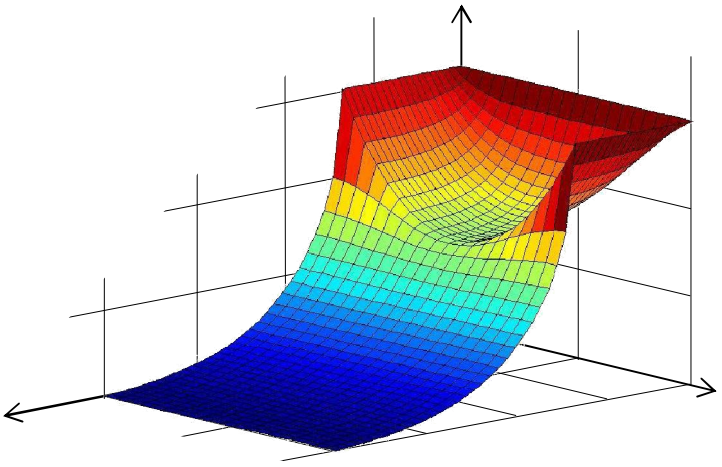

Stellingen
Behorend bij het proefschrift:
"Sub-micro grinding of a food product"

Stéphen Hennart
7 December 2011

A decrease in antifungal agent particle size increases the specific protection against mould growth.

Reducing the grinding media size by a given factor makes the ball milling process more efficient than increasing the rotation speed by the same factor.

The efficiency of a stirred media mill is defined by the transfer of energy inside the mill. Best energy transfers are reached when the surface area of the rotating impellors in contact with the centrifuged packed bed of grinding media is maximized.

Any present measuring instrument for particle size is insufficient to allow satisfactory interpretation unless combined with an imaging technique.

Both Journalists and Scientists are committed to the truth. They also suffer from the same problem: the reliability of their sources.

Natural competition and rewarding within a society leads to sustainable outstanding results that threat can never reach.

The more rules, more rules are violated. It should be possible to minimize the number of rules to the point where no rules are broken by the decent majority.

Food technologists should not mind eating the cheese rind. Just as water management engineers should not mind living below sea level.

Justice is not Science. If you go to court, do not apply scientific thinking. Playing with emotions will give you better chances.

A democracy can not be based on the laws defined by a religion.

These propositions are regarded as opposable and defendable, and have been approved as such by the supervisor Prof.dr. A. Schmidt-Ott.

Stellingen
Behorend bij het proefschrift:
"Sub-micro grinding of a food product"

Stéphen Hennart
7 December 2011

Een vermindering van de deeltjesgrootte van een schimmelwerend middel verhoogt de specifieke bescherming tegen schimmelgroei.

Het verminderen van de maalkogel grootte met een bepaalde factor, maakt het maal proces efficiënter dan de omwentelingssnelheid met dezelfde factor te verhogen.

De efficiëntie van een kogelmolen wordt bepaald door de energieoverdracht in de molen. De beste energieoverdrachten worden verkregen als de oppervlakte van de roterende schoepen in contact met het gecentrifugeerde maalkogels is gemaximaliseerd.

Elk huidig meetinstrument voor deeltjesgrootte is ontoereikend om bevredigende interpretatie te krijgen tenzij gecombineerd met beeldvormende techniek.

Zowel journalisten als wetenschappers dienen waarheidsgetrouw te handelen. Beiden leiden onder hetzelfde probleem: de betrouwbaarheid van hun bronnen.

Binnen een maatschappij leiden natuurlijke competitie en beloningen tot duurzame uitstekende resultaten die nooit bereikt kunnen worden door bedreigingen.

Hoe meer regels, hoe meer overtredingen. Het moet mogelijk zijn het aantal regels te verminderen tot het punt waarop de regels door de welwillende meerderheid niet meer overtreden worden

Voedingsdeskundigen zouden zich niet moeten storen aan het eten van de kaaskorst. Zoals de waterbeheersingingenieurs zich niet zouden moeten storen aan het wonen beneden de zeespiegel.

Rechtspraak is geen wetenschap. Denk niet wetenschappelijk als u naar de rechter stapt. Het bespelen van emoties geeft u betere kansen.

Een democratie kan niet gegrondvest zijn op door een religie bepaalde wetten.

Deze stellingen worden opponeerbaar en verdedigbaar geacht en zijn als zodanig goedgekeurd door de promotor Prof.dr. A. Schmidt-Ott.

Sub-micron grinding of a food product

Proefschrift

ter verkrijging van de graad van doctor
aan de Technische Universiteit Delft,
op gezag van de Rector Magnificus prof. ir. K.C.A.M. Luyben,
voorzitter van het College voor Promoties,
in het openbaar te verdedigen op 7 december 2011 om 12 uur

door

Stéphen Ludovic Alexandre HENNART

Diplome d'Ingénieur
Institut National des Sciences Appliquées de Rouen, France
geboren te Rouen, Frankrijk.

Dit proefschrift is goedgekeurd door de promotor:
Prof dr. A. Schmidt Ott

Copromotor: Dr. ir. G.M.H. Meesters

Samenstelling promotie commissie:

Rector Magnificus	voorzitter
Prof. dr. A. Schmidt Ott	Technische Universiteit Delft, promotor
Dr.ir. G.M.H. Meesters	Technische Universiteit Delft, copromotor
Prof. dr. G. Schembecker	TU Dortmund, Duitsland
Prof. Dr.-Ing. A. Kwade	TU Braunschweig, Duitsland
Prof. dr. S. Luding	Technische Universiteit Twente
Prof. dr. G.J. Witkamp	Technische Universiteit Delft
Dr.ir. P. van Hee	DSM Food Specialties
Prof. dr. S.J. Steven Picken	Technische Universiteit Delft, reservelid

Dr. ir. P. van Hee en Dr. ir. W.J. Wildeboer hebben als begeleiders in belangrijke mate aan de totstandkoming van het proefschrift bijgedragen.

The research described in this thesis was performed at the Department of Research and Development, DSM Food Specialties, Delft, the Netherlands and was co funded by the Marie Curie actions of the European Commission and DSM Food Specialties BV.

ISBN / EAN: 978-90-9026489-9

Summary

This thesis describes how the activity of a preservative product used in food coatings can be optimized. This project is partly sponsored by the European Marie Curie Framework projects as part of the BioPowders research training network. DSM Food Specialties hosts and co finances this project.
The research project focuses on food coating such as cheese coatings. A preservative additive is often incorporated to prevent microbial growth on the food products. The shelf life of the food product is defined as the time without any microbial growth. The preservative being poorly water soluble is mainly present in the form of particles and slowly dissolves and diffuses in the coating.
The approach in this research is to reduce the particle size of the preservative particles in the coating. At a given concentration, the number of particles and the total surface area of product available increases with decreasing particle size. This enables to reduce the distances between the particles. The increase in specific surface area improves the product dissolution rate. At a given concentration in the food coating, the product diffuses along shorter distances when decreasing product particle size. This is shown to improve the shelf life of the food product.
The smaller particles are obtained by milling and specific efforts are made to understand and characterize the milling process.

The preservative product initially of a mean size of 15µm ($d_{4,3}$), is ground in a stirred media mill down to sub micron sizes. Part I of the thesis presents in the first chapter how the process parameters influence the time of grinding and the level of the contamination by heavy metals.
Particles in a stirred media mill can undergo different breakage mechanisms depending on the strength of the product and the forces applied by the grinding media on the particles. In the second chapter of Part I the grinding mechanisms are determined. The particles mainly break under long stresses of high intensities and shear stresses. The particles are broken by cleavage and abrasion.
In the third chapter of Part I is attempted to characterize the milling of the preservative products by using a grinding time prediction by a model based on population balances. The grinding profile of the preservative product is defined as the mean particle size as function of the number of stress events or “stress number”, SN. SN represents the number of stresses that an initial particle needs to undergo during the grinding process to reach the desired fine particle size. That representation of the grinding profile is product specific. As presented in chapter 4 of Part I, no significant differences are observed between the grinding profiles measured in different tested mills. Any similar stirred media mill is therefore expected to present a similar grinding profile.
A correlation is found between the mill parameters (mill rotation speed, surface area of grinding media in contact with the impellors and the grinding media size) and the breakage mechanism and the grinding profile.

In order to fully characterize the ground particles, different techniques commercially available for particle sizing are tested. The results are presented and discussed in the first chapter of the second part of this thesis. The minimal product particle size is ca 0.2µm. Different techniques point out as well the presence of larger particles. It is seen by imaging techniques such as SEM and Cryo-TEM that those larger particles are most likely aggregates of the ground particles.
The stability of the ground particles is further investigated in the second chapter of Part II. The stability of the particle suspension is determined by measuring the initial sedimentation rate. This measurement technique shows differences in the aggregate size for different pH values. Changing the pH values influences the zeta-potential of the particle surface. Using the DLVO theory, the stability of ground particles shows a good correlation with the energy barrier between the particles. The higher the energy barrier the less aggregation occurs and the smaller the aggregates are. The energy barrier increases with an increase of electrostatic repulsion, i.e. the zeta-potential. The particle suspension becomes more stable when driving away the pH from the iso-electric point.

The ground particles are tested in cheese coating. The use of preservative particles from different sizes is presented and discussed in Part III.
Using an accelerated shelf life test, it is shown experimentally that protection against fungal growth increases when higher product concentrations are used. Also micronized product particles provide the longest protection against mould growth. A decrease in product particle size increases protection against fungal growth.
A model is designed and the different aspects regulating the concentration of the product in the coating are included: the product diffusion, the product dilution, the particle distribution, the product degradation and the limit of sensitivity of the microbe to the product.
The weakest point in a coating is the point where the concentration first reaches the limit of sensitivity of the microbe to the product. That point is the position in the middle of two particles.
It is seen from the model that the distribution of the particles in the coating is of great importance. Reducing the particle size or increasing the concentration enables the increase of the specific number of particles. Thus the distribution of particles in the matrix changes and the distances between the particles reduce. The diffusing molecules in the coating reach the position in middle of two particles faster; this increases the shelf life of the food product.

Stéphen Hennart

Samenvatting

Dit proefschrift beschrijft hoe de activiteit van een conserveermiddel gebruikt in voedsel beschermlaag geoptimaliseerd kan worden. Dit project wordt mede gesponsord door de Europese Marie Curie Framework projecten, als onderdeel van de BioPowders Research Training Network. DSM Food Specialties host en mede financiert dit project.
Het onderzoeksproject richt zich op voedsel caotings, zoals de kaas korst. Een conserveermiddel additief wordt vaak opgenomen om microbiële groei te voorkomen op de voedingsmiddelen. De houdbaarheid van het voedingsmiddel wordt gedefinieerd als de tijd zonder dat er microbiële groei optreedt. Het conserveermiddel is slecht oplosbaar in water en is voornamelijk aanwezig in de vorm van deeltjes die langzaam oplossen zich verspreiden in de coating.
De aanpak van dit onderzoek is het verminderen van de deeltjesgrootte van het conserveermiddel in de coating. Bij een gegeven concentratie, neemt het aantal deeltjes en de totale oppervlakte toe met afnemende deeltjesgrootte. Dit laat vermindering van de afstanden tussen de deeltjes toe. De toename van het specifieke oppervlak verbetert de oplossnelheid van het product. Bij een bepaalde concentratie in de voedsel beschermlaag, het product verspreidt zich langs kortere afstanden, bij afnemende deeltjesgrootte. Het is aangetoond dat de houdbaarheid van het voedsel hiermee verbetert.
De kleinere deeltjes worden gemaakt door het maalproces. En specifiek onderzoek is gedaan om dit proces te begrijpen en te karakteriseren.

Het conserveermiddel heeft in eerste instantie van een gemiddelde grootte van 15μm (d4, 3). En wordt gemalen in een geroerd media molen tot sub-micron maten. Deel I van het proefschrift behandelt in het eerste hoofdstuk hoe de proces parameters de tijd van malen en het niveau van de besmetting door zware metalen beïnvloeden.
Deeltjes in een geroerde media molen kunnen verschillende breuk mechanismen ondergaan, afhankelijk van de sterkte van het product en de krachten die ontstaan door het maalproces op de product deeltjes. In het tweede hoofdstuk worden de maalmechanismen bepaald. De deeltjes breken voornamelijk onder lang aangebrachte spanning van hoge intensiteiten en schuifspanningen. De deeltjes worden gebroken door splitsing en slijtage.
In het derde hoofdstuk is geprobeerd om het malen van de conserveermiddel producten te karakteriseren met behulp van een maalduur voorspelling en een model gebaseerd op populatie gemiddelden. Het maalprofiel van het conserveermiddel wordt gedefinieerd als de gemiddelde deeltjesgrootte als functie van het aantal botsingen genoemd, "stress-number", SN. SN staat voor het aantal botsingen dat een initieel deeltje ondergaat tijdens het maalproces om de gewenste fijne deeltjesgrootte te bereiken. Het maalprofiel heeft en product specifieke afbeelding. In hoofdstuk 4 wordt gepresenteerd dat er geen significante verschillen tussen de maalprofielen van verschillende geteste molens bestaan. Het wordt daarvan verwacht dat enkele soortgelijke geroerd media molen een vergelijkbaar maalprofiel hebben.

Er is een correlatie gevonden tussen de parameters van de molen (rotatiesnelheid, oppervlakte van het maalmedia in contact met de roeiers en de maalmedia grootte), het breuk mechanisme en het slijp profiel.

Om de gemalen deeltjes te karakteriseren (deel 2), zijn verschillende deeltjesgrootte meetapparaten uit de handel getest. De resultaten worden gepresenteerd en besproken in het eerste hoofdstuk. De minimale product deeltjesgrootte is ca. 0.2 μm. Verschillende deeltjesgrootte bepaling technieken wijzen op de mede aanwezigheid van grotere deeltjes. Door beeldvormende technieken zoals SEM en Cryo-TEM wordt zichtbar gemaakt dat die grotere deeltjes waarschijnlijk aggregaten van de gemalen deeltjes zijn.

De stabiliteit van de gemalen deeltjes wordt verder onderzocht in het tweede hoofdstuk. De stabiliteit van de suspensie wordt bepaald door het meten van de initiële sedimentatie snelheid van de deeltjes. De meettechniek toont de verschillen in de grootte van de aggregaten voor verschillende pH-waarden. Het veranderen van de pH is van invloed op de zeta-potentiaal van het deeltjes oppervlak. Met gebruik van de DLVO theorie is een goede correlatie te zien tussen de stabiliteit van de gemalen deeltjes en de energie barrière tussen de deeltjes. Hoe hoger de energie barrière hoe minder aggregatie optreedt en hoe kleiner de aggregaten. De energie barrière neemt toe met een toename van de elektrostatische repulsie, i.e. de zeta-potentiaal. De deeltjes suspensie wordt stabieler waneer de pH zich verder van het iso-elektrisch punt verwijdert.

De gemalen deeltjes zijn getest in kaas korsten. Het gebruik van conserveermiddel deeltjes van verschillende grootte wordt gepresenteerd en besproken in Deel III.

Met behulp van een versnelde houdbaarheid test, is het experimenteel aangetoond dat de bescherming tegen schimmelvorming toeneemt wanneer een hoger product concentratie wordt gebruikt. Daarnaast verhoogt de bescherming tegen schimmelgroei bij afname van de grote van de product deeltjes.

Een model is ontworpen met de verschillende parameters die de concentratie van het product in de korst regelen: de product diffusie, de product oplosbaarheid, de deeltjes distributie, de product degradatie en de grens van gevoeligheid van de microben.

Het zwakste punt in een coating is het punt waar de concentratie het eerst de grens van de gevoeligheid van de microbe bereikt. Dit punt bevindt zich op de positie in het midden van de twee deeltjes.

Het model toont dat de verdeling van de deeltjes in de coating van groot belang is. Het verminderen van de deeltjesgrootte of het verhogen van de concentratie bepaalt de toename van het specifieke aantal deeltjes. Dus de verdeling van de deeltjes in de matrix verandert en de afstanden tussen de deeltjes vermindert. Nu bereiken de zich in de coating verspreidende moleculen, het zwakste punt sneller; dit verhoogt de houdbaarheid van het voedsel product.

Stephen Hennart

Table of content

General Introduction

1. ANTIMICROBIAL PROTECTION OF FOOD SURFACES

In the food industry several research groups are working on the protection of food and food surfaces against mold growth. The challenges are optimization of the protection systems to enhance the shelf life of food products. In various studies (Teerakarn et al. [1], Gill et al. [2], Vojdani et al. [3], Ouattara et al. [4], Warin et al. [5], Ozdemir and Floros [6, 7]) the food surface is protected by a coating containing antimicrobial products. The antimicrobial product is often a poorly soluble compound. A large part of the active molecules is then in a particulate form. The antimicrobial particles are dispersed in the coating.

From the previous research cited above it is known that the different aspects regulating the concentration of the product in the coating are product diffusion, product dissolution, particle distribution, product degradation and the sensitivity of the microbe to the product (minimum concentration necessary to inhibit the growth of the organism).

The present work is based on the idea that the particle size has an influence on the shelf life of a food product protected by a film which contains the anti-microbial particles. Indeed, a reduction in particle size should increase the product specific surface area and the number of particles per unit of coating surface area. The surface area has an influence on the particle dissolution properties and the product diffusion. The number of particles has influence on the distribution of particles in the coating. The smaller the particles the more effect of the parameters is expected.

The system studied is Plasticoat® produced by DSM Food Specialties, The Netherlands. Plasticoat® is used as cheese coating and contains a poorly soluble antifungal active product.

In the work presented in this thesis, the first aim is to be able to produce extremely fine antimicrobial powders. The particle size desired is in the sub-micron range. Secondly, the fine particles are analyzed in terms of particle size and their physical stability to maintain this size (stability versus agglomeration). Lastly, the influence of the particle size on the shelf life is studied for particle distribution in films or coatings. That work is applied and verified to the use of fine antifungal particles in a cheese coating.

This thesis covers the work carried out at DSM Food Specialties and the Delft University of Technology, Faculty of Chemical Engineering, in the Nano Structured Materials Section. The work is partly carried out as a Marie Curie training (Project number MRTN-CT-2004-512247, BioPowders), sponsored by the European Union under the 6th Framework program. DSM Food Specialties extends this work and

supplies the equipment and antifungal product, as well as the labs to do the experiments and the application testing. At Delft University of Technology, several experiments are performed too, and measurements on the compounds used are done there as well.

2. PRODUCTION OF SUB-MICRON PARTICLES.

Different methods are available to produce small particles. Particles can be obtained by bottom up approaches like controlled precipitation or cryogenic spraying for example. The invert approach – top-down – consists in particle size reduction [8, 9].

Published research shows a large potential of ball milling to produce sub-micron milled particles. Inorganic material, like aluminum particles [10] and some organic pigments particles [11] are, for example, reduced to the sub-micron size range. Grinding in wet ball mills is used in nanotechnology to produce very fine powder mainly in the field of inorganic products, for example for silica particles or metals. Grinding enables in such applications a particle size reduction to less than 50 nm [8, 12, 13].

Grinding of organic products is studied in the pharmaceutical industry. In most cases, grinding is carried out using additives such as polymers or cyclodextrines. Those additives enable finer grinding, better physical stability and/or chemical stability. An example is given by Horter and Dressman [14]; when the dissolution process is a rate-determining step, an improvement in the dissolution rate of poorly water-soluble drugs is required for enhancement of the gastrointestinal absorption. Grinding with polymers is known to be one pharmaceutical approach to improve the dissolution rate of drugs (Yamada et al. [15]; Mura et al. [16]; Saito et al. [17]; Vippagunta et al. [18]) and may be useful for enhancement of the gastrointestinal absorption of poorly water-soluble drugs. The polymer acts as a surfactant to enhance the physical stability of the ground particles.

Stirred media mills are therefore expected to be capable of reducing the particle size of antimicrobial products to be used in the food coatings. Many polymers used in the pharmaceutical industry do not have a food grade status. Where grinding without additives is possible, costs are limited and no toxicological issues are raised.

Several research groups are focusing on the milling process using stirred media mills. Different important aspects and issues regarding the milling process are pointed out:

- The effect of process parameters on the final particle size and time of grinding.

Many researchers investigate for mineral products the effect of process parameters on the particle size and the time of grinding. Gao et al. [19] investigate the mill speed, the slurry density, the grinding media density and the dispersant concentration on the power draft. The rotation speed of the shaft is found by Gao et al. to be the dominant factor influencing the power; the effect is not linear. Another investigation by Herbst

and Sepulveda [20] focuses on the effect of the grinding chamber volume, the grinding medium size and its density on the mill power draft of a vertical stirred ball mill. A coarser grinding medium size and a higher medium density are all found to increase the mill power draft. Another work by He et al. [21] studies the effect of dispersant concentration and of the mill load on the cumulative energy efficiency. For a specific energy consumption, a higher bead load enables smaller particle size to be reached.

Hou et al. [22] investigate the milling of titanium oxide and studied among others the rotation speed of the shaft in the vertical mill. By using the Tagushi method, Hou shows that the effect of the shaft decreases with the product particle size. Previous studies by Jankovic [23] shows the dependence of the product particle size on the parameters. The study of Jankovic focuses on milling zinc particles and evaluates the effect of the mill design, the grinding media properties, the rotation speed and the slurry density. An optimum of the grinding media size was found between 1.7 – 1.2mm for grinding the coarse product particles of 46µm. The optimum of the grinding media size is found to be different for other product particle size and grinding 7µm zinc particles is optimum with 0.85 – 0.6mm grinding media, in the set of experiments from Jankovic. In general, grinding medium smaller than the optimum grinding media size for the starting product size is getting more efficient with decreasing product size.

- Heavy metals contamination issues.

The effect of the mill parameters on the contamination level by different bead materials is investigated by Howorth et al. [24]. The differences in contamination by Cerium and Yttrium grinding media when grinding quartz and alumina lead Howorth to the following conclusions: The material hardness of the medium is a relevant factor; the harder the medium the less contamination is detected. The product milled is of importance as well; milling quartz particles generates more medium wear as milling alumina. Further studies focus on wear and costs: bead wear, as function of its property and especially size, is widely studied by Breitung-Faes et al. [25]. The grinding medium wear is increasing with the grinding medium size. Becker and Schwedes [26] investigate the comminution of fused corundum and silicon carbide. They show that the amount of grinding bead wear is a function of the specific energy input and that in this case the wear of grinding beads is determined by the structure and the hardness of beads as well as by the hardness and the shape of the feed particles.

- The particle breakage mechanism in the mill.

The nature and intensity of the applied stresses on the particles affect the particle size reduction process. In comminution three main breakage mechanisms are identified (Redner [27]; Austin [28]; Gao et al. [29]):

1. Abrasion occurs when stress is applied on particles along the tangential axis (shear).
2. Cleavage of particles occurs when intense stresses are slowly applied on a particle (compression).
3. Fracture occurs through rapidly applying intense stresses (impact).

Determination and quantification of the mechanisms can be done using different approaches. The breakage mechanisms can be determined from the particle size evolution by determining the probability for formation of fragments with a specific size after breakage of the initial particle. Besides this method other methods are described in literature for determination of the particle breakage behavior. Menacho [30] derives the different breakage mechanisms from the cumulative breaking factors. Menacho's model uses abrasion and fracture as the two extreme mechanisms to describe the evolution of the particle size distribution during grinding. Varinot et al. [31] use the representation of Menacho and concentrated on the influence of the operating parameters on the fracture and abrasion mechanisms.

- Modeling and characterization of mills.

During a ball milling process the minimal particle size reachable is often limited by a process of agglomeration or compaction of product particles [32]. It is a challenge to build a model capable of describing a grinding process and its agglomeration component.
As broadly reported in literature [33], several types of models can be useful for the prediction of the grinding process, up scaling, etc. Population balance modeling (PBM) often is the best way to fit experimental data. The PBM is a mathematical tool to study and describe the evolution of for example particle size in a particle size reduction process.
Varinot [34] shows that grinding processes can be described with PBM using only two fitting parameters. The PBM in this case only describes the particle size reduction process. When agglomeration occurs, the PBM can also be used to describe a particle size increase, but more parameters are required to describe this process. A full model would represent a characteristic description of a mill and enable mill comparison and mill up-scaling.

According to Kwade and Schwedes the breakability of the product defines also the mechanism under which the particles will break. Stadler et al. [35] and Kwade et al. [36] describe milling experiments using two key parameters. The first one is the stress energy (SE) and represents the energy of a collision between two grinding media in the mill. The second parameter is the stress number (SN) which is the number of collisions that a product particle requires to break into pieces of a target size. Those parameters are found sufficient to describe the milling of one given product in a defined mill. Whether this concept can be generalized to the grinding of a given product in any mill is examined in this thesis.

- The stability of the ground particles.

Previous research by Mende et al. [37] on sub-micron grinding of inorganic products shows that the stability of the product and its final particle size are a function of the electrostatic properties of the particles and therefore the pH of the solution.

Stirred ball mills are units simple to operate. According to similar investigations, the media mills should enable a particle size reduction to the sub-micron range of the studied product.
The first chapter of the first part of the thesis investigates the influence of the process parameters on the grinding time, the particle size and the heavy metal contamination levels. The grinding mechanism resulting from the motion of the grinding media and the rotation speed will be determined in a second chapter. To have a full characterization of the milling of the studied product, a model is built using population balances and the concept of stress energy and stress number. That model is presented in chapter 3 and tested on different mills in chapter 4.

The particle stability issues will be discussed in the second part of the thesis.

3. CHARACTERIZATION OF GROUND PARTICLES

In this work frame, it is important to determine the final particle size distribution of the milled particles. That enables evaluation of the efficiency of the grinding process.
It is also important to evaluate the stability versus aggregation of the milled particles. It is shown in previous studies that milled particles can quickly aggregate (Mende et al [37]). Aggregated milled particles can be seen as large particles in the particle size distribution.

3.1. Particle size measurements

In order to fully characterize the ground particles, different techniques commercially available for particle sizing are tested. The results are presented and discussed in the first chapter of the second part of this thesis. The different techniques available on the market can be drawn together in several groups [38, 39]:

- Image analysis techniques: In the present research, SEM and a variant of TEM, Cryo-TEM, are tested. Cryo TEM stands for cryogenic TEM. The technique consists in using a classical TEM system to look through cryogenically frozen particle suspensions.
- Static light scattering based techniques: Static light scattering is used join to specific systems used for the detection of extra fine particles:
  - Polarization Intensity Differential Scattering (PIDS) uses polarized light to filter out the signal of the coarse particles.
  - High resolution CCD detectors are introduced to obtain a much higher resolution on the diffraction pattern.
  - Blue wave technology makes use of a combination of lasers of different wavelengths. [40]

    - Backscattering detection makes use of extra detectors at angles ranging from 60 to almost 180°.
- Techniques based on the Brownian motion of the particles: Thermal motion of particles is referred to as Brownian motion. The speed of the particles is proportional to their size. Several techniques use this principle to measure particle sizes:
    - Photon correlation spectroscopy (PCS) is based on the measurement of the diffusion coefficient of the particles
    - Photon Cross Correlation Spectroscopy (PCCS) is similar to PCS but corrects for multiple scattering.
    - The Heterodyne principle is the comparison of the wavelength of the initial beam to the wavelength of the back scattered beam. The backscattered beam presents a shift in wavelength because of the Doppler Effect.
    - Particle Tracking is a technique directly measuring the speed of the scattering pattern of individual particles.
- Centrifugation: The speed of sedimentation of a particle in a centrifuged system is a function among others of the particle size. [41]
- Field flow fractionation techniques: The approach is to separate the particle size distribution in a flow before measuring the very narrow particle size distribution exiting the fractionation system.

3.2. Characterization of the particle stability

As shown by Mende et al [37], after grinding the particles can form aggregates, which is undesirable. Focus is required on the prevention of aggregation after wet grinding of poorly soluble crystalline organic compounds.
When two colloidal particles approach one another, attractive and repulsive forces come into play. Particles can approach each other because of Brownian motion and convective transport. The main attraction and repulsion forces are the van der Waals force and the electrostatic interaction force, respectively.
The previous research by Mende et al. [37] on sub-micron grinding of inorganic products shows that the stability of the product and its final particle size are a function of the electrostatic properties of the particles and therefore the pH of the solution.

The detection of aggregates is, in practice, not always straightforward. Different particle sizing techniques can give different results depending on the measurement conditions. Imaging techniques enable a visual representation of the aggregates in suspension. Sedimentation measurements are another approach to the characterization of the aggregates [42].

In the present thesis, Part II, chapter 2, the suspension stability was analyzed as function of pH and ionic strength by light scattering and sedimentation measurements. The findings of these measurements are correlated with zeta-potential measurements through the DLVO theory.

4. APPLICATION TO FOOD SURFACES

As mentioned in the first section of this introduction, the different aspects regulating the concentration of the product in the coating are diffusion, degradation, dilution, the particle distribution and the sensitivity of the mold to the product. The present work studies the behavior of a poorly water soluble preservative used onto food surfaces into coating (see figure 1). Figure 1 illustrates the studied system.

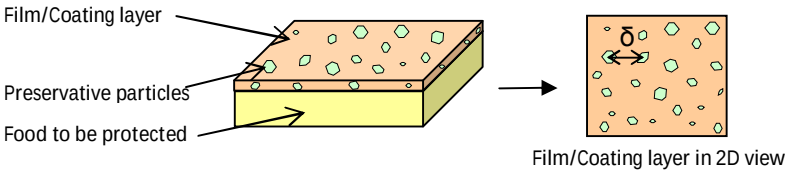

Figure 1 – Schematic view of the studied particle dispersion in a coating and its equivalent 2D representation (δ is the distance between particles).

The objective is to investigate the effect of product particle size on shelf life. In the third part of the thesis, a model is built. It aims at evaluating the influences of all five above-mentioned parameters on shelf life. An accelerated shelf life test is carried out to experimentally investigate the influence of particle size on shelf life. Finally, the experimental results are presented and discussed and the model is validated.

5. REFERENCES

[1] A. Teerakarn, D.E. Hirt, J.C. Action, J.R. Rieck, P.L. Dawson, Nisin Diffusion in Protein Films: Effect of Film Type and Temperature, Journal of Food Science 67(8) (2002) 3019–3025.

[2] C.O. Gill, A review. Intrinsic bacteria in meat, Journal of Applied Bacteriology 47 (1979) 367–378.

[3] F. Vojdani, J.A. Torres, Potassium Sorbate Permeability of Methyl-cellulose and hydroxypropyl methyl-cellulose coatings: Effect of fatty acids, Journal of Food Science 55 (1990) 841–846.

[4] B. Ouattara, R.E. Simard, G. Piette, A. Begin, R.A. Holley, Diffusion of acetic and propionic acids from chitosan-based antimicrobial packaging films, Journal of Food Science 65 (2000) 768–773.

[5] F. Warin, V. Gekas, A. Voirin, P. Dejmek, Sugar diffusivity in agar gel/milk bilayer systems, Journal of Food Science 62 (1997) 454–456.

[6] M. Ozdemir, J.D. Floros, Film composition effect on diffusion of potassium sorbate through whey protein films, Journal of Food Engineering 68 (2003) 511–516.

[7] M. Ozdemir, J.D. Floros, Analysis and modeling of potassium sorbate diffusion through edible whey protein films, Journal of Food Science 65 (2001) 149–155.

[8] J. Hu, K.P. Johnston, R.O. Williams, Nanoparticles Engineering Process for Enhancing the dissolution rates of Poorly water soluble drugs, Drug Development and industrial Pharmacy 30(3) (2004) 233–245.

[9] G. Gordillo, X. Hailey, L. Agyarko, P.D. Mansoori, Nanopowder Production (2004) Ed.: University of Illinois at Chicago.

[10] J.Y. Qiu, Y. Hotta, K. Watari, K. Mitsuishi, M. Yamazaki, Low-temperature sintering behavior of the nano-sized AlN powder achieved by super-fine grinding mill with Y_2O_3 and CaO additives, Journal of the European Ceramic Society 26(4-5) (2006) 385–390.
[11] E. Bilgili, R. Hamey, B. Scarlett, Nano-milling of pigment agglomerates using a wet stirred media mill: Elucidation of the kinetics and breakage mechanisms, Chemical Engineering Science 61(1) (2006) 149–157.
[12] C. Bernhardt, E. Reinsch, K. Husemann, The influence of suspension properties on ultra-fine grinding in stirred ball mills, Powder Technology 105(1-3) (1999) 357–361.
[13] H. Bel Fadhel, C. Frances, A. Mamourian, Investigations on ultra-fine grinding of titanium dioxide in a stirred media mill, Powder Technology 105(1-3) (1999) 362–373.
[14] D. Horter, J. B. Dressman, Influence of physicochemical properties on dissolution of drugs in the gastrointestinal tract, Advanced Drug Delivery Reviews 46 (2001) 75–87.
[15] T. Yamada, N. Saito, T. Imai, M. Otagiri, Effect of grinding with hydroxypropyl cellulose on the dissolution and particle size of a poorly water-soluble drug, Chemical and Pharmaceutical Bulletin 47 (1999) 1311–1313.
[16] P. Mura, M.T. Faucci, P.L. Parrini, Effects of grinding with micro-crystalline cellulose and cyclodextrins on the ketoprofen physicochemical properties, Drug Development and Industrial Pharmacy 27 (2001) 119–128.
[17] M. Saito, T. Ugajin, Y. Nozawa, Y. Sadzuka, A. Miyagishima, T. Sonobe, Preparation and dissolution characteristics of griseofulvin solid dispersions with saccharides, International Journal of Pharmaceutics 249 (2002) 71–79.
[18] S.R. Vippagunta, K.A. Maul, S. Tallavajhala, D.J. Grant, Solid-state characterization of nifedipine solid dispersions, International Journal of Pharmaceutics 236 (2002) 111–123.
[19] M. Gao et al, International Journal of Mineral Processing 44-45 (1996) 641–652.
[20] J.A. Herbst, J.L. Sepulveda, Fundamentals of fine and ultra-fine grinding in a stirred ball mill, International Powder and Bulk Solids Handling Conference Chicago IL (1978) 452–470.
[21] M. He, Y. Wang, E. Forssberg, Parameter effects on wet ultrafine grinding of limestone through slurry rheology in a stirred media mill, Powder Technology 161 (2006) 10–21.
[22] T.-H. Hou, C.-H. Su, W.-L. Liu, Parameters optimization of a nano-particle wet milling process using the Taguchi method, response surface method and genetic algorithm, Powder Technology 173 (2007) 153–162.
[23] A. Jankovic, Variables affecting the fine grinding of minerals using stirred mills, Minerals Engineering 16 (2003) 337–345.
[24] C.J. Howorth, W.E. Lee, W.M. Rainforth, P.F. Messer, Contamination Rates from Ce- and Y-TZP Ball Milling Media, British ceramic, transactions and journal 90 (1990) 18–21.
[25] S. Breitung-Faes, A. Kwade, Nano particle production in high-power-density mills, Chemical engineering research and design 86 (2008) 390–394.

[26] M. Becker, J. Schwedes, Comminution of ceramics in stirred media mills and wear of grinding beads, Powder Technology 105 (1999) 374–381.
[27] S. Redner, Statistical model for the fracture disordered media, In Fragmentation ed. J. P. Hulin, Elsevier, London (1990) 321–328.
[28] L.G. Austin, Some topics for research on fine grinding, IFPRI Annual Meeting Harrogate (1992).
[29] M. Gao, E. Forssberg, Prediction of product size distributions for a stirred ball mill, Powder Technology 84(2) (1985) 101–106.
[30] J.M. Menacho, Some solutions for the kinetics of combined fracture and abrasion breakage, Powder Technology 49 (1986) 87–86.
[31] C. Varinot, S. Hiltgun, M.-N. Pons, J. Dodds, Identification of the fragmentation mechanisms in wet-phase fine grinding in a stirred bead mill, Chemical Engineering Science 52(20) (1997) 3605–3612.
[32] F. Stenger, W. Peukert, The role of particle–particle interactions in submicron grinding in stirred ball mills, Mineral Processing 42 (2001) 477–486.
[33] M. Sommer, F. Stenger, W. Peukert, N.J. Wagner, Agglomeration and breakage of nanoparticles in stirred media mills — a comparison of different methods and models; Chemical Engineering and Science 61 (2006) 135–148.
[34] C. Varinot, H. Berthiaux, J. Dodds, Prediction of the product size distribution in associations of stirred bead mills, Powder Technology 105(1-3) (1999) 228–236.
[35] R. Stadler, R. Polke, J. Schwedes, F. Vock, Naßmahluing in Rührwerksmühlen, Chemie Ingenieur Technik 62(11) (1990) 907–915.
[36] A. Kwade, L. Blecher, J. Schwedes, Motion and stress intensity of grinding beads in a stirred media mill. Part 2: Stress intensity and its effect on comminution, Powder Technology 86(1) (1996) 69–76.
[37] S. Mende, F. Stenger, W. Peukert, J. Schwedes, Mechanical production and stabilization of submicron particles in stirred media mills, Powder Technology 132 (2003) 64–73.
[38] A. Grubenmann, Particle Size Distribution and Aspect Ratio of Organic Pigments, Particle and Particle Systems Characterization 3(4) (1986) 179–186.
[39] H. Lange, Comparative Test of Methods to Determine Particle Size and Particle Size Distribution in the Submicron Range, Particle and Particle Systems Characterization 12(3) (1995) 148–157.
[40] D. M. Scott, Characterizing Particle Characterization. Particle & Particle Systems Characterization 20(5) (2003) 305–310.
[41] H. R. Laapas, U.-R. Lahtinen, The Determination of Particle Size Distribution Using Combined gravitational and centrifugal sedimentation analysis, Particle and Particle Systems Characterization 1(1) (1984) 127–131.
[42] L.-S. H. Lum, S. G. Malghan, S. B. Schiller, Standard reference materials for particle size analysis of ceramic powders by gravity sedimentation, Powder Technology 87 (1996) 233–238.

Part I

Grinding to Sub-Micron Scale

Chapter 1

Study of The Process of Stirred Ball Milling of Poorly Water Soluble Organic Products using Factorial Design.

This chapter has been published as S.L.A. Hennart, M.C. Domingues, W.J. Wildeboer, P. van Hee, G.M.H. Meesters, Powder Technology 198(1) (2009) 56–60.

Abstract – The objective of this work was to investigate the mechanism of very fine grinding in a wet ball mill as a function of process parameters, i.e. rotation speed of the mill and grinding medium bead size. The ball mill used was a Dynomill and the grinding medium consisted of zirconium oxide beads. The product is a poorly water-soluble organic compound. Laser diffraction was used to analyze the particle size distribution.
During grinding the average particle diameter of the product was reduced to a minimum size, which was constant within the range of tested operating conditions.
The grinding parameters were studied to control the grinding process with respect to the required grinding time for reaching the minimum particle size and wear of the set-up.
The grinding time was strongly dependent on the grinding medium bead size and on the rotation speed. The grinding process became faster when the rotation speed increased and the grinding medium bead size decreased. The wear of the set-up, and therefore the contamination of the final product with heavy metals, strongly increased with the rotation speed. A similar trend was observed with an increase of grinding medium bead size. The degradation rate of the product was not significant in the range of grinding parameters studied.

1. INTRODUCTION

Poorly water soluble products are challenging for formulation scientists. Dealing with the low solubility requires innovative research for the optimization of the application of the product in case the product is only active in its soluble form. In the field of pharmaceuticals for example, target release and bio-availability are strongly affected by the dissolution properties of the product. One way to increase the solubility and solubilisation rate of the product is to reduce the particle size distribution of the powder material [1]. A decrease in particle size results in an increase of the specific surface area and thus increases the area that is available for dissolution of the product.

Small particles can be produced with high shear wet ball milling and thus to improve the product efficacy [2]. The grinding process needs to be well understood in order to reach the desired particle size and product quality. Important parameters are particle size, grinding time and the contamination of the product by wear of the mill. The

grinding process in a ball mill is influenced by several parameters. Molls and Hornle [3] described 44 of them, which shows the complexity of the grinding process.

Over the last 35 years, many researchers investigated for mostly mineral products the effect of the parameters on the power draft. Gao et al. [4] investigated the mill speed, the slurry density, the grinding media density and the dispersant concentration. The rotation speed of the shaft is found by Gao et al. to be the dominant factor influencing the power; the effect was not linear. Other investigation by Herbst and Sepulveda [5] focused on the effect of the grinding chamber volume, the grinding medium size and its density on the mill power draft of a vertical stirred ball mill. A coarser medium size and a higher medium density were all found to increase the mill power draft. Another study by He et al. [6] studied the effect of dispersant concentration and of the mill load on the cumulative energy efficiency. For a specific energy consumption, higher bead load enables to reach smaller particle size.

Hou et al. [7] investigated the milling of titanium oxide and studied among others the rotation speed of the shaft in the vertical mill. By using the Tagushi method, Hou showed that the effect of the shaft is decreasing with the product particle size. Previous studies by Jankovic [8] showed dependence of the product particle size on the effect of the parameters. The study of Jankovic focuses on milling zinc particles and evaluates the effect of the mill design, the grinding media properties, the rotation speed and the slurry density. An optimum of the grinding media size was found between 1.7 and 1.2 mm for grinding the coarse product particles of 46 µm. The optimum of the grinding media size is found to be different for other product particle size and grinding 7 µm zinc particles is optimum with 0.85–0.6 mm grinding media, in the set of experiments from Jankovic. In general, grinding medium smaller than the optimum grinding media size for the starting product size is getting more efficient with decreasing product size. The study from Jankovic shows as well that the effect of the speed of rotation of the shaft in a mill is stronger when milling in coarse product size range, inversely grinding of fine product size is less influenced by the rotation speed. Further Jankovic expects that higher speeds would result in greater efficiency for smaller grinding media.

The effect of the mill parameters on the contamination level by different bead material has been investigated by Howorth et al. [9]. The differences in contamination by Cerium and Yttrium grinding media when grinding quartz and alumina lead Howorth to the following conclusions: The material hardness of the medium is a relevant factor; the harder the medium the less contamination is detected. The product milled is of importance as well; milling quartz particles generates more medium wear as milling alumina. Further studies focused on the wear and costs: bead wear, as function of its property and especially size, has been widely studied by Breitung-Faes et al. [10]. The grinding medium wear is increasing with the grinding medium size. Becker and Schwedes [11] investigated the comminution of fused corundum and silicon carbide. They showed that the amount of grinding bead wear is a function of the specific energy input and that in this case; the wear of grinding beads

is determined by the structure and the hardness of beads as well as by the hardness and the shape of the feed particles.

The present paper focuses on the more important parameters, i.e. rotation speed of the stirrer and grinding medium bead size. All other parameters (e.g. flows, product concentration, temperature, etc) were kept constant. Factorial design enables analysis of process parameters as independent variables. This tool is especially efficient for complex systems with multiple variables and responses, such as ball mills. The statistical computation provides a quantitative overview of the process parameters on the basis of a restricted number of experiments. In the present study the variables are rotation speed of the stirrer in the mill and the grinding medium bead size. The response variables are grinding time and heavy metal contamination level.

2. EXPERIMENTAL WORK

2.1. Grinding process

This work focuses on the grinding of a poorly water soluble poly crystalline compound. The material has a starting mean product particle size ($d_{4,3}$) of 15 µm; its density is of 1300 kg m^{-3}. Grinding has been performed using a ball mill (Dynomill, Bachofen AG, Switzerland). Grinding experiments have been performed in the absence of additives. Particle size distributions have been measured with a laser diffraction size analyzer (LS230 equipment from Beckman Coulter).

Experiments were carried out using a Dynomill from Bachofen AG (Basel, Switzerland). The ball mill was operated in a recirculation mode. The poorly water soluble organic product was suspended in water (4.8% w/w, 500mL solution). Figure 1 shows the circulation of the product suspension through the grinding chamber (volume of the chamber: 300 mL, pump speed: 2mL.s^{-1}) that was filled at 80% (bulk volume) with grinding beads (Zirconium oxide, Yttrium stabilized beads from Tosoh, Japan). The product suspension was drawn out through a 0.1 mm gap to prevent the grinding medium to exit the milling chamber. The system was cooled to keep a constant temperature throughout the entire system.

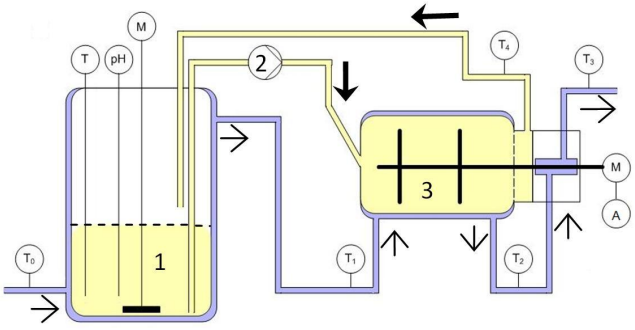

Figure 1 . Grinding set-up and controls, where *T* is a temperature measurement and pH is a pH control point. Arrows show the circulation of the cooling water (→) and

product (➔). The product is pumped from the stirred tank marked as 1 by the pump 2 to the grinding chamber 3. M stands for motor and A for Amp meter.

The particle size distribution was measured as a function of time throughout the grinding process. Figure 2 shows an example of data that were obtained during a grinding experiment.

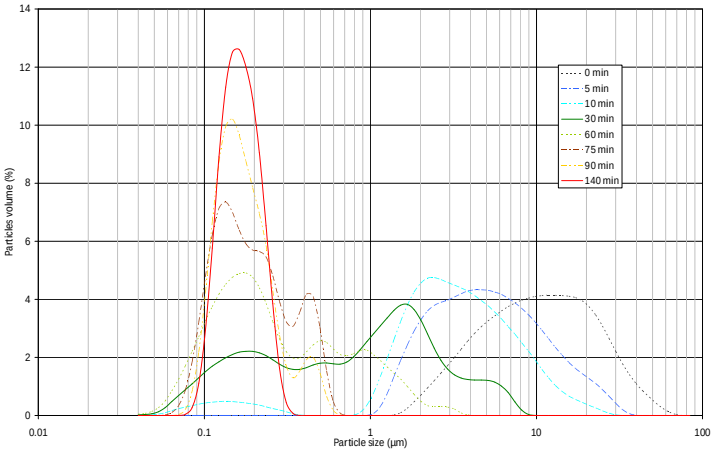

Figure 2 . Evolution of the particle size distribution as function of the grinding time (process parameters: rotation speed: 2000 rpm, grinding media size: 0.5 mm).

2.2. Factorial design.

The factorial design software (Statgraphics Plus 5.1, StatPoint, Inc) defines the measurements that need to be performed to obtain the desired correlations between process parameters. This work aims at finding the influence of rotation speed and grinding media bead size on grinding time. Two rotation speeds were studied, i.e. 2000 rpm and 6000 rpm. The grinding beads sizes that were studied are 0.3, 0.5 and 0.8 mm. The heavy metal contamination was studied on the basis of a 2-level factorial design using 0.3 and 0.8 mm grinding beads. The experimental design consisted of 6 experiments. The experiments were carried out in random order. Several response variables were created. The influence of the operating parameters on grinding time and the time to reach a product at particle sizes of 5 µm, 2 µm, 1 µm, 0.5 µm and 0.2 µm were used as response variables. When considering the heavy metal contamination level, the quantity of zirconium, iron, chromium and nickel after 3 h of grinding was used as a response variable. For each response variable the statistical program ran an analysis of variance giving the influence of each process parameter (grinding medium bead size and rotation speed) on the studied response.

3. EXPERIMENTAL RESUTLS

3.1. The effect grinding medium bead size and rotational speed on grinding time

The first objective was to analyze the effect of grinding medium bead size and rotational speed on grinding time on the basis of factorial design. The calculations were done using Statgraphics 5.1 software ANOVA (ANalysis Of VAriance). The effect was measured as the average response at a high parameter value minus the average response at a low parameter value. Figure 3 shows that the influence of grinding medium bead size and rotational speed on grinding time increases exponentially as the final product particle size decreases. The influence of these parameters on grinding time is thus very strong, especially when sub-micron product particles are desired.

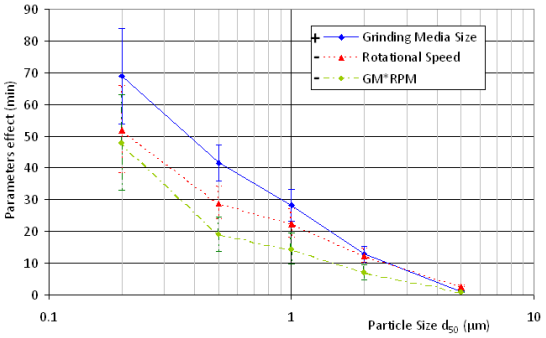

Figure 3. Impact of grinding medium bead size, rotational speed and final product particle size (d_{50}) on grinding time.

The influence of rotational speed alone, and the product of rotational speed and grinding medium bead size is negative (negative in this case implies shorter grinding time). Thus, at higher rotational speed, a shorter grinding time is required. Opposite to this the grinding medium bead size has a positive effect on grinding time, i.e. smaller grinding beads give a shorter grinding time to reach a certain product particle size.

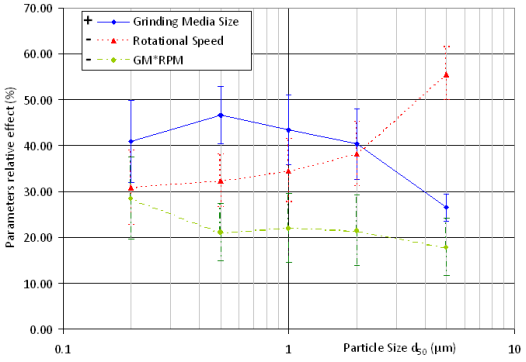

Figure 4 . Relative effect of the different parameters and combination of parameters on the time of grinding to reach different particle sizes.

Figure 4 shows the normalized data from Figure 3 in order to compare the relative effects of the grinding parameters. The rotation speed is the most important parameter for grinding of coarse particles. To reach sub-micron particles, the grinding medium bead size is the dominant factor. This is in accordance with the results from Jankovic [8].

As detailed in the Introduction section, the strongest effect of the rotation speed is observed in the coarse product size range and the finer product size range is less influenced by the speed. This is confirmed by the observations from Hou et al. [7], the relative effect of the rotation speed is decreasing with the product particle size.

In a previous study [12] the grinding mechanism in the same stirred ball mill for the same product was determined. Coarse particles mainly undergo cleavage and the production of extra fine particles results from an abrasion mechanism. Cleavage occurs by the application of low and high forces such as compaction due to the centrifugal motion of the bed of grinding medium. Thus the individual grinding medium particles are not of importance, but the loading of medium in the grinding chamber and the intensity of the forces in the mill are key factors.

The grinding medium loading was kept constant in this work. In the case of cleavage, the intensity of the applied forces and therefore the speed of centrifugation are much more important than the number of contacts and thus the grinding medium bead size. Abrasion is the result of tangential forces applied on the mother particle. Typically those forces are also present due to the centrifugal motion of the bed of grinding media. The speed and the energy of the impacts are then less important than the number of the potential impacts. The number of those impacts depends on the number of grinding beads that are present in the mill. At constant grinding medium loading the number of grinding beads increases with decreasing the medium bead size.
By taking into consideration the grinding mechanism, it becomes clear that the impact of the grinding medium bead size and rotational speed (Figure 4) is dependent on the size of the product particles being broken. The grinding medium bead size is more relevant than the rotational speed for production of fine particles. The number of impacts determined by the number of grinding beads is then dominant. In case of coarse product particles, the breakage is initiated by high centrifugal forces of compression in the packed bed of grinding beads, thus showing that the rotation speed is a dominant factor for these product particle sizes.
Jankovic [8] observed an optimum grinding media size for each product size. In the present case, the optimum grinding media size is not known for the starting material but the grinding media used is probably smaller than the optimum since as in the case of Jankovic's studies, the effect of the grinding media increases when the product size decreases. Further, Jankovic expected that a higher speed would result in greater efficiency for smaller grinding medium. This aspect is observed here as well: the combined effect of the grinding media and the rotation speed on the grinding time is significant. That interaction effect (noted GM * RPM as indicated in Figure 4) is nearly

constant for all product particle sizes. “GM * RPM” is a notation used to refer to the combined effect of the grinding media and the rotation speed on the grinding time (Figure 3 and Figure 4) or on the contamination level (Figure 5 left and right). Schwedes et al. [13] described that a stirred ball mill can be described using two parameters:

$$SE \sim m \cdot v_{tip}^2 \sim d_{GM}^3 \cdot v_{tip}^2 \quad (1)$$

with *m* the mass of one grinding medium bead and SE the stress energy (assimilated to the kinetic energy of a grinding medium). The number of stresses, i.e. the stress number, is equivalent to the number of impacts. The stress number is proportional to the frequency of impacts and thus on the number of grinding beads and the rotation speed of the mill. At constant loading of grinding medium the number of beads increases with the decreasing grinding medium bead size. Therefore, as for the stress energy, the stress number is dependent on the grinding medium bead size and the rotation speed. Nevertheless, the interaction is constant: Stress energy and stress number do not depend on the time of grinding. At any time of grinding, the influence of one parameter on the other parameter is the same and this is in accordance with the results of the factorial design.

3.2. The effect of grinding medium bead size and rotational speed on heavy metal contamination.

The forces applied in the grinding chamber are of great magnitude and high frequency. The stainless steel grinding chamber and the grinding medium (zirconium oxide stabilized with yttrium) undergo wear. Heavy metals can therefore enter the final suspension. Stainless steel is typically composed of iron, chromium, nickel and carbon. Carbon contamination is rather difficult to detect since the grinded product is organic and contains carbon atoms. The focus was therefore on the heavy metals. The content of iron, chromium, nickel and zirconium was determined using an atomic absorption spectrophotometer. Table 1 shows the influence of the rotational speed, v_{tip}, and the grinding medium bead size, d_{GM}, on the heavy metal content.

Table 1 . Heavy metal content after 3 hours grinding
(in part per million, ppm, ± 0.05ppm)

d_{GM} (mm)	V_{tip} (rpm)	Zr	Cr	Fe	Ni
0.8	6000	103	80	295	59
0.8	2000	9.9	1.7	6.8	1.5
0.3	6000	56	20	73	15
0.3	2000	7.9	0.29	1.8	0.6

The contamination by heavy metals is strongly dependent on the grinding conditions. The contamination by zirconium or iron ranges from a few ppm to a couple of hundreds ppm. The contamination by zirconium is limited because the grinding medium is relatively hard in comparison to the grinding chamber that is composed of

stainless steel. Table 1 presents the heavy metal contamination after 3 h of grinding. The required grinding time to reach a specific product particle size might be shorter than 3 h. Contamination levels can therefore be reduced in some cases. An optimum balance needs to be found between heavy metal contamination and the product particle size that is reached. The biggest impact is found for the rotation speed. At higher speeds the more the heavy metal concentrations increase. The effect of the grinding medium bead size is less important. The number of impacts between the grinding beads and the grinding chamber wall thus seems to have a smaller impact than the collision force (refer to Eq. (1)).
The results from Breitung-Faes et al. [10] showed that the bigger the grinding media the more contamination would occur. This effect is seen here and it is very limited. The hardness of the product material as mentioned by Becker and Schwedes [11] determines the bead wear as well. The present organic product milled is supposed much less harder than a metal or ceramics (as used in the references) and thus the wear of the grinding media is very limited.
The conclusions from Howorth [9] are consistent with the present observation. Howorth indicated that the harder the medium the less contamination would be detected. The present experiments are carried out with zirconium oxide, which is one of the hardest materials used as grinding media. Its wear is according to Howorth and as observed here very limited.

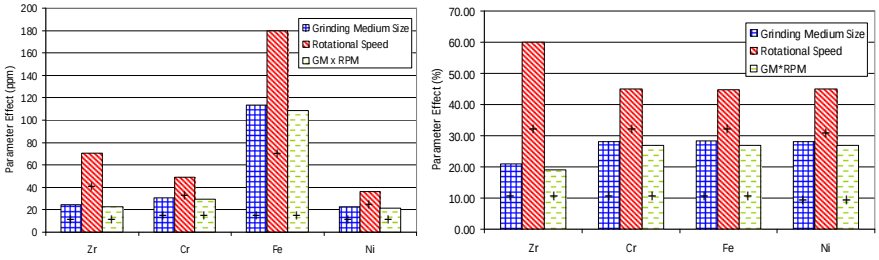

Figure 5 . Parameter effect (left) and relative effect (right) of grinding medium size and rotational speed on the heavy metal contamination after 3 h grinding.

The stainless steel composition is constant. Wear should therefore be similar for all metals that are present in stainless steel. This is confirmed by Figure 5. No estimate of sampling variability is available since there are no degrees of freedom remaining to estimate the experimental error. The number of experiments carried out is not sufficient here to consider both the error and an effect of the parameter at the second order (thus the combined effect of the grinding medium size and the rotation speed).

Figure 6 shows a photograph of the grinding chamber after 100 experiments. The contamination by zirconium is dependent on the grinding medium bead size, the rotational speed and the product of the two. Most of the wear of the grinding beads

are expected to be caused by interparticle collisions, because the beads are much harder than the stainless steel grinding chamber.

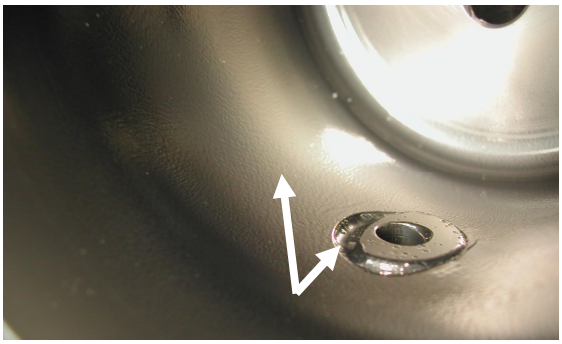

Figure 6 . Picture of the inside of the grinding chamber after more than 100 experiments. Arrows indicate area with visible wear of the grinding chamber. Radius of the grinding chamber: 39 mm, depth: 84 mm; Size of the pressure control hole indicated by the arrow: 7 mm.

4. CONCLUSION

The particle size reduction process follows specific breaking mechanisms depending on the size of the product particles. The breakage of coarse particles is most affected by the rotational speed and the breakage of small particles by the grinding media size. The rotational speed has a somewhat higher impact on the heavy metal contamination level than grinding medium bead size and the product of the two parameters. Higher rotational speeds and/or larger grinding medium particles give more heavy metal contamination when the grinding time is kept constant.

5. NOMENCLATURE

m : Mass of a grinding medium [kg]
d_{GM} : Diameter of the grinding medium [mm]
v_{tip} : Tip speed [rpm] or [$m.s^{-1}$]
GM : Grinding media
RPM : Rotation speed

6. REFERENCES

[1] Roman Shimanovich, A case study in improving in vivo exposure of a poorly soluble compound through several pharmaceutical approaches, Improving Solubility Conference, London (2008).
[2] E. Merisko-Liversidge, G.G. Liversidge, E.R. Cooper, European Journal of Pharmaceutical Sciences 18 (2003) 113–120.
[3] H.H. Molls, R. Hornle, DECHEMA, Monography 69(Tl 2) (1972) 631–661.
[4] Gao et al., International Journal of Mineral Processing 44–45 (1996) 641–652.

[5] J.A.Herbst, J.L. Sepulveda, Fundamentals of fine and ultra-fine grinding in a stirred ball mill, International Powder and Bulk Solids Handling Conference Chicago, IL, (1978) 452–470.
[6] M. He, Y. Wang, E. Forssberg, Parameter effects on wet ultrafine grinding of limestone through slurry rheology in a stirred media mill, Powder Technology 161 (2006) 10–21.
[7] T.-H. Hou, C.-H. Su, W.-L. Liu, Parameters optimization of a nano-particle wet milling process using the Taguchi method, response surface method and genetic algorithm, Powder Technology 173 (2007) 153–162.
[8] A. Jankovic, Variables affecting the fine grinding of minerals using stirred mills, Minerals Engineering 16 (2003) 337–345.
[9] C.J. Howorth, W.E. Lee, W.M. Rainforth, P.F. Messer, Contamination rates from Ce and Y-TZP ball milling media, British ceramic. Transactions and Journal 90 (1990) 18–21.
[10] Sandra Breitung-Faes, Arno Kwade, Nano particle production in high-power density mills, Chemical engineering research and design 86 (2008) 390–394.
[11] M. Becker, J. Schwedes, Comminution of ceramics in stirred media mills and wear of grinding beads, Powder Technology 105 (1999) 374–381.
[12] S.L.A. Hennart, W.J. Wildeboer, G.M.H. Meesters, Identification of the grinding mechanisms and their origin in a stirred ball mill using population balances, Chemical Engineering Science 64 (2009) 4123–4130.
[13] A. Kwade, L. Blecher, J. Schwedes, Powder Technology 86 (1996) 69–76.

Part I - Chapter 2

Identification of the Grinding Mechanisms and Their Origin in a Stirred Ball Mill Using Population Balances.

This chapter has been published as S.L.A. Hennart, W.J. Wildeboer, P. van Hee, G.M.H. Meesters, Chemical Engineering and Science 64 (2009) 4123–4130.

Abstract – The objective of this work was to understand the origin of the stresses and the nature of the grinding mechanisms in a high-shear ball mill. The ball mill used was a Dynomill and the grinding media consisted of zirconium oxide beads. The ground powder was a poorly water soluble product. The particle size distribution was analyzed with laser diffraction.
A population balance model enabled to calculate the breakage function from the experimental data. The breaking parameters were used to determine the grinding mechanism at different grinding conditions. The grinding mechanism depends on the orientation and intensity of the forces applied on the particles. The grinding mechanisms were determined from the grinding experiments and correlated to the movement of the grinding media in the grinding chamber and the applied mechanical stresses.

The observed grinding mechanisms are cleavage and some fracture for coarse particles (15µm), cleavage and abrasion for intermediate particles (0.8µm) and cleavage for fine particles (smaller than 0.15µm).
The grinding mechanisms are related to the movement of the grinding media in the grinding chamber. Cleavage and abrasion of particles are the result of compression forces and shear in the centrifuged packed bed of grinding beads. The grinding mechanism does not change when changing the operating conditions and the packed bed of media is similar in the studied ranges of operating conditions.

1. INTRODUCTION

The latest research in grinding focuses among others on the development of models to predict the grinding behavior of particles [1]. Population balance modeling (PBM) often is used to fit experimental data. The PBM is a mathematical tool to study the evolution of for example particle size in a particle size reduction process. One particular aspect of PBM is that the breakage behavior of each particle of a given size class can be calculated.
The present work uses PBM for further investigations of the grinding behavior of particles using a ball mill (Dynomill, Bachofen AG, Switzerland). The grinding mechanism depends on the material properties of the product, such as particle strength and size, and on the orientation and intensity of the forces exerted onto the particles. The forces result from the movement of grinding media in the grinding

chamber. The grinding mechanisms are determined from the grinding experiments and correlated to the movement of the grinding media in the grinding chamber and the applied mechanical stresses. The objective is to understand the origin of the stresses and the nature of the grinding mechanisms in a high-shear stirred ball mill. This study concentrates on a single product that is a poorly water soluble compound.

2. GRINDING THEORY

The nature and intensity of the applied stresses on the particles affect the particle size reduction process. In comminution the following three main breakage mechanisms have been identified [2, 3, 4].

- Abrasion occurs when stress is applied on particles along the tangential axis (shear). Particle breakage in this cases gives a bimodal particle size distribution comprising fine particles that are released from the surface of the initial particle and particles with a size close to that the initial particles.

- Cleavage of particles occurs when intense stresses are slowly applied on a particle (compression). This produces fragments of sizes 50–80 vol% smaller than the initial particles.

- Fracture occurs through rapidly applying intense stresses (impact). The particle size distribution in this case will range between 20 and 70 vol% of the size of the initial particle (Figure 1).

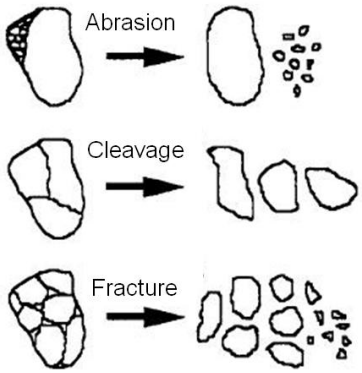

Figure 1. Fragmentation mechanisms (adopted from Varinot et al. [5]).

The evolution of the particle size distribution over time provides qualitative information on the dominant breakage mechanism during grinding (as in Figure 4). A quantitative measurement of the breakage mechanism can be obtained by calculation of the relative size distribution of the fragments. One way to represent the distribution is to plot the volume fraction of fragmented particles as a function of the particle size relative to the size of the initial particles. An example is given in Figure 2.

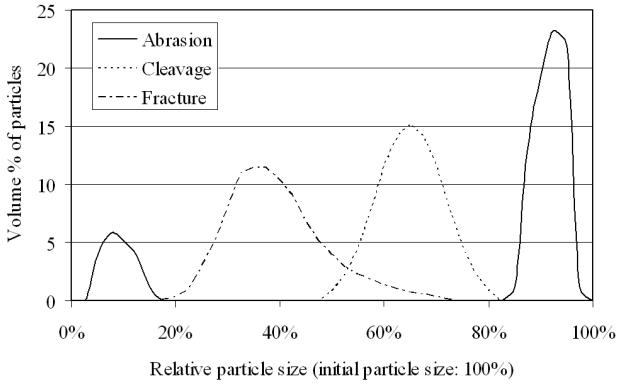

Figure 2. Particle size distribution of fragments representing different theoretical examples of the breakage mechanisms indicated in Figure 1.

The particle size distribution as function of time provides information on the evolution of all particles and fragments during the grinding process. The breakage mechanisms can be determined from the particle size evolution by determining the probability for formation of fragments with a specific size after breakage of the initial particle.

Besides this method other methods have been described in literature for determination of the particle breakage behavior. Menacho [6] derived the different breakage mechanisms from the cumulative breaking factors. Menacho's model used abrasion and fracture as the two extreme mechanisms to describe the evolution of the particle size distribution during grinding. Varinot et al. [5] used the representation of Menacho [6] and concentrated on the influence of the operating parameters on the fracture and abrasion mechanisms. The fragmentation process is complex and can be simplified by considering only the abrasion and fracture mechanisms. Cleavage is then considered as an intermediate between abrasion and fracture even if it results from slightly different forces.
In order to obtain a precise description of the grinding process both the qualitative analysis of experimental data and the non-cumulative breakage function have been applied in this work. All three main breakage mechanisms have been used to describe the breakage behavior of particles from different size classes.

3. PROCESSING OF THE EXPERIMENTAL DATA.

Experiments were carried out using a Dynomill from Bachofen AG (Basel, Switzerland) to study particle breakage mechanisms. The ball mill was operated in a recirculation mode. The ground product is a suspension of poorly water soluble organic powder in water. Figure 3 shows the circulation of the product suspension (4.8 wt%, 500mL) through the grinding chamber (volume of the chamber: 300 mL), which is filled at 75 vol% (bulk volume) with grinding media (0.3, 0.5 or 0.8 mm zirconium oxide, yttrium stabilized beads from Tosoh, Japan). The product suspension is drawn out

through a 0.1 mm gap to prevent the grinding medium to exit the milling chamber. The system is cooled to keep a constant temperature in the entire system.

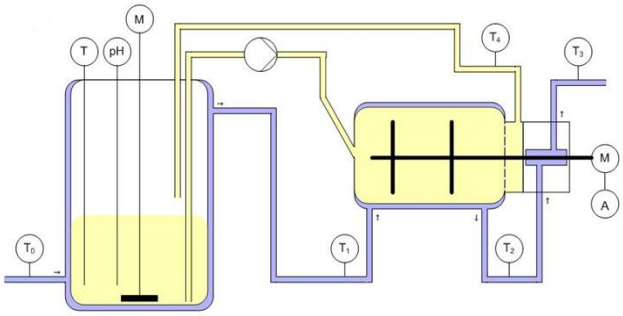

Figure 3 . Grinding set-up and controls, where *T* is a temperature measurement and pH is a pH control point.

Samples were taken from the stirred vessel at different times during grinding. The particle size distributions of the samples were measured with a laser diffraction particle size analyzer (LS230 equipment from Beckman Coulter) (Figure 4).

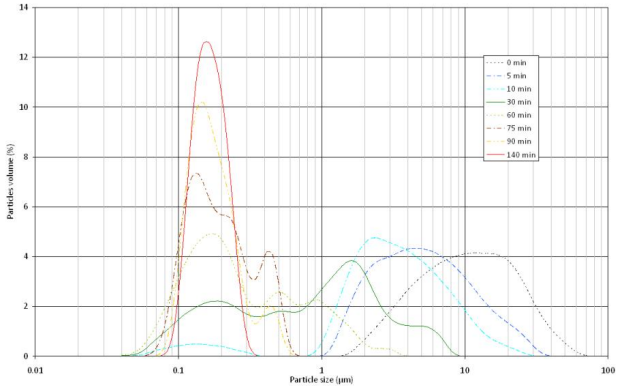

Figure 4. Evolution of the particle size distribution at different grinding times. (0.8 mm grinding media, 4500 rpm shaft speed)

As discussed in the previous paragraph the probabilities for formation of particles with a certain size after breakage of an initial particle need to be calculated. Population balances are used to calculate these probabilities from the experimental data.

The quantity of particles in size class *i* (V_i) can be described with the following equation [7]:

$$\frac{dV_i}{dt} = -S_i V_i + \sum_{j=1}^{i-1} b_{ij} S_j \cdot V_j \qquad \text{with} \qquad \sum_{i=j+1}^{n} b_{ij} = 1 \text{ and } n \geq i \geq j \geq 1 \qquad (1)$$

where *i* and *j* are specific size classes and *n* is the total number of size classes. *t* and V_i represent time and volume fraction in size class *i*.
The differential equation (1) can be solved analytically after it has been rewritten as an oversize cumulative size distribution form [8]. The cumulative volume fraction R_i represents the volume fraction of particles larger than the lower limit of the particle in size class (x_i):

$$\frac{dR_i}{dt} = -S_i R_i + \sum_{j=1}^{i-1} (S_{j+1} B_{ij+1} - S_j B_{ij}) \cdot R_j \quad \text{with } R_i(t) = \sum_{j=1}^{i} V_j \text{ and } B_{ij} = \sum_{k=i+1}^{n} b_{kj} \qquad (2)$$

The selection function S_i represents the probability of a particle in class size *i* to break. The breakage function b_{ij} is defined as the probability of formation of a particle of size class *i* after breakage of a particle from class *j*.
Many studies [9, 10] showed that for short grinding times the first order solution (Eq. (3), H_i=0 in Kapur [8] solution) is sufficient to describe the particle size evolution (see Figure 5).

$$R_i(t) = R_i^{\,0} \cdot \exp(K_i \cdot t) \qquad (3)$$

This solution (Eq. (3)) leads to the following expression (Eq. (4)) of the selection and breakage functions [9].

$$S_i = -K_i\,,\; b_{ij} = \frac{S_{i-1} - S_i}{S_j} \quad \text{or in a cumulative way: } B_{ij} = \frac{S_i}{S_j} \qquad (4)$$

The representation of b_{ij} as a function of x_i/x_j (Figure 7) gives the relative particle size distribution expressed as the equivalent volume percentage of the fragments resulting from breakage of a particle from size class *j*.

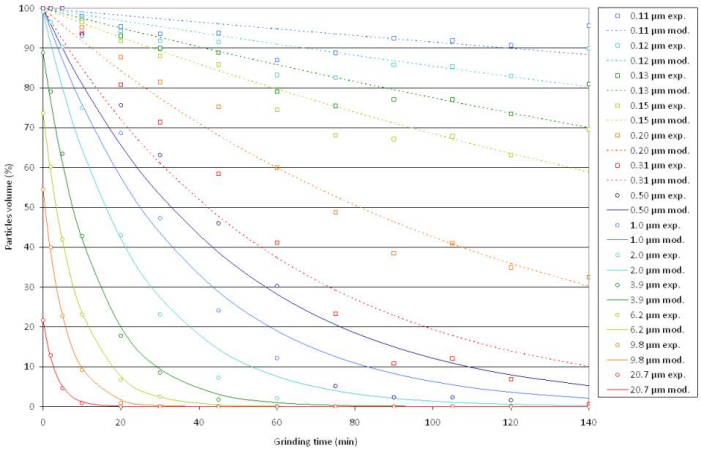

Figure 5 . Fitting results of the First order solution of the population balance modeling. (The lines are the fitted curves to the experimental points.)

4. STUDY OF THE BREAKING BEHAVIOR OF PARTICLES DURING THE GRIDNING PROCESS

4.1. Experimental observations

The grinding mechanisms can be studied by comparing the experimental data with the characteristic behavior of the grinding mechanisms as illustrated in Figure 4.

The initial particle size distribution of the material slowly shifts to smaller particle sizes during the first 5 min of grinding. The first breakage events only require a small amount of energy. This breakage leads to only a few daughter particles and therefore cleavage is the dominant grinding mechanism.

In a later stage during grinding, smaller particles appear and the distribution becomes bimodal. The particle size measurements have been complemented with scanning electron microscopy (SEM) pictures taken from samples dried at room temperature at different grinding time. Figure 6 shows that the decrease in particle size between 5 and 10 min of grinding leads to coarse particles covered by many fine particles. This behavior is typical for the abrasion breakage mechanism.

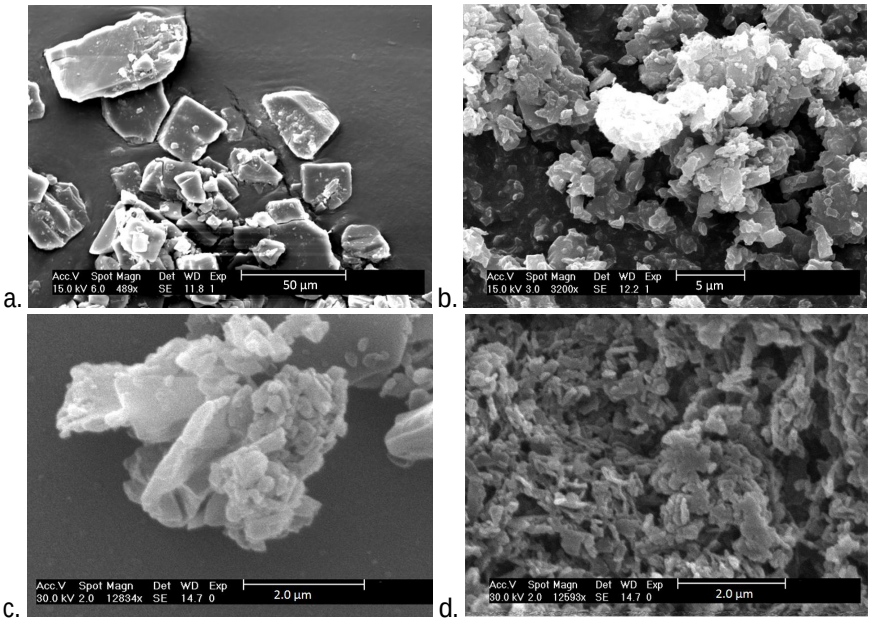

Figure 6. Scanning electron microscopy imaging of particles after different grinding times: (a) starting material; (b) 10 min grinding; (c) 30 min grinding and (d) end product after freeze drying—140 min grinding.

The formation of intermediate sized particles is observed after circa 30 min of grinding. This broad range of particles shows that the breakage is mainly resulting from a complex breaking process which includes abrasion, cleavage and/or fracture. The SEM image in Figure 6c shows a large amount of fines, intermediate sized

particles and coarse particles. The presence of fines is characteristic of the abrasion mechanism. It is not easily visible on the picture if the other broken particles are resulting from a cleavage or fracture process. The breakage of intermediate sized particles is mainly resulting from a double breaking process which includes abrasion and cleavage or fracture.

Finally, all intermediate sized particles break down to the final particle size. The difference between those particle sizes is not big and breakage can therefore be classified as a cleavage process. SEM picture (Figure 6d) was made of a freeze dried sample. Particles therefore agglomerated but the single structure can still be observed.

4.2. Use of PBM to determine breaking mechanisms

The qualitative analysis of the trends of the breakage mechanisms can also be studied using the population balance model as described in paragraph 3. The breakage behavior illustrated in Figure 7 shows similar results as the breakage mechanisms shown in Figure 4.

Coarse particles that are present at the start of the grinding process sustain a complex breakage mechanism.

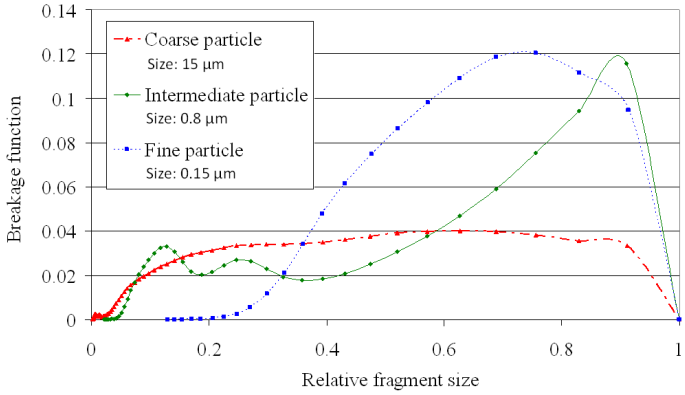

Figure 7 . Calculated breakage functions of fine, intermediate and coarse particles. (0.8 mm grinding media, shaft speed: 4500 rpm)

From Figure 7 the fragments size distribution is identified as ranging from 20 to 90 vol% of the initial size of the particles. Comparison with Figure 2 leads to the conclusion that the fragmentation process is a combination of the cleavage and fracture mechanisms. The probability for breakage of large particles is higher than for small particles and the weakest particles such as agglomerates or particles with weak axes caused by impurities for example will break quicker.

Particles of intermediate size mainly reduce in size due to abrasion and cleavage as shown in Figure 7. A large amount of fragments consists of fines (below 10 vol% of the initial particles), which are the result of the abrasion mechanism. Some of the fragments have an intermediate size (60–80 vol% of that of the initial particle), which

is typical for the cleavage process. These particles do not consist of for example agglomerates since they have been already broken in the first stage. Theses particles require more specific energy to break, which is typical for the abrasion and cleavage mechanisms. The preference between the two mechanisms depends then on the orientation of the forces and is discussed in the following Section 4.3.
The smallest particle classes are the hardest to break. These particles require more specific energy to break. This means applying a higher stress for a longer period of time. Therefore, particles of smaller sizes undergo mainly cleavage.

4.3. Origin of the mechanical stresses

Blecher and Schwedes [11] carried out numerical calculations of the flow pattern of a fluid inside the grinding chamber. Studies carried out at high Reynolds numbers showed that the fluid circulation occurs along the stirrers to the grinding chamber and back to the stirrer shaft in between the stirrer blades (Figure 8, further discussion is held in part 5). Kinetic energy calculations showed that more than 85% of the energy is concentrated in 10% of the volume of the chamber. Those high energy zones are located at the tip of the stirrer blades and along the walls of the grinding chamber. A higher inertia of the grinding beads, i.e. the bigger their size and relative density, causes the particles to move more independent from the liquid phase. Therefore, the flux of grinding medium particles through the high energy zone is lower. The velocity of the media in the high energy zones is much higher along the stirrers than along the walls.

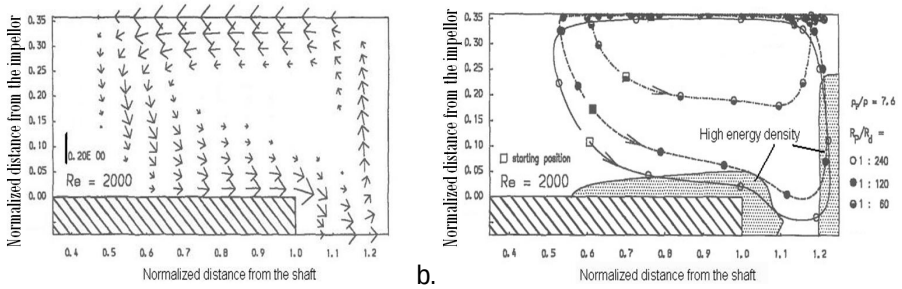

Figure 8 . (a) Flow pattern inside the grinding chamber and (b) trajectories of beads with different relative radii (adopted from Blecher and Schwedes 1996).

Kwade [12] defines three impact processes on the basis of the calculations of Blecher:
(A) Grinding media accelerated from the stirrer towards the grinding chamber.
(B) Grinding media pressed against the walls by centrifugal forces.
(C) Grinding media in the bed of centrifuged beads with different velocities.

Kwade [12] describes the frequency of the impact by the movement of the grinding media. A bead will move towards the grinding chamber (Mechanism A) once per rotation where in the centrifuge bed a single bead will generate several impacts per rotation (Mechanisms B and C).

Mechanism A is not frequent enough to be significant in comparison with the other mechanisms. Kwade [12] has compared the impact energy to the breaking energy of limestone particles. He showed that only limestone particles smaller than 10µm are broken by the second mechanism (B), i.e. the shear between the grinding beads and the walls.

Therefore, the main impacts in the grinding chamber are tangential collisions between grinding beads (Mechanism C). The resulting forces will be applied in the same direction to the product particle squeezed in between the media.

The forces applied on the product particles leading to breakage are therefore mainly tangential forces in the centrifuge bed of particles. The movement of the grinding media results in slow but high energy forces typical of shear and compression processes. Those forces are known (cf. paragraph 2) as the origin of respectively abrasion and cleavage mechanisms. This confirms the above studies of the grinding mechanisms.

5. STUDY OF THE INFLUENCE OF THE OPERATING PARAMETERS ON THE BREAKAGE MECHANISMS.

The PBM study was used to investigate the effects of rotation speed and grinding media size on the breakage mechanisms. The varying conditions result in different stress distributions in the ball mill due to a different kinetic energy of the grinding beads. The resulting fragment size distributions are presented in Figure 9 for different stress energy.

The stress energy has been described by Kwade, Blecher and Schwedes [14] as a function of the kinetic energy of a grinding media moving of size d_{GM} at the tip speed velocity v_d (Eq. (5)).

$$E = d_{GM}^{3} \cdot \rho_{GM} \cdot v_d^{2} \tag{5}$$

The results show that there are small variations in the breakage mechanism for all coarse, intermediate sized and fine particles. This implies that the breakage mechanisms are not influenced by changes in operating conditions within the tested range.

The study from Blecher and Schwedes [11] mentioned above is based on a Reynolds numbers of 2000, corresponding to a laminar zone when using a disc agitator (Figure 10). The determination of the Reynolds number (Eq. (6)) requires the velocity of the fluid, which was approximated by to be the tip speed (v_d) of the stirrer blades (radius R_d), the viscosity (η) and density of the slurry (ρ).

$$Re = \frac{v_{GM} \cdot R_d \cdot \rho}{\eta} \quad (6)$$

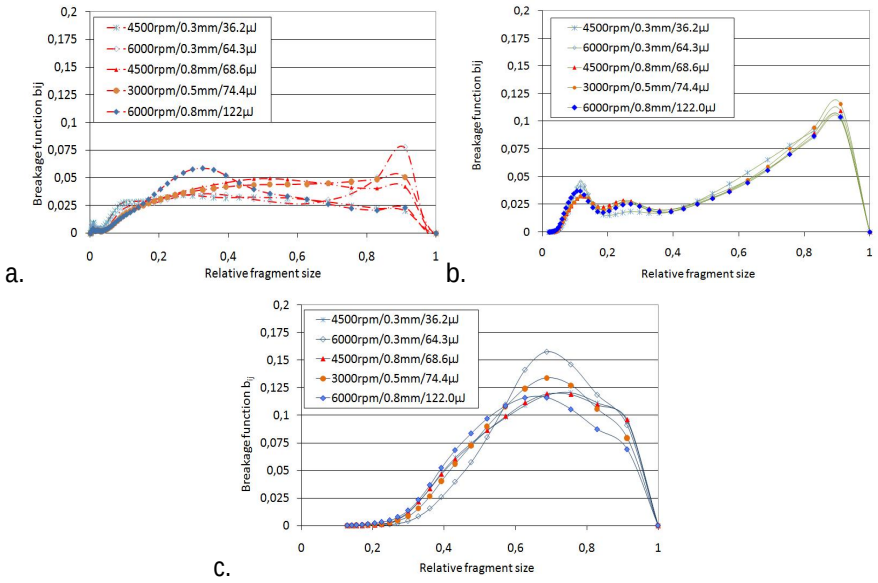

Figure 9. Relative fragments size distribution for breakage of coarse (a), intermediate (b) and fine (c) particles at different conditions v, d_{GM} and stress energy E.

The viscosity and density factors are determined from the suspension. In this study, the suspension consists of 4.8 wt% powder in water, the density is approximated at 1048 kg m^{-3}, the diameter of the stirrer blades is 6.4 cm. The viscosity of the initial slurry was measured with a rheometer at 0.01 (±0.005) Pa s. The viscosity increases further during grinding because of the increase of number and surface area of product particles.

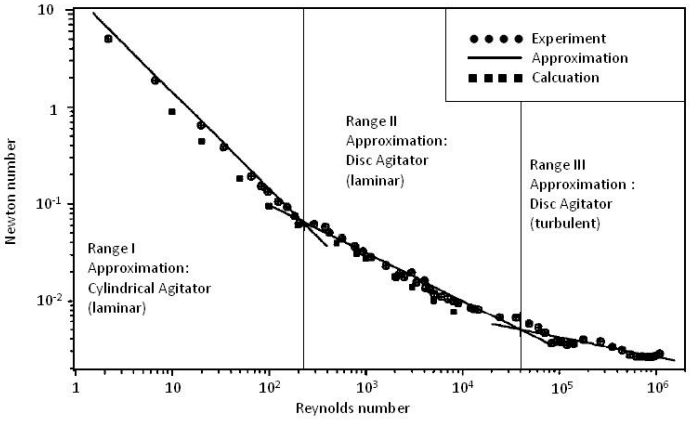

Figure 10. Power characteristic of the stirred ball mill. Adopted from Blecher and Schwedes [11].

Blecher and Schwedes [11] describe "laminar flow" with a disc agitator for Reynolds numbers in the range of *Re*=200 to *Re*=40 000. In this paper, the Reynolds numbers for the different conditions in Figure 9 vary between 10^4 and 10^5 for the initial suspension and the Reynolds number decreases with an increase of the viscosity in grinding time. As described by Blecher and Schwedes [11] the Newton number *Ne* (Eq. (7)) describing the power consumption in the mill is a function of the inverse of the Reynolds number. Variations in high Reynolds number imply only small variations in the Newton number used to calculate the flow pattern.

$$Ne = \frac{P}{v_d^{\,3} \cdot R_d^{\,2} \cdot \rho} = \frac{0{,}2 \cdot P}{Re \cdot \eta \cdot v_d^{\,2} \cdot R_d} \tag{7}$$

with *P* the specific power input.

The movement of the fluid in the grinding chamber is different from the one of the grinding media. The fluid motion depends on its viscosity, density and the stirrer size and tip speed. It is therefore, accepted that the maximum speed of the fluid is the tip speed of the impellor. The motion of the grinding media follows partially the movement of the fluid, depending on the ratios between the grinding bead size and the stirrer size and between the bead density and the fluid density.

Cases calculated by Theuerkauf and Schwedes [13] are for high fluid Reynolds number (16 000) combined with beads having almost no velocity lag and being neutrally buoyant. The grinding media follows therefore the fluid flow pattern and the high energy zone are specifically at the wall of the grinding chamber.

The study made by Blecher et al. [14], Figure 8, combine lower fluid Reynolds number (200 and 2000) with grinding media of different ratios (up to 7.6 in the density and a ratio of 1/240 between the grinding media size and the disc radius). The grinding media does not follow as in the present case exactly the fluid flow pattern. But as in the study of Theuerkauf and Schwedes [15], it is well defined that high energy zones are specifically at the wall of the grinding chamber.

The present paper uses slightly higher fluid Reynolds number ($10^4 < Re < 10^5$). And according to Blecher and Schwedes [11] and Figure 10, the present conditions are at the upper limit of the disc agitator laminar regime. The grinding media used is small compared to the disc radius: 1/80 to 1/213 and the media density ratio is of 5.6.

In laminar disc agitator regime, the flow pattern of the grinding media should be closely similar to the one calculated by Blecher et al. [14] for Reynolds number of 2000 and equivalent ratios of grinding media properties as in the present paper. The flow pattern presents a high energy zone at the wall of the grinding chamber and the forces applied on the product particles leading to breakage are therefore mainly tangential forces in the centrifuge bed of particles. The movement of the grinding

media results in slow but high energy forces typical of shear and compression processes. Those forces are known (cf. paragraph 2) as the origin of, respectively, abrasion and cleavage mechanisms. This confirms the studies of the grinding mechanisms. When changing slightly the process parameters, the regime remains constant and the grinding media present always a high energy zone where forces are typical of the observed grinding mechanisms.

6. CONCLUSION AND OUTLOOK

The objective of the work was to determine the grinding mechanisms in a stirred ball mill by using population balances. The main grinding mechanisms are cleavage and some fracture for coarse particles (15µm) cleavage and abrasion for intermediate particles (0.8µm) and cleavage for fine particles (relative size smaller than 0.15µm). The results of the studies are in line with the observations of the evolution of the particle size distribution over grinding time. The movement of the grinding media in the grinding chamber confirms the grinding mechanisms as resulting from characteristic forces. Cleavage and abrasion of particles are typical from compression forces and long shear that are present in the centrifuged packed bed of grinding beads.

The mechanism of grinding itself is not varying when changing the operating conditions; the motion of grinding media and thus the characteristic forces are of same nature in the studied ranges.

7. NOMENCLATURE

b_{ij} : Breakage function [-]
B_{ij} : Cumulative breakage function [-]
d_{GM} : Diameter of the grinding media [mm]
E : Stress energy [J]
K_i : Agglomeration selectivity function [-]
Ne : Newton number
P : Specific power input [$W.kg^{-1}$]
Re : Reynolds number [-]
R_d : Radius of the stirrer [m]
$R_i(t)$: Cumulative weight fraction from size class 1 to i at time t [-]
R_i^0 : Cumulative weight fraction from size class 1 to i at time t=0 [-]
S_i : Selectivity function [-]
t : Time [min]
v, v_d : Tip speed [rpm] or [$m.s^{-1}$]
v_{GM} : Speed of grinding media [$m.s^{-1}$]
$V_i(t)$: Volume fraction of particle from size class i (at time t) [-]
x_i : Lower size of particles of class i [µm]

η : Viscosity of the slurry [Pa.s]
ρ : density of the slurry [$kg.L^{-1}$]
ρ_{GM} : density of the grinding media [$kg.L^{-1}$]

8. REFERENCES.

[1] E. Bilgili, R. Hamey, B. Scarlett, Nano-milling of pigment agglomerates using a wet stirred media mill: Elucidation of the kinetics and breakage mechanisms, Chemical Engineering Science 61(1) (2006) 149–157.

[2] S. Redner, Statistical model for the fracture disordered media, In Fragmentation, ed. J. P. Hulin Elsevier, London (1990) 321–328.

[3] L.G. Austin, Some topics for research on fine grinding, IFPRI Annual Meeting Harrogate (1992).

[4] M. Gao, E. Forssberg, Prediction of product size distributions for a stirred ball mill, Powder Technology 84(2) (1985) 101–106.

[5] C. Varinot, S. Hiltgun, M.-N. Pons, J. Dodds, Identification of the fragmentation mechanisms in wet-phase fine grinding in a stirred bead mill, Chemical Engineering Science 52(20) (1997) 3605–3612.

[6] J. M. Menacho, Some solutions for the kinetics of combined fracture and abrasion breakage, Powder Technology 49 (1986) 87–86.

[7] K. Sedlatschek, L. Bass, Contribution to the theory of milling processes, Powder Metallurgy Bulletin 6 (1953) 148–153.

[8] P.C. Kapur, Kinetics of batch grinding, Trans of AIME 247 (1970) 309–313.

[9] H. Berthiaux, C. Varinot, J. Dodds, Approximate calculation of breakage parameters from batch grinding tests, Chemical Engineering Science 51(19) (1995) 4509–4516.

[10] C. Varinot, H. Berthiaux, J. Dodds, Prediction of the product size distribution in associations of stirred bead mills, Powder Technology 105(1-3) (1999) 228–236.

[11] L. Blecher, J. Schwedes, Energy distribution and particle trajectories in a grinding chamber of a stirred ball mill, International al Journal of Mineral Processing 44-45 (1996) 617–627.

[12] A. Kwade, Determination of the most important grinding mechanism in stirred media mills by calculating stress intensity and stress number, Powder Technology 105 (1999) 382–388.

[13] J. Theuerkauf, J. Schwedes, Investigation of Motion in Stirred Media Mills, Chemical Engineering and Technology 23 (2000) 203–209.

[14] L. Blecher, A. Kwade, J. Schwedes, Motion and stress intensity of grinding beads in a stirred media mill, Powder Technology 86 (1996) 59–68.

[15] J. Teuerkauf, J. Schwedes, Theoretical and experimental investigation on particle and fluid motion in stirred media mills, Powder Technology 105 (1999) 406–412.

Part I - Chapter 3

Characterization and Modeling of a Sub-Micron Milling Process Limited by Agglomeration Phenomena.

This chapter has been submitted as S.L.A. Hennart, P. van Hee, V. Drouet, M.C. Domingues, W.J. Wildeboer, G.M.H. Meesters, Chem Eng Sci (accepted).

Abstract – The objective of this work was to characterize a sub-micron grinding process in a wet stirred media mill including the agglomeration of fines inside the grinding chamber. To do so a population balance model has been developed. A Dynomill stirred media mill was used and the grinding medium consisted of zirconium oxide beads. The product under investigation was poorly water-soluble. The particle size distribution of the initial powder ranged from 1 to 100 um. Laser diffraction was used to analyze the particle size distribution.

During grinding the average particle diameter of a particulate product is reduced to a minimum value. These grinding experiments showed that for a specific product this minimum value is a fixed constant within the range of tested operating conditions. This minimum average particle diameter could be influenced by modification of the particle surface properties with surface active agents.

The minimum mass mean particle diameter is a result of grinding and simultaneous agglomeration of broken particles. To build a representative model, a dynamic population balance model was developed. The crystallite size as measured with X-Ray diffraction was chosen as the minimum achievable particle size by grinding. Simulations showed that the applied population balance model is an adequate tool to forecast the evolution of the particle size reduction process and the time required to reach the final product specifications.

The product could be defined as “very brittle” using the approach from Kwade [1] and Stadler and Schwedes [2]. The shear induced by the translation movements of the grinding beads was thus enough to break the particles.
The median particle size of the broken particles (x_{50}) was plotted as function of the number of stress events (SN) in the mill. This number of stress events was calculated for one initial product particle. That is the representative number of stresses that needs to be applied on an initial particle to break it into fractions with the desired fine particle size. SN is proportional to the number of media contacts and their frequency and the probability that a media contact leads to particle breakage. That frequency of media contact is defined as the angular rotation speed (ω) of the mill corrected by an efficiency factor (γ_F). The stress number SN is characteristic of the ground product.

The efficiency factor γ_F describes the efficiency with which the impellor transfers its energy to the grinding medium. γ_F was a function of the mill design and more specifically the impellor shape. Factor γ_F is taken as the surface of the impellor in contact with the grinding media.

This approach leads to a general representation of the grinding profile of the studied product in a stirred media mill.

1. INTRODUCTION

The development of grinding technology for the production of very fine powders has focused on the limit of grinding. During a ball milling process the minimal particle size reachable is often limited by a process of agglomeration or compaction of product particles [3]. The objective of this work is to build a model capable to describe a grinding process and its agglomeration component.

As broadly reported in literature [4], several types of models can be useful for the prediction of the grinding process, up scaling, etc. Population balance modeling (PBM) often is the best way to fit experimental data. The PBM is a mathematical tool to study and describe the evolution of for example particle size in a particle size reduction process.

Varinot [5] showed that grinding processes can be described with PBM using only two fitting parameters. The PBM in this case only describes the particle size reduction process. When agglomeration occurs the PBM can also be used to describe a particle size increase, but more parameters are required to describe this process. The purpose of this work is to combine the grinding process and the agglomeration process in a PBM. The resulting PBM contains four fitting parameters two describing the grinding process and two describing the agglomeration process. The model is then used for the prediction of the particle size versus the grinding time.

Kwade et al. [1] and Stadler et al. [2] describe milling experiments using two key parameters. The first parameter is the stress energy (SE) and represents the energy of a collision between two grinding media in the mill. The second parameter is the stress number (SN), which is the number of collisions that are required to break a product particle into fractions with the target size. These two parameters were found sufficient to describe the milling of a given product in a defined mill. This paper examines whether this concept can be generalized to the grinding of a given product in any mill.

2. MATERIAL AND METHODS

2.1. The experimental set-up.

This work focuses on the grinding of a poorly water soluble compound. Grinding has been performed using a stirred media mill (Dynomill, Bachofen AG, Switzerland). In a first study grinding experiments have been performed in absence of additives. In a second study various surfactants have been tested to reduce the agglomeration behavior of the particles. Particle size distributions have been measured with a laser diffraction size analyzer (LS230 equipment from Beckman Coulter).

Experiments were carried out using a Dynomill from Bachofen AG (Basel, Switzerland). The stirred media mill was operated in a recirculation mode. The poorly water soluble organic product was suspended in water (4.8 wt%, 500mL solution). Figure 1 shows the circulation of the product suspension through the grinding chamber (volume of the chamber: 300 mL) that was filled at 80% (bulk volume) with grinding beads (Zirconium oxide, Yttrium stabilized beads from Tosoh, Japan). The product suspension was drawn out through a 0.1 mm gap to prevent the grinding medium to exit the milling chamber. The system was cooled to keep a constant temperature throughout the entire system.

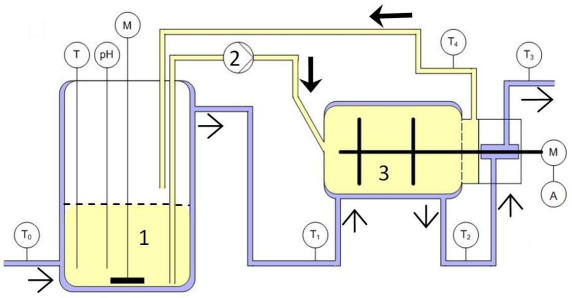

Figure 1 . Grinding set-up and controls, where T is a temperature measurement and pH is a pH control point. Arrows show the circulation of the cooling water (→) and product (➔). The product is pumped from the stirred tank marked as 1 by the pump 2 to the grinding chamber 3. M stands for motor and A for Amp meter.

The particle size distribution was analyzed throughout the grinding process by taking samples from the stirred vessel. Figure 2 is an example of such particle size measurements. These data were used to develop the PBM describing the evolution of the particle size distribution during grinding.

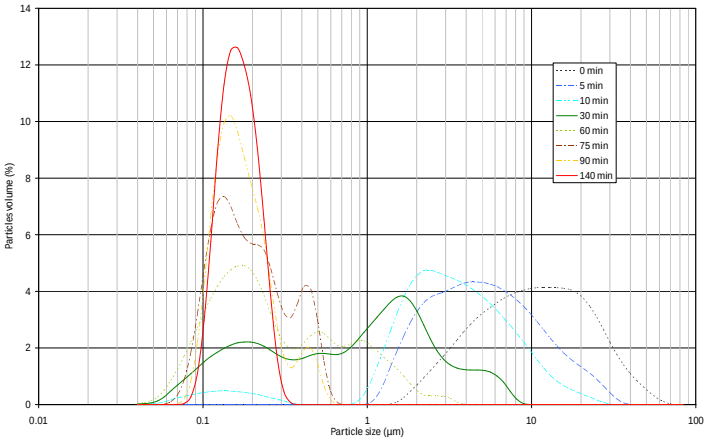

Figure 2 . Evolution of the particle size distribution as function of grinding time after start of the circuit operation t_Z.

2.2. X-Ray Diffraction

X-Ray diffraction (XRD) was used to measure the crystallite size in crystals. Stenger et al. [6] showed that the crystalline structure can change in grinding processes. The study on tin oxide by Stenger et al. showed that high stresses damage the crystalline structure causing the formation of amorphous segments and fragmentation of crystallites. Thus, for some inorganic materials a decrease in crystallite size has been observed during grinding even when the particles are larger than the crystallite size itself. Stenger et al. also showed that the final particle size of grinding is in the same order as the crystallite size.

The ground product in this study is an organic polycrystalline material. The crystallite size "L_v" was measured by XRD in concentrated slurries using the Scherer formula. The broadness of the diffraction peaks is inversely proportional to the volume weighted crystallite size [7]:

$$L_v = \frac{0.9 \cdot \lambda}{B \cdot \cos \Theta} \tag{1}$$

With B the full-width at half maximum of the peak from the diffraction curve at the angle Θ when using X-Ray wavelength λ.

2.3. Population Balance modeling

The population balance model describes changes in the quantity of particles (V_i) in each particle size class i. The following equations describe the size-discrete, volume (or mass) fraction frequency of the population balance model (PBM) for batch grinding [8]:

$$\frac{dV_i}{dt_Z} = -S_i V_i + \sum_{j=1}^{i-1} b_{ij} S_j \cdot V_j \qquad \text{with} \qquad \sum_{i=j+1}^{n} b_{ij} = 1 \text{ and } n \geq i \geq j \geq 1 \tag{2}$$

where i and j are the size-class indices running from 1 to n; t_Z and V_i representing respectively time after start of the circuit operation and volume fraction in size class i. The differential equation (2) can be solved analytically after it has been rewritten as an oversize cumulative size distribution form [9]. The cumulative volume fraction R_i represents the volume fraction of particles larger than the lower limit of the particle in size class (x_i):

$$\frac{dR_i}{dt_Z} = -S_i R_i + \sum_{j=1}^{i-1} (S_{j+1} B_{ij+1} - S_j B_{ij}) \cdot R_j \quad \text{with } R_i(t) = \sum_{j=1}^{i} V_j \text{ and } B_{ij} = \sum_{k=i+1}^{n} b_{kj} \tag{3}$$

Many studies [10,11] consider the first order solution (H_i=0 in Kapur [9]) sufficient to describe the particle size evolution for short grinding times (Equation 4). Long grinding times give more effect to the secondary term relative to the first order term, in the second order solution (Equation 5).

$$R_i(t) = R_i^{\,0} \cdot \exp(-S_i \cdot t_Z) \tag{4}$$

The second order solution (Equation 5) enables the consideration of a delay to breakage [12], which is omitted by the first order solution. Particles in low cumulative classes do break but the daughter particles remain mainly above the size class and therefore the representation of the mass fraction in time shows a delay to breakage.

$$R_i(t) = R_i^0 \cdot \exp(G_i \cdot t_Z + H_i \cdot t_Z^2) \tag{5}$$

Further studies [12] including delay to grinding used a numerical approach based on a time variant model. Equation 3 becomes then:

$$\frac{dR_i}{dt_Z} = -S_i(t_Z)R_i + \sum_{j=1}^{i-1}(S_{j+1}(t_Z) \cdot B_{ij+1} - S_j(t_Z) \cdot B_{ij}) \cdot R_j \tag{6}$$

The addition of a time dimension in the model only enables a better fitting to the model to the experimental data and does not enable a physical understanding of the model parameters. Regarding the objectives of the present paper to have a representative model still which parameter can be related to the process parameters by a physical meaning; the time variant model is not an option because it includes an unknown part of the process.

The quality of the fitting can be defined by a sum-of-squared residual ratio to the number of data point defined by:

$$F = \frac{\sum_{i=1}^{N}\sum_{q=1}^{\Omega}\left(R_{iq,mod} - R_{iq,exp}\right)^2}{N \cdot \Omega} \tag{7}$$

With $R_{iq,mod}$ and $R_{iq,\ exp}$ the prediction and the experimental value of the cumulative volume fraction at sample point q. N being the number of classes (in the present publication, N=83).

2.4. Characterization of the mill

A simple approach to the characterization of the mill was inspired from the approach of Stadler et al [2] developed by Kwade et al [1]. Stadler and Kwade described the grinding process by the stress energy (SE), the stress number (SN) and the grinding energy (E_m). The model descriptions assume that grinding takes place upon collision between the grinding beads. The number of the impacts necessary for a particle to break into particles of a target particle size is defined as the Stress Number (SN). The energy of one impact is the Stress Energy (SE). The grinding energy (E_m) is the total specific energy used for grinding.

The SE is taken as the maximum kinetic energy of the grinding beads in the mill. That corresponds to a particle moving at equal velocity as the tip of the impeller. SE is defined in equation (8).

$$SE = \frac{\pi}{6} \cdot d_{GM}^{\ 3} \cdot \rho_{GM} \cdot v_{tip}^{\ 2} \tag{8}$$

With d_{GM} being the diameter of a grinding medium, ρ_{GM} the density of the grinding media and v_{tip} the tip speed of the impellor.

The specific energy used for grinding (E_m) is proportional to the maximal energy applied per initial product particle ($E_{/P,\,max}$) multiplied by the number of particles (N_P). The maximum energy applied to an initial particle during grinding is the multiplication of the SE and the SN (equation 9).

$$E_{m,real} = \frac{N_P}{m_P} \cdot E_{/P,max} = \frac{N_P}{m_P} \cdot SE \cdot SN \tag{9}$$

with m_P the total mass of product particle and N_P the number of initial product particles.

The stress number (SN) is calculated in the following manner (Stadler and Kwade). The number of stress events (SN, equation (10)) on an initial product particle is determined by the total number of media contact (N_C) and the probability that a product particle is sufficiently stressed and caught at a contact point between two grinding beads (P_S). The number of stress events SN is defined per initial product particle. SN from grinding experiments at different product particle concentrations or with different mills having different volumes should be constant for a given particle size. The SN should be calculated as such as being purely dependent on the product and its target particle size.

$$SN = \frac{N_C \cdot P_S}{N_P} \tag{10}$$

With N_P the number of initial particles.

The number of contact (N_C) according to Kwade [13] is proportional to the number of grinding beads, grinding time (residence time) and the frequency of the grinding bead impacts. The same definition is used in this paper.
As defined by Kwade, the frequency of impact is proportional to the rotation speed of the mill. A correction is proposed to correct for the mill size and design. Each mill has a different efficiency for energy transfer from the impeller to the grinding beads. Later, Kwade [14] distinguishes the effective specific energy transferred to the particles for breakage and the total specific energy (energy used for breakage and energy dissipations). This efficiency influences the frequency of impacts and is proposed to be corrected defined by an efficiency factor γ_F. γ_F is a function of the transfer of energy from the impellor to the grinding media. That transfer is a function of the impellor size and shape as described by Bunge [15], Blecher [16] and Jayasundara [17]. It is defined as the total surface area of impeller in contact with the grinding medium (see figure 3). The number of contacts is thus defined as follows:

$$N_C = \frac{m_{total,GM}}{\frac{\pi}{6} \cdot d_{GM}^{\ 3} \cdot \rho_{GM}} \cdot (\gamma_F \cdot \omega) \cdot t \qquad (11)$$

With $m_{total,GM}$ the total mass of grinding media in the chamber, ω the angular rotation speed of the stirrer, t the time of grinding, d_{GM} the diameter of a grinding medium, ρ_{GM} the density of the grinding media and γ_F the surface area of the impellor in contact with the grinding media.

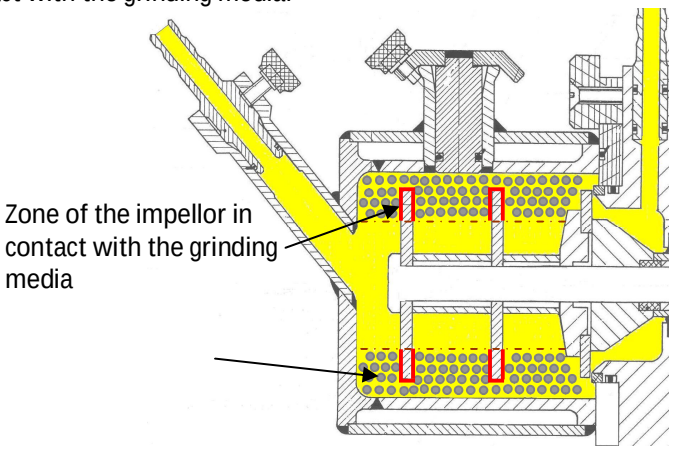

Figure 3 . Scheme of the inside of the mill. The red line represents the part of the impellor in contact with the grinding medium when the mill is in operation. All grinding beads are supposed to be on the outside of the grinding chamber because of the centrifugal force.

The probability P_S is found to be dependent on the breakage mechanism. Two approaches were defined by Stadler et al [2], Bunge [18] and Kwade and Schwedes [19]: The grinding beads generate two types of impact:

- Frontal impacts of two grinding beads (Figure 4 left)
- Shear stresses generates by grinding beads "rolling" on each other (Figure 4 right)

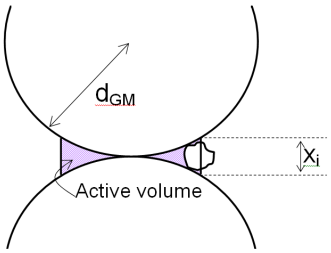

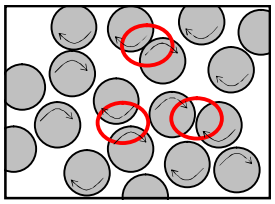

Figure 4 . Left – Frontal impacts between too grinding beads that may catch product particles. Right – translation and rotation movements that generate shear stresses between grinding medium particles

In the case of frontal impact, the probability is defined by the active volume in between the grinding beads. The active volume is a function of the product particle size and the grinding medium bead size as illustrated in figure 4 left. That volume is proportional to the diameter of the grinding media (d_{GM}) and thus the probability P_S can be defined as proportional to d_{GM}. The stress number can thus be defined as in equation (12) by combining this with equation (10) and (11):

$$SN_{frontal} \propto \frac{m_{total,GM}}{\frac{\pi}{6} \cdot d_{GM}^{\ 2} \cdot \rho_{GM}} \cdot \frac{(\gamma_F \cdot \omega) \cdot t}{N_P} \tag{12}$$

For the other breakage mechanism the shear stresses acting between the grinding medium surfaces are potentially sufficient to break weak particles (aggregates or weak structures). The probability of such stress to occur is higher since it is linked to the surface area of the media. The probability is defined by Stadler et al [2] and Bunge [15] as proportional to the surface area of one grinding medium bead. The stress number is then defined by combining this with equation (10) and (11):

$$SN_{shear} \propto \frac{m_{total,GM}}{\frac{1}{6} \cdot d_{GM} \cdot \rho_{GM}} \cdot \frac{(\gamma_F \cdot \omega) \cdot t}{N_P} \tag{13}$$

The frontal impacts are of the highest impact energy in the mill and will therefore be sufficient to break any particles that can be milled. The shear stresses are expected to be lower in intensity and thus enough to break only weak particles (agglomerates or crystalline particles with a weak crystal structure). It is not yet known how to define the limits of the two mechanisms that act on the product particles and how to forecast the behavior of a product in the mill on the basis of the material properties. Nevertheless, tools defined hereafter can help to determine which mechanism is applicable.

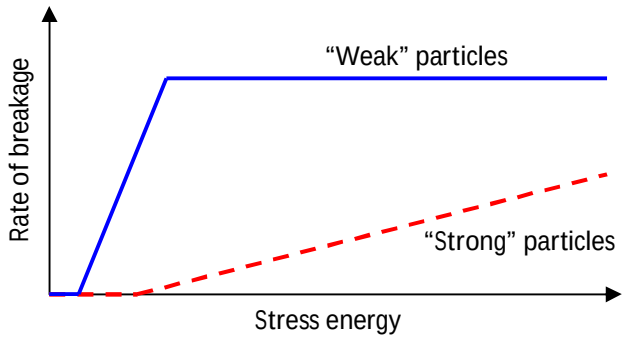

Figure 5 . Schematic representation of the rate of breakage as function of the stress energy for materials of different strength: weak particles (line) and strong particles (dashed line).

A weak material is easy to break and low values of the SE are already sufficient to break all particle sizes of this material. Therefore from all stresses in the grinding chamber, the shear stresses are sufficient to break product particles. The consequence is that above a minimum value of the SE, the breakage rate is only dependent on the number of stress events. Above a minimum value of the stress energy the result of stressing a particle does not depend on the stress energy because every stress energy is sufficient to reach the finest possible product fineness. This is schematically shown in figure 5. The line indicates the rate of breakage of weak particles as function of the applied stress energy. Under these conditions the stress energy (SE) is independent of the stress number (SN). When increasing the stress energy SE by a factor f, the grinding energy ($E_{m,max}$) should be multiplied by the same factor f; thus the slope of the curve describing the grinding energy ($E_{m,max}$) versus stress energy (SE) should be 1.

In the case of a material which is hard to break, not all stress events can deliver energy which is high enough to break the particles. The product will be milled at a rate depending on the stress energy (SE) and the stress number (SN). The stress energy (SE) is not constant for different stress numbers (SN) and the slope of curve of the grinding energy versus the stress energy ($E_{m,max}$ vs SE) is lower than 1.

Kwade [20] carried out a study for grinding limestone and found a slope of ca 0.33. In the case of fused aluminum a lower slope of 0.26 was found . Limestone and fused alumina are thus expected to be products that are hard to break. Following the definition of P_S for hard materials, P_S is proportional to the diameter of the grinding beads to the power 1. On the other hand, pigment grinding and yeast cell disintegration revealed very high factors, which approach a value of 1. These products are easily broken in the mill and follow the definition of P_S being proportional to the surface area of the grinding medium.

For hard materials SE and SN define how fast particle will break. For a given SE breakage to a given particle size will require a specific SN. The correlation between SE and SN is thus supposed to be purely product dependent.

For soft materials the SE is constant for different SN, which implies that breakage only depends on the SN. The grinding profile of a product in a stirred media mill is the correlation between the product quality (x_{50} for example) as function of SN.

All grinding experiments were operated in a circuit operation mode as shown in figure 1. The product particles were pumped from a tank to the grinding chamber and back to the tank. The ratio between the tank volume and grinding chamber free volume was approximately 2:1. The real grinding time – or residence time (t) has therefore been approximated to be the time (t_Z) after start of the circuit operation corrected by the volume ratio (equation 14).

$$t = t_Z \cdot \frac{V_{GC} - V_{T,GM}}{V_{suspension}} \quad (14)$$

With V_{GC} the volume of the grinding chamber, $V_{T,GM}$ the volume occupied by the grinding media and $V_{suspension}$ the total volume of suspension of product particles.

3. RESULTS AND DISCUSSION

Grinding experiments were carried without additives, varying the grinding medium size and/or the rotation speed. The data obtained were fitted with the PBM that is presented in section 3.1. Different models were tested to reach the following criteria:

The model should correlate the fitting parameters to the process parameters with a physical meaning with the aim to better understand the grinding process.

The quality of the model should be sufficient to calculate, in a studied domain, the time of grinding and the evolution of the particle size distribution in time.

3.1 Milling in absence of additives.

A stirred media mill is a complex system with many parameters that influence the process of grinding. The more important parameters are rotation speed, grinding medium size hardness and density, filling ratio, product concentration, etc. This study focuses on grinding medium size and rotation speed. The grinding medium used is made of Zirconium oxide stabilized with Yttrium. The sizes of the grinding beads (d_{GM}) are of 0.3, 0.5 and 0.8 mm. The rotation speed ranges from 2000 to 6000 rpm. Filling ratio of the mill is 80%. Considering the size of the impellor blades, the tip speed ranges from 6.80 m/s to 20.41 m/s. The results are presented in Table 1.

Table 1 . Relation between particle size and grinding time after start of the circuit operation as function of the grinding medium bead size and rotation speed. (time t_Z required to reach $d_{4,3}$ of 0.20 µm)

		Average Diameter Grinding Media (mm)		
		0.300	0.500	0.800
		Final mass mean diameter x_{70} (Time of grinding to final product t_Z)		
Rotation Speed (rpm)	2000	0.181 µm (53 min)	0.173 µm (116 min)	0.175 µm (260 min)
	3000	0.180µm (47 min)	0.188 µm (120 min)	0.179 µm (175 min)
	4500	0.184 µm (29min)	0.183 µm (69 min)	0.175 µm (145 min)
	6000	0.177 µm (26 min)	0.183 µm (50 min)	0.176 µm (112 min)

In all experiments a similar final particle size was reached regardless of grinding medium size and rotation speed. The grinding time was, however, strongly dependent on both parameters. The model to be developed should therefore allow to define the time required for grinding as function of its parameters, which themselves should be defined as a function of the process parameters.

3.2 Milling in presence of surfactants

The free energy of particles increases with an increase in specific surface area. When particles form agglomerates the total surface area decreases. As a result the free energy is lowered and the system is more stable. Agglomerates are formed when particles overcome the inter-particle energy barrier [21].
The driving forces for agglomeration are Brownian motion and fluid motion. In a stirred media mill particles can be pressed together between two grinding beads or between grinding beads and the wall of the stirred media mill. When particles are pressed together they can agglomerate or sinter. The resulting agglomerates can again be broken up into smaller particles in the stirred media mill.

Agglomeration can be prevented with additives that give electrostatic and/or steric repulsion between the particles. The choice of additives is dependent on the product and its application(s). Griffin [22,23] and Davies [24] calculated the hydrophilic-lipophilic balance (HLB) number for surfactants on the basis of the molecular weight of the hydrophilic and hydrophobic parts of the molecule. The HLB number helps to make a first selection of a stabilization system.

The grinding experiments from paragraph 3.1 were repeated with CTAB (Cetyltrimetyl-ammonium bromide), a cationic surfactant to stabilize the particle suspension and to prevent aggregation of small particles. As described for example by Bernhardt [25], the use of an additive will help to prevent broken particles from agglomerating. Therefore the final particle size reachable could be smaller when surfactants are used.

Figure 6 shows that an increase in surfactant concentration reduces the mean particle size after grinding. The observed effect is most likely due to stabilization of the particle suspension by the surfactant, which prevents/reduces particle agglomeration. The surfactant was present as micelles at the concentrations that were used (critical micelle concentration CTAB = 1 mmol.L^{-1}). These micelles could affect the particle size measurement. As a result a lower average particle size could be measured in the presence of surfactant micelles. The surfactant was added prior to grinding. The surfactant thus affected all particle size measurements in one grinding experiment. The particle size before grinding was the same in all experiments regardless of the use of surfactant. It may therefore be concluded that the micelles did not affect the particle size measurement in any of the experiments.

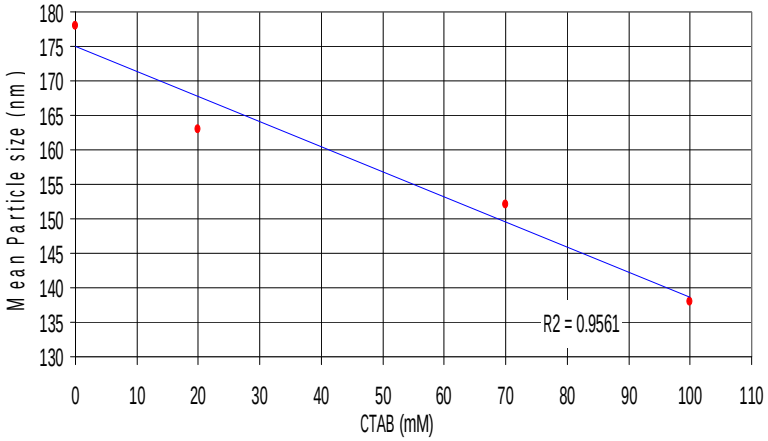

Figure 6 : Final particle size in ball milling as function of CTAB surfactant concentration.

The addition of surfactant can change the solubility and degradation rate of the product and thereby induce a particle size reduction. Solubility could be measured using filtration of dispersed suspensions (0,02µm filters) and HPLC techniques. Tests were performed to verify if the particle size decrease was related to a solubility increase. For CTAB concentrations of 0 and 100 mmol.L^{-1} the particle size changed from 0.18 to 0.14 µm after grinding, which implies an average single particle mass reduction of 47%. The concentration of total product in the liquid phase was 0.5% w/w in all experiments. In absence of surfactants the solubility was limited to 50 ppm. In the presence of surfactants (100mmol.L^{-1}) the solubility reached 170 ppm. The decrease of total particle mass due to solubilisation therefore was 2% w/w. This is much less than the decrease of 47% that is observed as the result of grinding. This proves that the surfactant prevents agglomeration of particles.
Another experiment was performed to determine the influence of the surfactant on the product solubility and the particle size analysis. 100 mM CTAB was added to a 180 nm particle suspension that did not contain surfactant. The particle size was measured before and after surfactant addition. Upon the addition of surfactant the particle size decreased from 180 to 170nm after several hours of magnetic stirring. The decrease in particle size could be related to solubilisation or desagglomeration of the particles. The particle size in presence of surfactant was thus much higher than 140nm, which was reached when surfactant was added prior to grinding. This confirms that the surfactant had a small effect on the particle size measurement.

The PBM describing should thus include agglomeration of fines and agglomerate break up. The particle size reduction process produces particles that are smaller than the final particle size, and these particles undergo agglomeration. In order to define the model, the minimal particle size needs to be determined.

3.3. Minimum reachable particle size.

Polycrystalline materials are made of primary crystalline structures often referred to as grains or crystallites.

Figure 7 shows that the mean crystallite size of the organic product did not change during grinding. The crystallites were in this case not broken and had an average size of approximately 45 nm. This is in contradiction with the observation from Stenger et al [6] and Knieke et al [26] for an inorganic product. An explanation could be that the elasticity and plasticity of the structure of the organic product is such that it does not undergo breakage under the conditions tested. The grinding experiments in this work resulted in a final particle size much larger than the crystallite size. This could be related to agglomeration, or the strength of the final particles in comparison to the grinding conditions. Since the crystallites are strong enough not to be broken, their size can therefore be taken as a minimum reachable particle size.

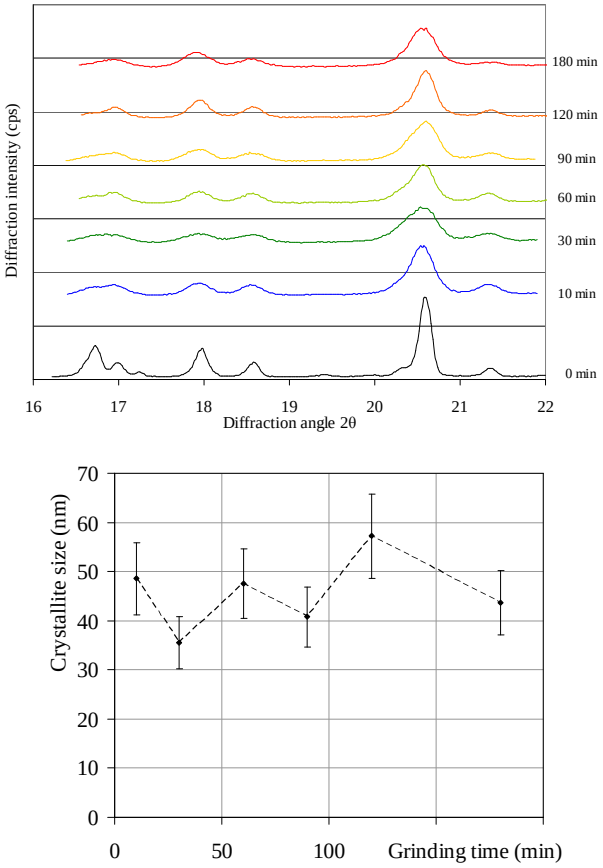

Figure 7 . X-Ray diffraction patterns (top) and crystallite size (bottom) at different grinding times.

The conclusion from this series of experiments is that ball milling is limited in the final particle size reachable by an equilibrium state between the grinding mechanism and a compaction/agglomeration mechanism. The absolute minimal particle size reachable can be considered as the crystallite size (crystallite size: 45nm). The model developed should include all those aspects and be simple enough to be linked to the process parameters.

3.4. Choice of the model

Both first (Equation 4) and second order (Equation 5) solutions of the population balance model (Equation 3) have been evaluated and a model was chosen on the basis of the above mentioned criteria.

Equation 4 and equation 5 were fitted to the experimental data and a sample of the result is plotted in figure 8 and figure 9. The figures only represent 10 of the 83 size classes being fitted. The fit was in all cases good for coarse sub-micron particles (above 2.0 µm). The fitting of intermediate sizes was slightly better when taking into account the delay phenomena described above with the second order solution, but for all size classes the value of the second order term H was equal to zero. In addition, in the grinding time at which the corresponding particles were being ground the secondary term $H_i.t^2$ remained small compared to $G_i.t$.

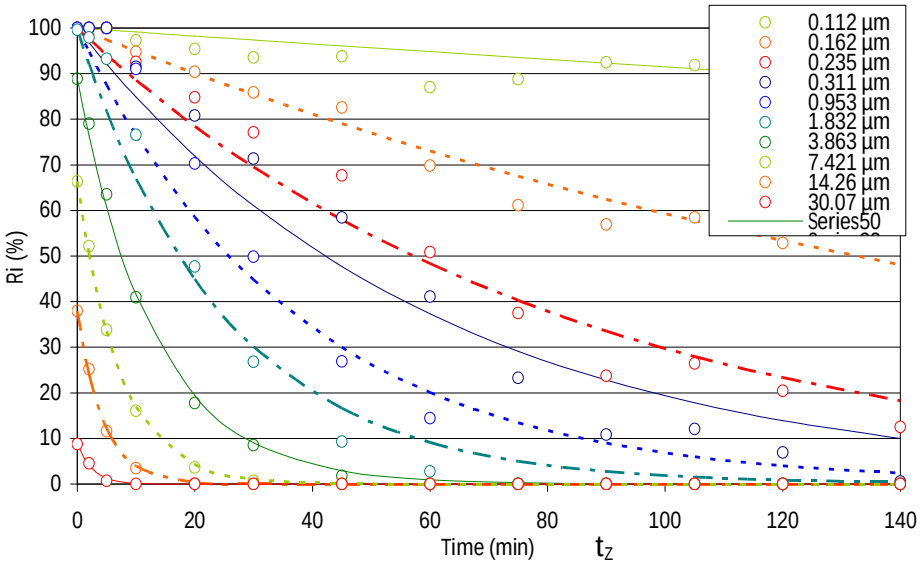

Figure 8 . Cumulative oversize fraction (R_i) as function of grinding time. The lines indicate the model predictions for the first order solution. The points indicate the actual measurement points. Each line corresponds to a specific size class.

Table 2 . Quality of the fitting (F function – equation 7) for the different approach

	First order solution	Second order solution
F	0.0014	0.0004

The quality of both fits is summarized in table 2. In comparison with literature values (F=0.0014, Bilgili et al [12]) the first model has sufficient accuracy to be used in the range of the studied process parameters, although the second order PBM gives a more accurate description. The first order solution was therefore used to correlate to the process parameters with a physical meaning.

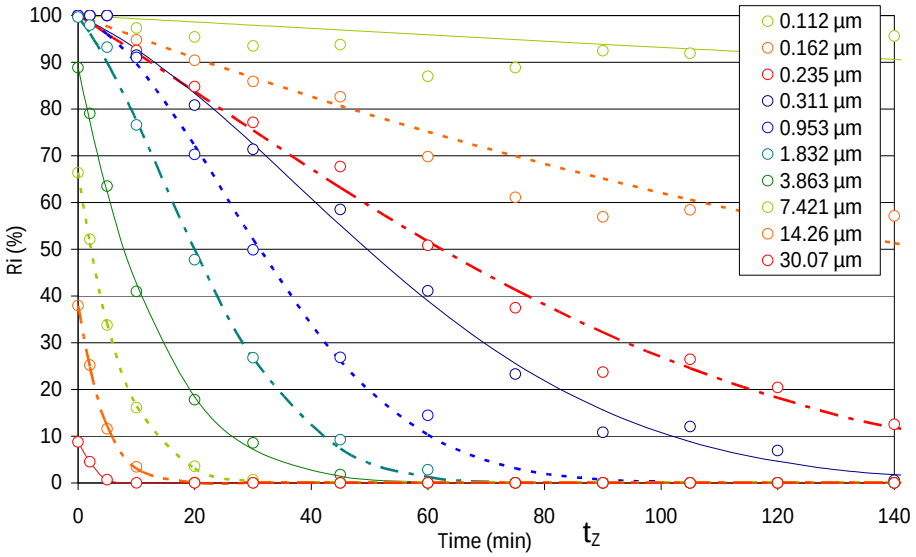

Figure 9 . Cumulative oversize fraction (R_i) as function of grinding time. The lines indicate the model predictions for the second order solution. The points indicate the actual measurement points. Each line corresponds to a specific size class.

3.5. Building up of the Model

The first order solution (equation 4) leads to the expression for the breakage and selection functions [10].

$$b_{ij} = \frac{S_{i-1} - S_i}{S_j} \quad \text{or in a cumulative way:} \quad B_{ij} = \frac{S_i}{S_j} \tag{15}$$

The parameter of this first order model, S_i, is the selection function. It represents the breakage probability for a particle in size class x_i. B_{ij} are the breaking factors. These represent the breakage probability for particles in size class x_i into fragments in size class x_j. The selection function is determined by fitting the exponential function of equation 4 to the experimental data. S_i can be represented as a function of the

particle size (figure 9). Comparison of S_i function for all experiments shows that the curve consists of two straight lines in all experiments. The intersection point ω of the lines corresponds to the final particle size after grinding. The value of ω is independent of the operating parameters when grinding without additives.

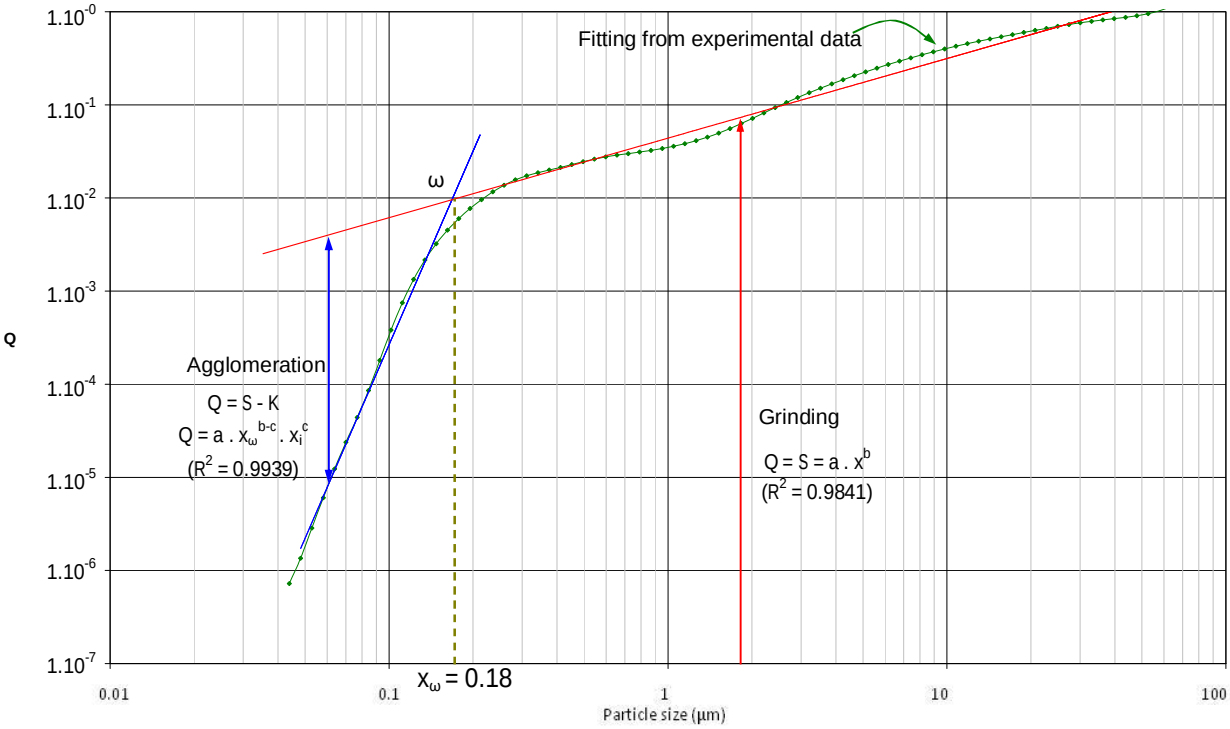

Figure 10 . Selection functions Q as a function of particle size. ω indicates the equilibrium point reached at the corresponding x_ω size.

The curve presents a drop for particles smaller than the equilibrium point, which is due to agglomeration. The probability for obtaining particles smaller than this size therefore decreases more rapidly.
The ground product is polycrystalline. Its crystallite size was determined by X-Ray diffraction (crystallite size: 45nm). Since the crystallite size did not change during grinding it can be taken as the minimal reachable particle size. The pure breaking mechanism would therefore lead to particles of the size of the crystallites. In order to make the model more representative of what is occurring in the grinding chamber, the pure breaking process is compensated by an agglomeration mechanism that leads to an equilibrium corresponding to the final particle size reachable.

The selection function can be expressed as a power law [27,28]. Assuming that grinding can be described with the same power function for all particle sizes, even for particles smaller than x_ω, the application domain can be divided in two parts. The

entire model is the function Q. Breakage is characterised by the selection function S and agglomeration by a selection function K. For particles bigger than x_ω there are only breakage events: $Q_i=S_i$ and the curve is a straight line (power function). For particles smaller than x_ω agglomeration compensates a part of breakage and $Q_i=S_i-K_i$. The values of the selection function for breakage of particles smaller than at the equilibrium point, $S(x_i<x_\omega)$, are obtained by extrapolation of the selection function for bigger particles.
In its matrix form the model becomes:

$$\frac{dV(x_i)}{dt_Z} = -SV(x_i) + bSV(x_i) + KV(x_i) - aKV(x_i) \tag{16}$$

$V(x_i)$ represent the volume fraction at time t of particles in class size x_i.
The factors corresponding to a fraction of $V(x_i)$ to be added or deleted during the time interval dt are:

- S, the part which disappears by breakage
- bS, the part which appears by breakage of particles from higher size classes
- K, the part which appears by agglomeration of smaller particles
- aK, the part which disappears by agglomeration to higher size classes

The function $Q_i=f(x_i)$ can therefore be described as the equations of two power functions:

$$\begin{cases} \text{If } x_i > x_\omega ; Q_i = S_i = a \cdot x_i^b \\ \text{If } x_i < x_\omega ; Q_i = S_i - K_i = a \cdot x_\omega^{b-c} \cdot x_i^c \end{cases} \tag{17}$$

The approach in equation 17 assumes that particles above 180 nm do not undergo aggregation, while particles below this size do. This assumption seems plausible because it is known that small particles have a higher aggregation rate than large particles in a shear field, as was shown by Wang [29,30]. There is no clear explanation, however, why this shift in aggregation rate is observed specifically at 180 nm for this product. Nevertheless, this value is used to discriminate between the two models of equation 17.

3.6 Study of the fitting parameters

Parameters a, b, c and ω help to understand the impact of the process parameters on the particle size reduction process. In this section equation 4 is used to describe the breakage mechanism. This equation has analogy with equations that are used in chemical reactions as is indicated in equation 18:

$$\frac{dR_i}{dt} = -S_i R_i \qquad\qquad \frac{dC_A}{dt} = -k_A C_A \tag{18}$$

In chemical reactions parameter k_A is the Arrhenius speed constant. Its expression is a power function similar to the expression the breakage selection function S:

$$S = a \cdot x_i^{\,b} \qquad k = A \cdot \exp\left(-\frac{E_a}{RT}\right) \tag{19}$$

Breaking factor “a” corresponds to A, which is a “frequency factor”. The unit of factor “a” should therefore be s^{-1} thus factor “a” is plotted versus the ratio between the rotation speed of the grinding machine in meters per seconds and the grinding media size in meter. Factor “a” is a function of the number of impacts per seconds. Figure 11a shows a linear correlation between factors “a” and the ratio of rotation speed and grinding media size. An increase in rotation speed and/or a decrease in grinding medium size (mass of grinding beads was kept constant) gives an increase in collisions in the grinding chamber and thus an increase in the frequency of breaking events (frequency factor “a”). The formula giving the value of parameter “a” as function of the ratio tip speed, v_{tip}, (unit: m/s) over the diameter of the grinding beads, d_{GM}, is:

$$a = 2.0 \cdot 10^{-6} \cdot \frac{v_{tip}}{d_{GM}} \tag{20}$$

Factor “b” corresponds to the activation energy. In case of grinding this corresponds to the energy required for breakage. Factor “b” is the same for each particle class in the case of grinding but varies according to the experimental conditions as function of the energy available for grinding. This energy is assimilated as the stress energy defined by Schönert [31] as the maximum kinetic energy of one grinding media (equation 8).

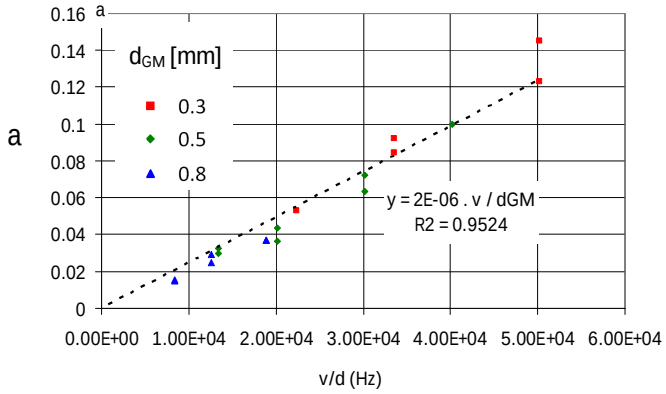

Figure 11 a. Model parameter as function of experimental conditions – Factor “a” as function of ratio v / d_{GM}.

The relation between “b” and log(SE) is not linear for all values of energy (figure 11b). For low energy (below 66.4 µJ) the relation between “b” and the logarithm of the stress energy has a linear trend. For higher energies “b” is constant at a value around 0.95. Factor “b” is the slope of the selection function as function of particle size. It can

therefore be seen as a breakage efficiency factor. The higher the stress energy the better the grinding should be. The correlation is exponential and is valid up to a given value of stress energy where the grinding efficiency cannot be much higher. Above that value the stress energy is sufficient to break any particle and increasing the energy will not enable better grinding. For mills with identical transfer of energy from the shaft to the product to be broken, the parameter b would only be a function of the ground product.

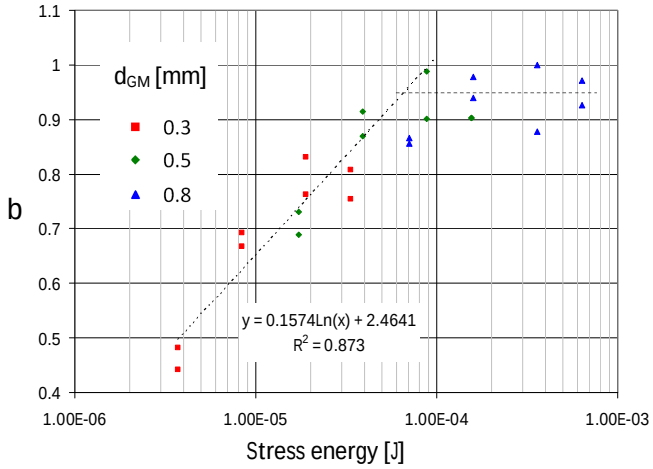

Figure 11 b. Model parameter as function of experimental conditions – Factor "b" as function of the stress energy.

The optimal conditions for factor "b" are therefore for a stress energy value of 66 µJ. Corresponding optimal conditions can be found along the iso-stress energy line (figure 12).

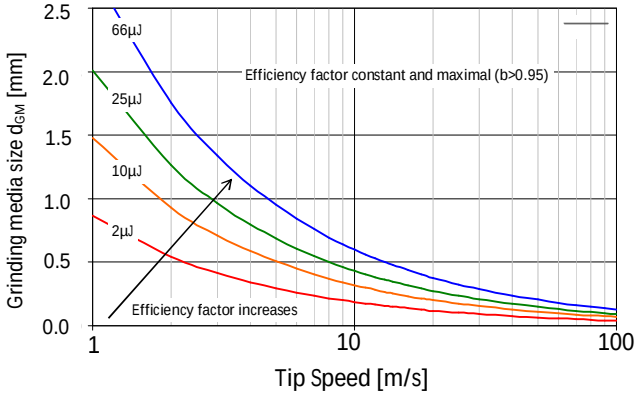

Figure 12 . Iso stress energy lines, obtained by plotting the grinding media size as function of the tip speed

Factor x_ω is constant in the present grinding conditions. As stated before this work assumes that particles above x_ω do not undergo aggregation, while particles below this size do. There is no clear explanation why this shift in aggregation rate is observed specifically at x_ω for this product. The observed behavior could also be related to:

1) decreasing particle inertia with decreasing particle size, which causes the grinding efficiency to decrease with particle size,

2) decreasing specific energy input with decreasing particle size.

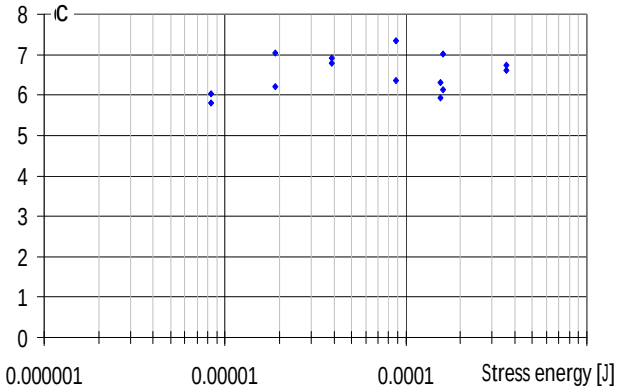

Figure 13 . Agglomeration efficiency factor "c".

Factor "c" can be seen as the efficiency factor of the agglomeration process by similarity with factor "b" in Equation 17. Factor "c" versus the stress energy (Figure 13) does not give a specific correlation. The variation of the factor is small and therefore considered as constant in the studied domain of energy.

3.7. Quality of the final model.

In order to check the quality of the model, one experiment is compared to the data obtained from the simulation.

Operating conditions are randomly chosen as rotation speed: 3000 rpm, grinding media size: 0.5mm. The ground product remains the same in terms of nature and particle size distribution, no additives were used.

The grinding time after start of the circuit operation (t_z) is defined as the time required to reach a given advancement in the grinding process. In general, $t(P\%<x_i)$ is the time of grinding required to reach P% (in mass) of particles below x_i. For example, the time required to reach 75% (P=0.75) of the particles have a particle size below 500nm is written as t(75%<500nm).

From equation (4) the time is calculated when $R_i(t) = 1-P$; thus:

$$t_z\left(P\% < x_i\right) = \frac{-1}{Q_i} \cdot \ln\left(\frac{1-P}{R_i^0}\right) \qquad (21)$$

Q_i is calculated from the model (equation 17) and the values of the parameters “a”, “b” and “c” from figure 10 and figure 12).For the simulation, factor “a” is calculated from equation 20, factor “b” is read from figure 10, factor “c” is taken as constant at 6.5 and the equilibrium point x_ω is also constant at 0.180 µm.

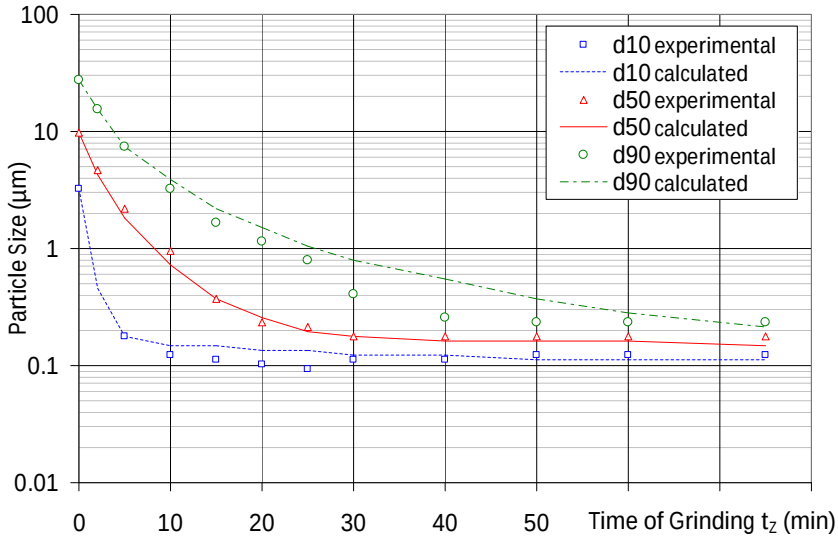

Figure 14 . Evolution of the d_{10}, d_{50} and d_{90} versus grinding time after start of the circuit operation (t_z). Lines indicate the values obtained through the model calculations. Points indicate the experimental data.

The selection functions were calculated according to equation 17 and the evolution of the particle size in time was compared to the one measured from the experiment (figure 14). The coefficient of variation between the experimental data and the forecast from the model is for d_{10} below 1.0%, for the d_{50} 3.7% and for the d_{90} 3.0%. The results are of very good quality and the model is therefore further used as for example in the following paragraph to determine the required grinding time.

3.8. Characterization of the mill.

As presented in section 2.4 the product breakage kinetics provide information on the efficiency of the grinding process and the grinding mechanism. In a first step the relation between the maximum grinding energy $E_{m,max}$ and the stress energy SE is plotted in figure 15.

The trend of the curve is as expected. At lower particle size a higher grinding energy is required at constant stress energy. The population balance model was used to calculate the grinding time. Data from the model calculations (lines in figure 15) fit the experimental data points.

The slope of the curve is approx. 1 in all cases. The product is thus a very brittle material as explained in paragraph 2.4). The stress number should thus be defined according to the equation for weak product particles. (Equation 13)

As developed in the theory, figure 16 shows that the stress number is not dependent on the value of the stress energy, which is in correspondence with the observed trends.

The characteristic plot for the milled product can thus be drawn as the median particle size (x_{50}) as function of the stress number (figure 17). The model calculations fit the experimental data. The concept proposed gives a good representation of the product being ground. The quality of the results is comparable to the data from Kwade [20]. The experimental data points range within a deviation from 20% of the average.

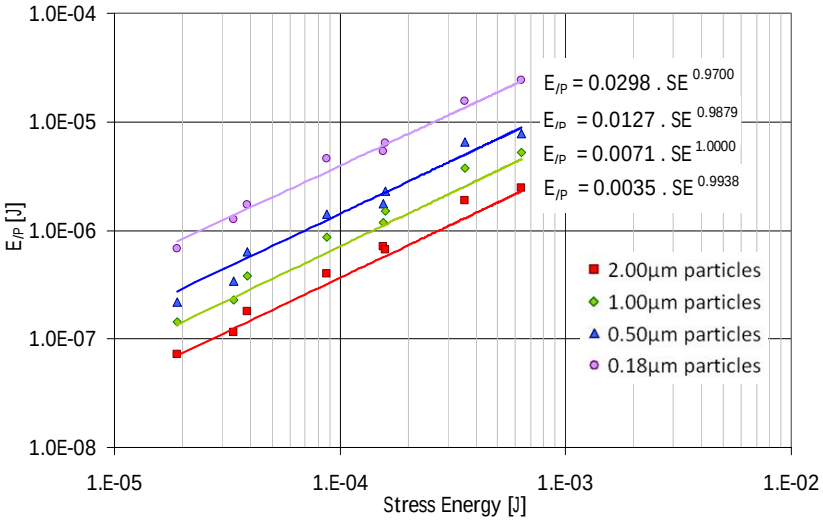

Figure 15 . Specific energy required as function of the stress energy (SE) for different median product size (2, 1, 0.5 and 0.18 µm product finesse) – points are experimental data and the lines indicate model calculations.

Should the product be milled in another mill, the corresponding characteristic line should remain unchanged. Up-scaling mills can be made using the characteristic graph from figure 17. The up-scaled process parameters can be calculated from the value of the SN for the desired particle size.

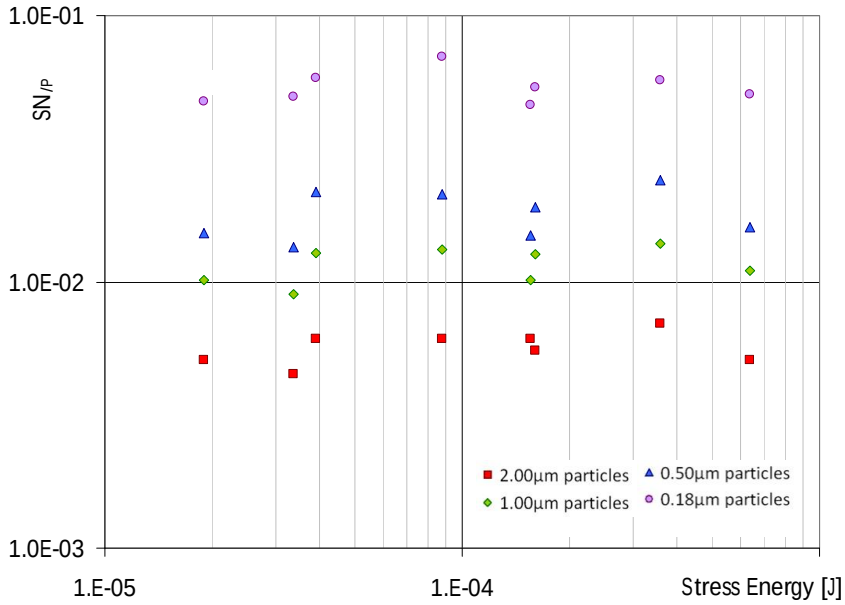

Figure 16 . Stress number as function of the stress energy for different product particle sizes (experimental data).

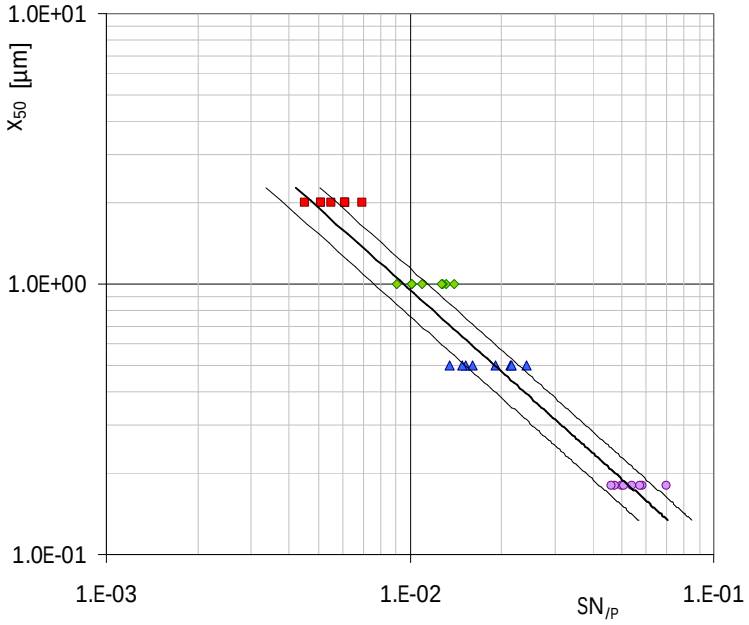

Figure 17 . Grinding profile of the product milled – Median Size (X_{50}) as function of the stress number (SN). Points are experimental data, line model calculations and dotted lines +/- 20% from the model calculations

The grinding profile presented in figure 17 is characteristic of the ground product. A more brittle product with the same initial particle size would present a characteristic line below the one in figure 17. Inversely, a product more difficult to grind would present a characteristic line above the one in figure 17. The more difficult a product is to break, the more stress events are required, and the higher is the value of the SN. To be able to compare the grinding profile of different product, the particle size would need to be normalized with the initial particle size (x_{50}/x_i) and the SN with the value of the SN at the initial particle size ($SN/SN(x_{50} = x_{50,i})$. An example is presented in figure 18. Since only one product was used in this study, this cannot be proven though.

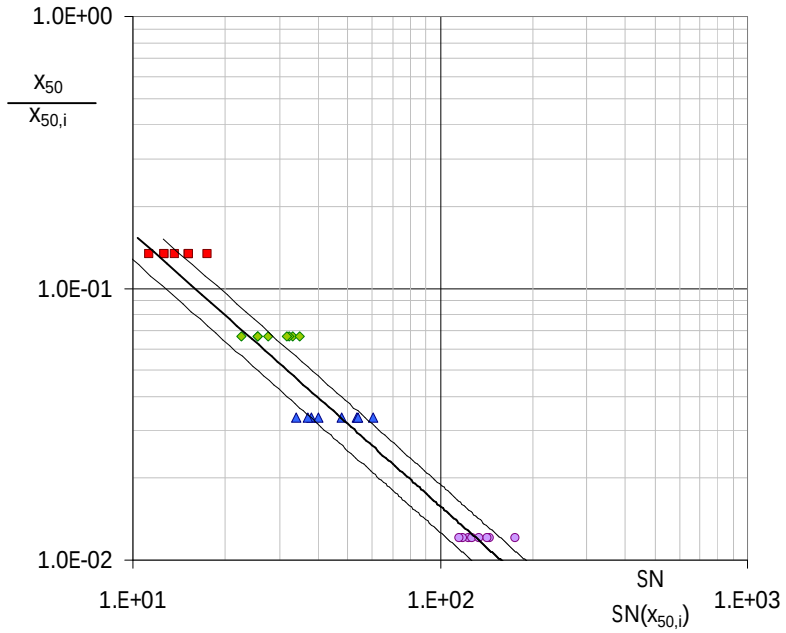

Figure 18 . Normalized grinding profile of the product milled

Various types of mills are commercially available. The three main types are presented in figure 19. Kwade [13] discussed the stress energy and stress number characterizing those mills. The design of a mill is optimized to enhance the power density in the mill. The design of the impeller and the grinding chamber is therefore strongly influence the motion of the grinding medium. The consequences are that both the stress energy (SE) and the surface area of the impeller in contact with the grinding media (factor γ_F) are strongly dependent on the mill design.
For a brittle material, as the one studied in this paper, the SN is determining the breakage. The surface area of the impeller in contact with the grinding medium (factor γ_F) is then the parameter dependent on the mill design influencing the value of the SN. Further research is needed to prove this.

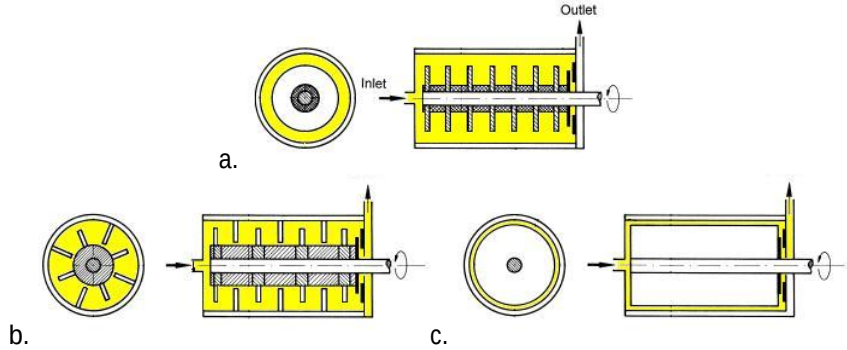

Figure 19 . Different types of mills and their stirrer (adopted from Kwade [4]):
a. Disc stirrer. b. pin-counter-pin stirrer. c. annular gap mill.

4. CONCLUSION AND OUTLOOK

The population balance model developed enables a better representation of a ball milling experiment by including the agglomeration process. The final population balance model describes specifically the studied grinding process and the product ground. In general such a population balance model can describe grinding processes using 4 fitting parameters. The breakage process is described by two parameters. The frequency factor ("a") is linear function of the ratio tip speed over grinding media size. Factor "a" is dependent on the mill characteristics. The second factor "b" is grinding efficiency factor, which is a linear function of the stress energy up to a point where the efficiency is at its maximum. Factor "b" is a function of the material properties. The modeling of such a grinding process by such a simple model enables a good forecast of the particle size versus the grinding time.

Using the approach from Kwade, Stadler and Schwedes the product could be defined as "very brittle". The product does not need high energy frontal impacts of grinding media to break. The shear induced by the translation movements of the beads is enough to break the particles.

A characteristic plot could be drawn. The median particle size of the broken particles (x_{50}) was plotted as function of the number of stress events (SN) in the mill. This number of stress events was calculated for one initial product particle. The stress number represents the number of stresses that an initial particle needs to undergo during the grinding process to reach the desired final particle size. SN is proportional to the total surface of the grinding beads. It is also proportional to a frequency of stress events. That frequency is defined as the angular rotation speed (ω) of the mill corrected by an efficiency factor (γ_F). The stress number is characteristic of the product ground. The same product ground in another mill – for example up-scaled – should present the same correlation between the product finesse (x_{50}) and the SN. This is not researched in this work but is part of future work.

The efficiency factor γ_F describes how good the impeller transfers its energy to the grinding medium. γ_F is expected to be the parameter dependent on the mill design and more especially the impeller shape. Factor γ_F is taken as proportional to the surface of the impellor in contact with the grinding medium.

Further research is needed to investigate materials with different properties, such as hardness, to explain how these properties can influence their breakage behavior.
Different mills in size and design should be tested with the same product suspension to determine how the efficiency factor of a mill is influenced and verify that factor γ_F is proportional to the surface of the impellor in contact with the grinding medium.
Additional experimental investigations using different surfactants would allow for studying the agglomeration parameters of the model and the agglomeration mechanism in more detail.

5. AKNOWLEDGMENT
The authors want to thank: Arno Kwade from the Technical University in Braunschweig, Germany for the helpful discussions; Pieter Vonk from DSM ACES, Geleen in the Netherlands for all interesting discussions regarding population balance modeling; Maria Christina Domingues, from the University of Coimbra, Portugal, and DSM Biotech Center in Delft, The Netherlands, assisting the authors for early stage grinding experiments; and Ida Kölmann, from the Technical University of Delft, assisting the authors with the X-Ray diffraction measurements.

6. NOMENCLATURE

A : Frequency factor (chemical reactions) [-]
a : Frequency factor [$\mu m^{-1}.min^{-1}$]
A_{1GM} : surface area of one grinding medium particle [m^2]
B : full-width at half maximum [-]
b : Grinding efficiency factor [-]
b_{ij} : Breakage function [-]
c : Agglomeration efficiency factor [-]
C_A : Concentration of a product A [$mol.L^{-1}$]
d_{GM} : Diameter of the grinding media [m]
d_{imp} : Diameter of the impellor [m]
E_A : Activation energy [$J.mol^{-1}$]
$E_{/P}$: Energy required to break a particle to a given size [J]
E_m : Energy per mass unit required for grinding [$J.kg^{-1}$]
k_A : Arrhenius speed constant [Hz]
K_i : Agglomeration selectivity function [-]
L_v : Crystalite size [m]
m_{GM} : mass of a single grinding bead [kg]
$m_{T,GM}$: Total mass grinding media [kg]
N_{GM} : Number of grinding beads [-]
n : number of size classes [-]
Q_i : Selectivity function [-]

R : Gaz constant, [$J.K^{-1}.mol^{-1}$]
$R_i(t)$: Cumulative weight fraction in size class i at time t [-]
SE : Stress energy [J]
S_i : Selectivity function [-]
SN : Stress number for a particle [m^4]
t : Grinding time [min] or [s]
t_Z : Grinding time after start of the circuit operation [min] or [s]
V_{GC} : Volume of the grinding chamber [m^3]
$V_i(t)$: Volume fraction of particle from size class i (at time t) [-]
$V_{T,GM}$: Volume of all grinding media
x_i : Lower size of particles of class i [µm]
x_ω : Minimal mean particle size when grinding ($x_{4,3}$) [µm]
v_{tip} : tip speed of the impellor [$m.s^{-1}$]
γ_F : Quality factor – Surface area of the impellor in contact with the grinding media [m^2]
λ : X-Ray wavelength [m]
ω_{imp} : angular rotation speed of the impellor [s^{-1}]
ρ_{GM} : density of the grinding media [$kg.m^{-3}$]
ω : Equilibrium point [-]

7. REFERENCES

[1] A. Kwade, L. Blecher, J. Schwedes, Motion and stress intensity of grinding beads in a stirred media mill. Part 2: Stress intensity and its effect on comminution, Powder Technology 86(1) (1996) 69–76.
[2] R. Stadler, R. Polke, J. Schwedes, F. Vock, Naßmahluing in Rührwerksmühlen. Chemie Ingenieur Technik 62(11) (1990) 907–915.
[3] F. Stenger, W. Peukert, The role of particle–particle interactions in submicron grinding in stirred ball mills, Mineral Processing 42 (2001) 477.
[4] M. Sommer, F. Stenger,W. Peukert, N.J.Wagner, Agglomeration and breakage of nanoparticles in stirred media mills — a comparison of different methods and models, Chem. Eng. Sci 61 (2006) 135–148.
[5] C. Varinot, H. Berthiaux, J. Dodds, Prediction of the product size distribution in associations of stirred bead mills, Powder Technology 105(1-3) (1999) 228–236.
[6] F. Stenger, S. Mende, J. Schwedes, W. Peukert, Nanomilling in stirred media mills, Chemical Engineering Science 60 (2005) 4557 – 4565.
[7] P. Scherrer, Gottinger Nachrichten 2 (1918) 98.
[8] K. Sedlatschek, L. Bass, Contribution to the theory of milling processes, Powder Metallurgy Bulletin 6 (1953) 148–153.
[9] P.C. Kapur, Kinetics of batch grinding, Trans of AIME 247 (1970) 309–313.
[10] H. Berthiaux, C. Varinot, J. Dodds, Approximate calculation of breakage parameters from batch grinding tests, Chemical Engineering Science 51(19) (1996) 4509–4516.
[11] C. Varinot, H. Berthiaux, J. Dodds, Prediction of the product size distribution in associations of stirred bead mills, Powder Technology 105(1-3) (1999) 228–236.

[12] E. Bilgili, R. Hamey, B. Scarlett, Nano-milling of pigment agglomerates using a wet stirred media mill: Elucidation of the kinetics and breakage mechanisms, Chemical Engineering Science 61 (2006) 149–157.
[13] A. Kwade, Determination of the most important grinding mechanism in stirred media mills by calculating stress intensity and stress number, Powder Technology 105(1-3) (1999) 382–388.
[14] A. Kwade, Mill selection and process optimization using a physical grinding model, Int. J. Miner. Process. 74S (2004) 93–101.
[15] L. Bunge, Dissertation, Technical University of Braunschweig (1993).
[16] L. Blecher, Dissertation, Technical University of Braunschweig (1992).
[17] C.T. Jayasundara, R.Y. Yang, A.B. Yu, D. Curry, Discrete particle simulation of particle flow in IsaMill—Effect of grinding medium properties, Chemical Engineering Journal 135 (2008) 103–112.
[18] F. Bunge, Dissertation, Technical University of Braunschweig (1991).
[19] A. Kwade, J. Schwedes, Breaking characteristics of different materials and their effect on stress intensity and stress number in stirred media mills Powder Technology 122 (2002) 109–121.
[20] A. Kwade, Dissertation, Technical University of Braunschweig (1996).
[21] S. Mende, F. Stenger, W. Peukert, J. Schwedes, Mechanical production and stabilization of submicron particles in stirred media mills, Powder Technology 132(1) (2003) 64–73.
[22] W.C. Griffin, Classification of Surface-Active Agents by 'HLB', Journal of the Society of Cosmetic Chemists 1 (1949) 311.
[23] W.C. Griffin, Calculation of HLB Values of Non-Ionic Surfactants, Journal of the Society of Cosmetic Chemists 5 (1954) 259.
[24] J.T. Davies, A quantitative kinetic theory of emulsion type, I. Physical chemistry of the emulsifying agent, Gas/Liquid and Liquid/Liquid Interface, Proceedings of the International Congress of Surface Activity (1957) 426–438.
[25] C. Bernhardt, E. Reinsch, K. Husemann, The influence of suspension properties on ultra-fine grinding in stirred ball mills, Powder Technology 105 (1999) 357–361.
[26] C. Knieke, M. Sommer, W. Peukert, Identifying the apparent and true grinding limit. Powder Technol. 195(1) (2009) 25-30.
[27] V.R. Koka, O. Trass, Analysis of the kinetics of coal breakage by wet grinding in the Szego mill, Powder Technolgy 43 (1985) 287–294.
[28] C. Gotsis, L.G. Austin, P.T. Luckie, K. Shoji, Modeling of a grinding circuit with a swing-hammer mill and a twin cone classifier, Powder Technolgy 42 (1985) 209–216.
[29] Q. Wang, Theoretical analysis of Brownian heterocoagulation of fine particles at secondary minimum, Journal of Colloid and Interface Science 145(2) (1991) 305–313.
[30] Q. Wang, A study on shear coagulation and heterocoagulation, Journal of Colloid and Interface Science 150(2) (1992) 418–427.
[31] K. Schönert, Aufbereitungstechnik 32(1991) 487.

Part I - Chapter 4

Comparison of Stirred Media Mills for Sub-Micron Grinding.

This chapter has been submitted as S.L.A. Hennart, P. van Hee, W.J. Wildeboer, G.M.H. Meesters, Chemical Engineering Science (2011)

Abstract – Hennart et al [1] determined the relation between process parameters and grinding kinetics by characterization of a product that was ground with a stirred media mill. In this work the same approach is used to compare the grinding kinetics in to different mills: the Dynomill KDL (Bachofen, Switzerland) and the Dispermat SL unit (VMA Getzmann, Germany).
The grinding time was calculated using a population balance model with two fit parameters, i.e. the frequency factor (a) and the grinding efficiency factor (b). The frequency factor is a linear function of the ratio of tip speed over grinding media size. It is dependent on the mill efficiency in both mills (γ_F). The mill efficiency was defined as the impellor area in contact with the grinding beads.
The grinding efficiency factor is a linear function of the stress energy up to a point where the efficiency is at its maximum. The experimental results show that the grinding efficiency factor is the same for both mills. It thus seems to be product dependent rather than mill dependent.
The stress number is a function of the number of grinding beads, grinding time and the frequency of the collision between grinding beads. The collision frequency was found to be a function of the rotation speed of the impellor and the surface area of the impellor in contact with the grinding beads. No significant differences could be observed between the grinding profiles for the two different mills after correction of the data for the mill efficiency in both mills.
In conclusion, this work shows that a direct comparison of the grinding kinetics in both mills is possible by correcting for the frequency factor on the basis of the impellor area in contact with the grinding beads.

1. INTRODUCTION

Several different types of ball-mills for extra fine milling are commercially available. Three main types are presented in figure 1. Comparison of mills is not an easy task. Shi et al. [1] for example studied differences between different mills. Their approach consisted of comparing the specific energy required to mill down a product to a given particle size. Their approach does not account for the amount of grinding medium that is required and the required grinding time.

Different approaches of mill characterization have been reported in literature. Several researches simulated the movement of the grinding medium and calculated the distribution of stress energies in the mill. Iwasaki et al [2] showed that these

computational simulations require expensive calculations. In addition, accurate estimation of the net energy that is applied to the product particles seems impossible.

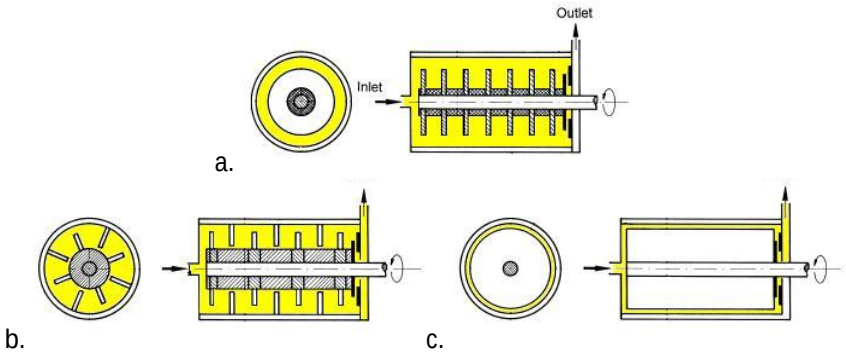

Figure 1 . Different types of mills and their stirrer (adopted from Kwade [3]):
a. Disc stirrer. b. pin-counter-pin stirrer. c. annular gap mill.

Kwade [4], Stadler and Schwedes [5] reported a full characterization on the limestone powder milling process. They used two parameters: stress energy and stress number. The stress energy (SE) represents the energy of a collision between grinding beads in the mill. The stress number (SN) is the number of collisions required to break an initial particle down to a given particle size. This approach takes into account all aspects of the milling process: milling time and the process parameters. A comparison of different mills with this approach was, however, not performed. Both stress energy (SE) and stress frequency are dependent on the mill design. The influence of mill design on both parameters is addressed in this work.

The present study follows the study by Hennart et al. [6] on the characterization of a ball milling process using population balance modeling. The final population balance model describes specifically the studied grinding process and the product ground. In general such a population balance model can describe grinding processes using 4 fitting parameters. The breakage process is described by two parameters. The frequency factor (“a”) is linear function of the ratio tip speed over grinding media size. It is dependent on the mill characteristics. The second factor “b” is the grinding efficiency factor, which is a linear function of the stress energy up to a point where the efficiency is at its maximum. It is a function of the material properties. Hennart et al. [6] showed that the model is able to describe the relation between particle size and grinding time. In the present study, the same approach is applied for two different mills: KDL Dynomill (Bachofen, Switzerland) and Dispermat LS (Getzmann, Germany)) with the same product and the same grinding medium. The main difference between the mills was the size of the grinding chamber and the shape of the impellor. The impact of the difference in mill design on both model parameters, i.e. frequency factor and grinding efficiency, was investigated.

2. MATERIAL AND METHODS

2.1. Grinding experiments on the Bachofen KDL Dynomill.

This work focuses on the grinding of a poorly water soluble compound. Grinding experiments were performed in absence of additives. Particle size distributions were measured using a laser diffraction size analyzer (LS230 equipment from Beckman Coulter).

Experiments were carried out using a Dynomill from Bachofen AG (Basel, Switzerland). The ball mill was operated in a recirculation mode. The poorly water soluble organic product was suspended in water (4.8 wt%, 500mL solution). Figure 2 shows the circulation of the product suspension through the grinding chamber (volume of the chamber: 300 mL) that was filled at 80% (bulk volume) with grinding beads (Zirconium oxide, Yttrium stabilized beads from Tosoh, Japan). The product suspension was drawn out through a 0.1 mm gap to prevent the grinding medium to exit the milling chamber. The system was cooled to keep a constant temperature throughout the entire system. The particle size distribution was analyzed throughout the grinding process by taking samples from the stirred vessel.

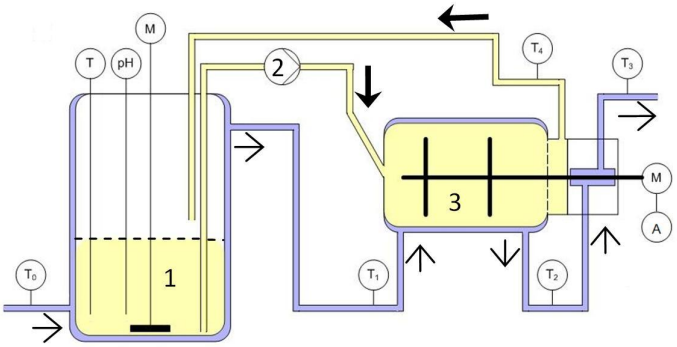

Figure 2 . Grinding set-up and controls, where T is a temperature measurement and pH is a pH control point. Arrows show the circulation of the cooling water (→) and product (➔). The product is pumped from the stirred tank marked as 1 by the pump 2 to the grinding chamber 3. M stands for motor and A for Amp meter.

2.2. Grinding experiments on the VMA Getzmann Dispermat SL mill.

There are few differences between the Dispermat SL unit and the KDL Dynomill unit. The grinding chamber of the Dispermat SL unit was smaller than that of the Dynomill KDL (125 mL and 300 mL, respectively). The impellor size and shape were also different. Figure 3 gives a schematical overview of the main differences between the two stirring systems.

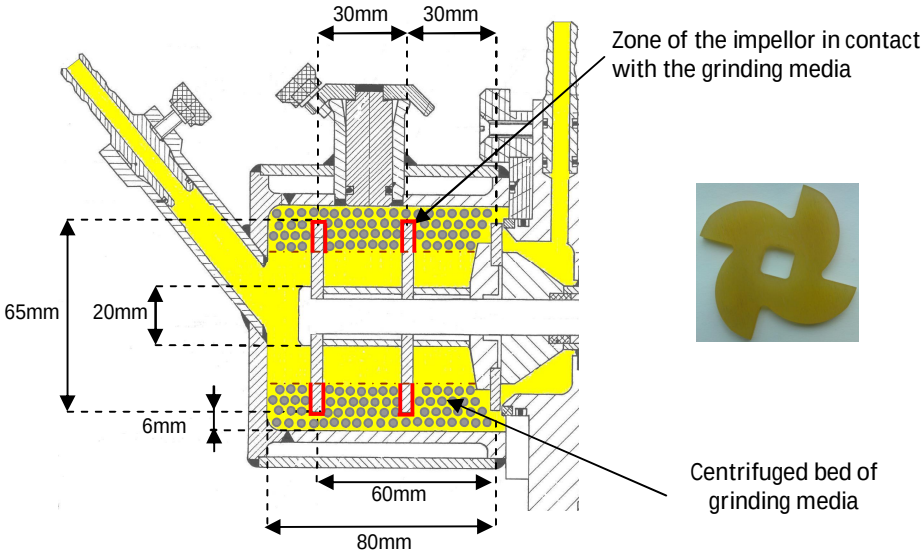

Dynomill KDL

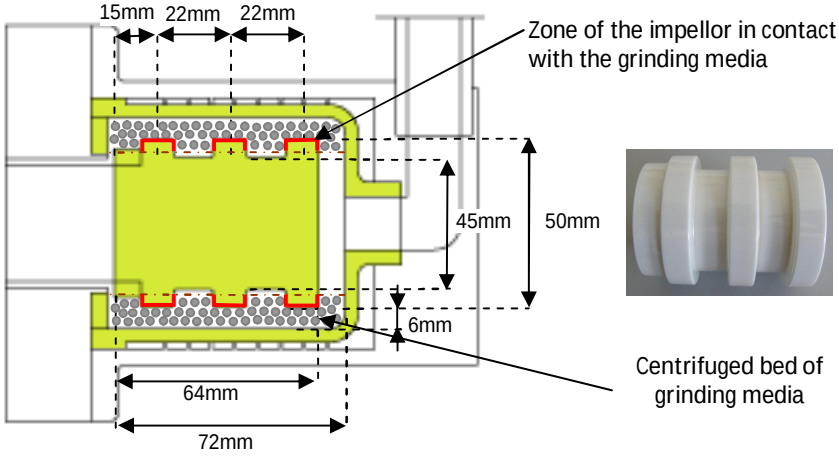

Dispermat SL

Figure 3 . Differences in impellor, size and shape between the two different mills tested.

Important differences are the thickness of the impellor tips: Dynomill KDL: 4 mm; Dispermat SL: 11 mm. The thickness of the centrifuged bed of grinding beads is indicated by the dash-dotted line. The thick lines represent the part of the impellor in contact with the grinding beads when the mill is in operation. All grinding beads are assumed to be centrifuged in a perfect bed.

The experiments in the Dispermat SL mill were carried out with the same product, at the same grinding medium filling ratio (80% of the grinding chamber is filled with grinding beads), with the same batch of grinding medium. The Dispermat mill was also operated in recirculation mode. The product particles were pumped from the vessel through the grinding chamber and back to the tank. The ratio between the tank volume and grinding chamber free volume was 2:1.
The product was circulated from the vessel through the mill and back to the vessel, which makes the actual grinding time shorter than the experimental time. The actual grinding time (t) was therefore approximated from the experimental time (t_Z), the vessel volume and the free grinding chamber volume using equation 1. For both mills the vessel volume and the free grinding chamber volume were maintained constant.

$$t = t_Z \cdot \frac{V_{GC} - V_{T,GM} - V_{imp}}{V_{suspension}} \quad (1)$$

With V_{GC} the volume of the grinding chamber, $V_{T,GM}$ the volume occupied by the grinding media, V_{imp} the volume occupied by the impellor shaft and blades, and $V_{suspension}$ the total volume of product particle suspension.

2.3. Mill characterization

The grinding kinetics can be determined from the relation between the median particle size and the stress number (SN) as was shown by Hennart et al [6], using the approach from Stadler et al [5] that was further developed by Kwade et al [4]. The number of stress events (SN, equation (9)) on the product particles was determined from the number of media contact (N_C), the number of product particles in the grinding chamber (N_P) and the probability that a product particle is sufficiently stressed and caught at a media contact (P_S).

$$SN = \frac{N_C \cdot P_S}{N_P} \quad (2)$$

The number of grinding medium contacts (N_C) is proportional to the number of grinding media, grinding time and the impact frequency [7]. The impact frequency is proportional to the rotation speed of the mill and to an efficiency factor γ_F. γ_F is a function of the transfer of energy from the impellor to the grinding beads. This energy transfer is a function of the impellor shape [8, 9, 10]. In this work we propose that γ_F is correlated to the total impellor surface area in contact with the grinding medium (see figure 3), which is a measure for efficiency of energy transfer from the stirrer to the grinding beads. γ_F is therefore regarded as an efficiency factor that is mill dependent.

$$N_C \propto \frac{m_{total,GM}}{\frac{\pi}{6} \cdot d_{GM}{}^3 \cdot \rho_{GM}} \cdot (\gamma_F \cdot \omega) \cdot t \qquad (3)$$

With $m_{total,GM}$ being the total mass of grinding beads in the chamber, ω the angular rotation speed of the stirrer, t the grinding time, d_{GM} the diameter of the grinding beads, ρ_{GM} the density of the grinding beads and γ_F the surface area of the impellor in contact with the grinding medium.

The probability P_S is dependent on the breakage mechanism. In the previous study [6] the same product was found to break at low impact energy. Breakage thus occurred under the influence of shear stresses acting between the medium bead surfaces. The breakage probability under these conditions is defined by Stadler et al [5] and Bunge [8] to be proportional to the surface area of one grinding medium bead. The stress number is therefore given by the following expression:

$$SN \propto \frac{6 \cdot m_{total,GM}}{d_{GM} \cdot \rho_{GM}} \cdot \frac{(\gamma_F \cdot \omega) \cdot t}{N_P} \qquad (4)$$

2.3. Calculation of the grinding time.

The grinding time t was calculated from the population balance model (PBM) that was described by Hennart et al [6]. The population balance model describes changes in the quantity of particles (V_i) in each particle size class i. The following equations describe the size-discrete, volume (or mass) fraction frequency of the population balance model (PBM) for batch grinding [11]:

$$\frac{dV_i}{dt_Z} = -S_i V_i + \sum_{j=1}^{i-1} b_{ij} S_j \cdot V_j \qquad \text{with} \qquad \sum_{i=j+1}^{n} b_{ij} = 1 \text{ and } n \geq i \geq j \geq 1 \qquad (5)$$

where i and j are the size-class indices running up to n; t_Z and V_i representing respectively time after start of the circuit operation and volume fraction in size class i. The differential equation 6 can be solved analytically after it has been written as an oversize cumulative size distribution form [12]. The cumulative volume fraction R_i represents the volume fraction of particles larger than the lower limit of the particle in size class (x_i):

$$\frac{dR_i}{dt_Z} = -S_i R_i + \sum_{j=1}^{i-1} (S_{j+1} B_{ij+1} - S_j B_{ij}) \cdot R_j \quad \text{with} \quad R_i(t) = \sum_{j=1}^{i} V_j \text{ and } B_{ij} = \sum_{k=i+1}^{n} b_{kj} \qquad (6)$$

Many studies [13,14] consider the first order solution (H_i=0 in Kapur [12]) sufficient to describe the particle size evolution for short grinding times (Equation 8). Hennart et

al[6] showed that the first order model has a sufficient accuracy for the conditions used in this study.
The first order solution to the population balance model (equation 8) was thus fitted to the experimental data.

$$R_i(t) = R_i^{\,0} \cdot \exp(-S_i \cdot t_Z) \tag{7}$$

The obtained selection function S_i is defined by four parameters (a, b, c and x_ω) as illustrated in figure 4.

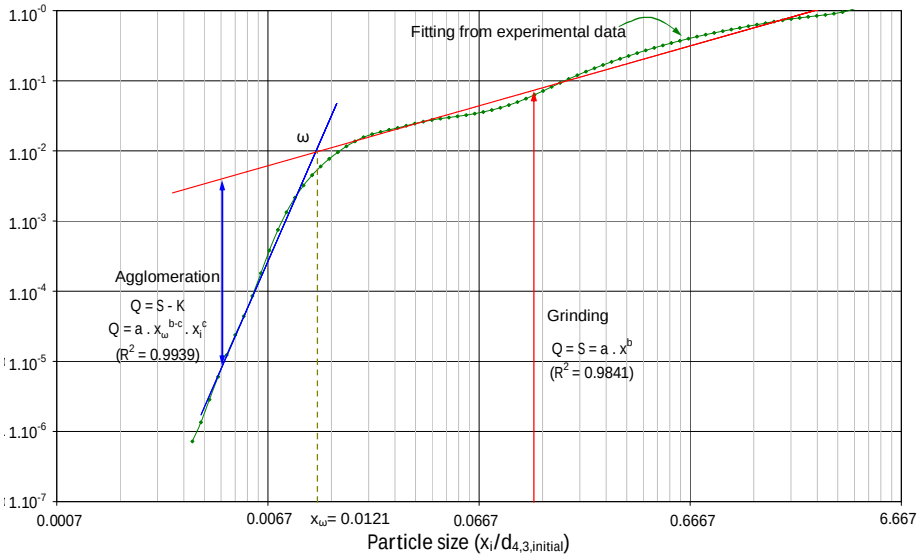

Figure 4 . Selection functions Q as a function of particle size ($x_i/d_{4,3,initial}$).

The function $Q_i=f(x_i)$ can therefore be described as the equations of two power functions:

$$\begin{cases} \text{If } x_i > x_\omega ; Q_i = S_i = a \cdot x_i^{b} \\ \text{If } x_i < x_\omega ; Q_i = S_i - K_i = a . x_\omega^{b-c} \cdot x_i^{c} \end{cases} \tag{8}$$

Factor “a” is the “frequency factor”. An increase in rotation speed and/or a decrease in grinding medium size (the mass of grinding beads was kept constant) gives an increase in collisions in the grinding chamber and thus an increase in the frequency of breaking events (frequency factor “a”). An increase as well in the surface area of the impellor in contact with the grinding media is expected to give an increase in the speed of the grinding beads and thus an increase in the frequency of breaking events. The formula giving the value of parameter “a” is a proportional to the ratio tip speed,

v_{tip}, (unit: m/s) over the diameter of the grinding media, d_{GM} and the factor γ_F. Factor "a" is expected to be mainly process related.

Factor "b" corresponds to an "activation energy". It is the grinding efficiency factor: the lower the stress energy, the lower the breakage probability. The maximum probability is reached above a stress energy limit. The stress energy was assumed to be the maximum kinetic energy of one grinding medium bead [14] (equation 8). Factor "b" is expected to be mainly product properties related (such as breakability, hardness, plasticity, elasticity, etc).

$$SE \propto \frac{\pi}{6} \cdot \rho_{GM} \cdot {d_{GM}}^3 \cdot {v_{tip}}^2 \qquad (9)$$

Where $\rho_{GM}$is the density of the grinding medium, d_{GM} the diameter of the grinding beads and v_{tip} the tip speed of the rotating impellor.

Factor "c" can be seen as the efficiency factor of the agglomeration process. Factor x_ω is the equilibrium point. In other words, x_ω is the mean particle size where the grinding and agglomeration processes are in equilibrium. "c" and x_ω were assumed to be independent of the process conditions that were applied in this work.

The model parameters were obtained for different experimental conditions.

$t_z(P\%<x_i)$ is the time of grinding required to reach a certain percentage (P%, in mass) of particles below x_i (equation 9). For example, the time required to reach 75% (P=0.75) of the particles have a particle size below 500 nm is written as t(75% < 500 nm). The time required to reach $R_i(t) = P$ is given by equation 4. Q_i was calculated from the model (equation 7); thus:

$$t_z\left(P\% < x_i\right) = \frac{-1}{Q_i} \cdot \ln\left(\frac{1-P}{R_i^0}\right) \qquad (10)$$

3. RESULTS AND DISCUSSION.

Experiments were carried out in both mills using the same range of stress intensities (SE ranging from 1.0×10^{-5} J to 1.0×10^{-3} J).

The product milled in the present research is identical to the one used in Hennart et al [6]. The product could be defined as "very brittle". The grinding profile of this product is the plot of its median particle size of the broken particles (x_{50}) as function of the number of stress events (SN) in the mill.

3.1. Model parameters

The model parameters were fitted from the experimental data (Figure 5). Parameter $x_{\omega,}$ the minimal final particle size, was constant throughout all experiments in both mills (0.180 µm). The same holds for factor "c" (c = 6.5).

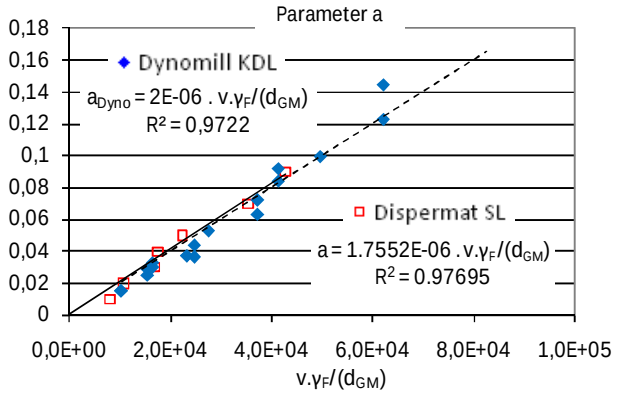

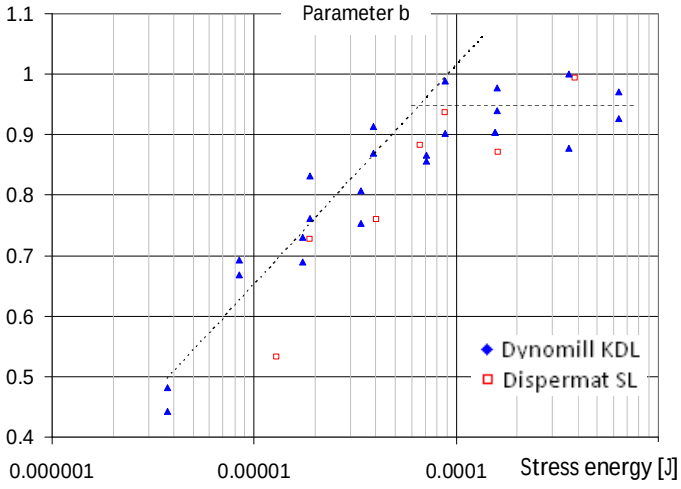

Figure 5 . Model parameters calculated for both Dynomill KDL and Dispermat SL.

Figure 5 shows the relation between the factor “a” and the ratio tip speed over grinding medium bead size. The data of both mills were corrected for γ_F. The graph shows both mills give a similar correlation and the data of both mills clearly show an overlap. This indicates that as expected in section 2.3, the factor “a” is a function of factor γ_F. An increase as well in the surface area of the impellor in contact with the grinding media gives an increase in the speed of the grinding beads and thus an increase in the frequency of breaking events. Values of factor γ_F for both mills are given in table 1.
Figure 5 shows that factor “b” is the same for both mills, which indicates that parameter b is only a function of the material properties.

Table 1 . Factor γ_F – Surface area of the impellor in contact with the grinding beads (m^2).

Mill	Factor γ_F (dm^2)
Dispermat LS	0.85
Dynomill KDL	1.23

3.2. Mill comparison using the efficiency factor

Figure 6 shows the relation between particle size after a certain grinding time and the stress number for both mills. The data of both mills were corrected for γ_F (Table 1). The graph shows that both mills give a similar correlation and the data for both mills clearly show an overlap. This indicates that the grinding mechanism is identical in both mills. In addition, the correction of the data for the mill efficiency gamma allows for a more general approach for comparison of the grinding kinetics in different mills. Following equation 4, for a given grinding medium bead size, rotation speed and quantity of product particles in the mill, the time of grinding can be shorten by increasing the surface area of the impellor in contact with the grinding beads, factor γ_F. The results that are presented in the graph are similar to that of Kwade [17].

It is expected that the correction factor can be applied for other stirred media mills. Further studies are, however, required to extend this approach for a broader range of mill designs and mill sizes.

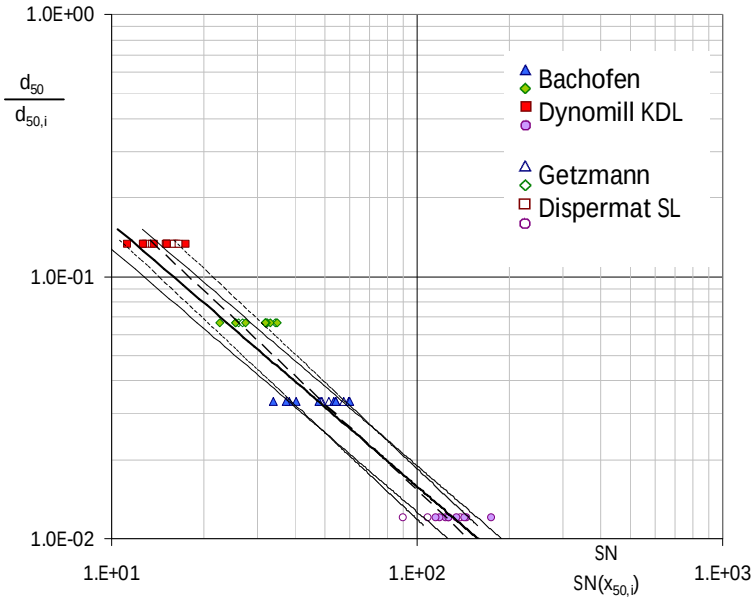

Figure 6 . Normalized grinding kinetics for an organic crystalline product: Median particle size versus SN per particle. Lines are model results from the Bachofen mill. Dashed lines are model results from the Getzmann Mill. In each case the thin line frame at +/- 20% the thick line corresponding to the model calculations.

Both mills were operated in recirculation mode using the same range of rotation speeds with the same grinding medium. Only the size of the grinding chambers and the impellor design were different for both mills. The graph in figure 6 indicates that the obtained grinding profile can be used to predict the grinding behavior in similar types of mills. Further studies are, however, required to extend this approach for a broader range of mill designs and mill sizes.

The grinding profile presented in figure 6 is characteristic of the ground product. A more brittle product with the same initial particle size would present a characteristic line below the one in figure 6. Inversely, a product more difficult to grind would present a characteristic line above the one in figure 6. The more difficult a product is to break, the more stress events are required, and the higher is the value of the SN.

4. CONCLUSION & OUTLOOK

The objective of this paper was to verify that the grinding profile defined by Hennart et al [1] is independent of the mill used. Two different mills were tested: the Dynomill KDL (Bachofen, Switzerland) and the Dispermat SL mill (VMA Getzmann, Germany). The experimental data were fitted by means of a population balance model from Hennart et al [1]. The breakage process was described in the population balance model by two parameters the frequency factor ("a") and the ginding efficiency (b). Factor "a" is a linear function of the ratio tip speed over grinding medium bead size and is dependent on the mill efficiency in both mills. The mill efficiency was defined as the impellor area in contact with the grinding beads.
The second factor "b" is the grinding efficiency factor, which is a linear function of the stress energy up to a point where the efficiency is at its maximum. Factor "b" was the same for both mills, which indicates that parameter b is only a function of the material properties.
The stress number is a function of the number of grinding beads, grinding time and the frequency of the collision between grinding beads. The collision frequency was found to be a function of the rotation speed of the impellor and the surface area of the impellor in contact with the grinding beads. No significant differences could be observed between the grinding profiles for the two different mills after correction of the data for the mill efficiency in both mills. It is therefore expected that the correction factor can be applied for other stirred media mills. Further studies are, however, required to extend this approach for a broader range of mill designs and mill sizes. In addition, the influence of product hardness and other product properties on the approach that was taken in this work should be investigated.

5. AKNOWLEDGMENT

The authors want to thank the company VMA Getzmann for welcoming the authors in their laboratories to carry out tests on the Dispermat SL unit.

6. NOMENCLATURE

a : Frequency factor [$\mu m^{-1}.min^{-1}$]
b : Grinding efficiency factor [-]
b_{ij} : Breakage function [-]
c : Agglomeration efficiency factor [-]
d_{GM} : Diameter of the grinding media [m]
K_i : Agglomeration selectivity function [-]
$m_{T,GM}$: Total mass grinding media [kg]
Q_i : Selectivity function [-]
$R_i(t)$: Cumulative weight fraction in size class i at time t [-]
S_i : Selectivity function [-]
SN : Stress number for a particle [m^4]
t : Grinding time [min] or [s]
t_Z : Grinding time after start of the circuit operation [min] or [s]
V_{GC} : Volume of the grinding chamber [m^3]
$V_i(t)$: Volume fraction of particle from size class i (at time t) [-]
$V_{T,GM}$: Volume of all grinding media
x_i : Lower size of particles of class i [µm]
x_ω : Minimal mean particle size when grinding ($x_{4,3}$) [µm]
γ_F : Surface are of the impellor in contact with the grinding media [m^2]
ω : angular rotation speed of the impellor [s^{-1}]
ρ_{GM} : density of the grinding media [$kg.m^{-3}$]

7. REFERENCES

[1] F. Shi, R. Morrison, A. Cervellin, F. Burns, F. Musa, Comparison of energy efficiency between ball mills and stirred mills in coarse grinding, Minerals Engineering 22(7-8) (2009) 673–680.
[2] T. Iwasaki, J.H. Kim, M. Satoh, Characterization of media mills based on mechanical energy applied to particles, Chemical Engineering Science 61(4) (2006) 1065-1073.
[3] A. Kwade. Wet Comminution in stirred media mills- research and its practical application. Powder Technology 105 (1999) 14–20.
[4] A. Kwade, L. Blecher, J. Schwedes, Motion and stress intensity of grinding beads in a stirred media mill. Part 2: Stress intensity and its effect on comminution, Powder Technology 86 (1996) 69–76.
[5] R. Stadler, R. Polke, J. Schwedes, F. Vock, Naßmahluing in Rührwerksmühlen. Chem Ing Tech 62(11) (1990) 907–915.
[6] S.L.A. Hennart, P. van Hee, V. Drouet, M.C. Domnigues, W.J. Wildeboer, G.M.H. Meesters, Characterization and Modeling of a Sub-Micron Milling Process Limited by an Agglomeration Phenomena, Submitted to Chemical Engineering Science (2009).
[7] A. Kwade, Determination of the most important grinding mechanism in stirred media mills by calculating stress intensity and stress number, Powder Technology 105 (1999) 382–388.
[8] L. Bunge, Dissertation, TU Braunschweig (1993).
[9] L. Blecher, Dissertation, TU Braunschweig (1992).

[10] C.T. Jayasundara, R.Y. Yang, A.B. Yu, D. Curry, Discrete particle simulation of particle flow in IsaMill—Effect of grinding medium properties, Chem. Eng. J. 135 (2008) 103–112.
[11] T. Iwasaki, J. H. Kim, M. Satoh, Characterization of media mills based on mechanical energy applied to particles, Chemical Engineering Science 61 (2006) 1065–1073.
[12] P.C. Kapur, Kinetics of batch grinding, Trans of AIME 247 (1970) 309–313.
[13] H. Berthiaux, C. Varinot, J. Dodds, Approximate calculation of breakage parameters from batch grinding tests, Chemical Engineering Science 51(19) (1996) 4509-4516.
[14] C. Varinot, H. Berthiaux, J. Dodds, Prediction of the product size distribution in associations of stirred bead mills, Powder Technology 105(1-3) (1999) 228-236.
[15] K. Schönert, Aufbereit.-Tech. 32 (1991) 487.
[16] P.W. Cleary, M. Sinnott, R. Morrison, Analysis of stirred mill performance using DEM simulation: Part 2 – Coherent flow structures, liner stress and wear, mixing and transport, Minerals Engineering 19 (2006) 1551–1572.
[17] A. Kwade, Dissertation, TU Braunschweig (1996).

Part II

Characterization of the Ground Particles

Chapter 1

Particle Size Characterization of Extra Fine milled Product.

This chapter has been submitted as S.L.A. Hennart, P. van Hee, W.J. Wildeboer, G.M.H. Meesters, Part. Part. Char. (September 2010 – awaiting first review)

Abstract – The present research aims to characterize the particle size distribution of sub micron particles suspended in a liquid. The particles milled are an organic poorly water soluble crystalline product. To characterize the size of these particles, different techniques have been tested: Imaging techniques (SEM, CryoTEM), static light scattering techniques, dynamic light scattering techniques, centrifugation and flow field flow fractionation.
The results indicate that the studied milled particles have a primary particle size close to 180nm and there is strong evidence of larger particles which are very likely aggregates. This is clearly seen from the Cryo TEM results.
All the above mentioned techniques should in principle be able to measure samples of dispersion containing particles of ca 180nm but several are disturbed by the presence of large aggregates. It is difficult to estimate the amount of aggregate present, but most of the time; one is interested in what the primary particle size distribution is.
It is clear that no single piece of equipment is capable of exactly determining the particle size distribution of our samples, but the static light scattering with low shear on mixing does give a good representation of what is seen with the image analysis by cryo TEM.

1. INTRODUCTION

The present research aims to characterize the particle size distribution of sub micron particles dispersed in a liquid.
The product particles are produced by extreme fine milling. The initial powder has a particle size in the micrometer range. It is suspended in water before being milled in a stirred media mill. After milling, the particle size is expected to be in the sub micron range. Previous study feature all details about the milling process [1,2].

In this work frame, it is important to determine the final particle size distribution of the milled particles. This enables the evaluation of the efficiency of the grinding process.
It is also important to evaluate the stability versus aggregation of the milled particles. It has been shown in previous studies that milled particles can quickly aggregate (Hennart et al. [2], Peukert et al [3].). The presence of aggregated milled particles can be seen as large particles in the particle size distribution.

In this work several techniques commercially available have been tested. All the tested techniques are capable to analyze sub micron particles dispersed in a liquid.

For each technique, particles milled and stored in the same conditions have been used. The size distribution has been measured with each sizing technique.

2. MATERIELS AND EQUIPMENT.

2.1. Production of the sub-micron particles by stirred media milling.

This work focuses on the grinding of a poorly water soluble poly crystalline compound. The material has a starting mean product particle size ($d_{4,3}$) of 15µm (measured with LS13320 equipment from BeckmanCoulter). Grinding has been performed using a ball mill (Dynomill, Bachofen AG, Switzerland) in the absence of additives. The ball mill was operated in a recirculation mode. The poorly water soluble organic product was suspended in water (pH stabilizes at 5.7). Figure 1 shows the circulation of the product suspension through the grinding chamber (volume of the chamber: 300 mL) that was filled at 80% (bulk volume) with grinding beads (Zirconium oxide, Yttrium stabilized beads from Tosoh, Japan). The product suspension was drawn out through a 0.1 mm gap to prevent the grinding medium to exit the milling chamber. The system was cooled to keep a constant temperature throughout the entire system.

Several commercially available techniques have been tested to measure the particle size distribution of the milled particles. The different techniques available on the market can be drawn together in several groups [4,5]:

Image analysis techniques

Static light scattering based techniques using:

- Polarization Intensity Differential Scattering (PIDS)
- High resolution CCD detectors
- Blue wave technology
- Backscattering detection

Techniques based on the Brownian motion of the particles. Those techniques uses:

- Photon correlation spectroscopy (PCS)
- Photon Cross Correlation Spectroscopy (PCCS)
- The Heterodyne principle
- Particle Tracking

Centrifugation

Flow field flow fractionation techniques

Other techniques available commercially which are not tested in this work are:

- Particle separation by size exclusion chromatography
- Acoustics and electro-acoustics

A detailed description of each technique is presented in the next section.

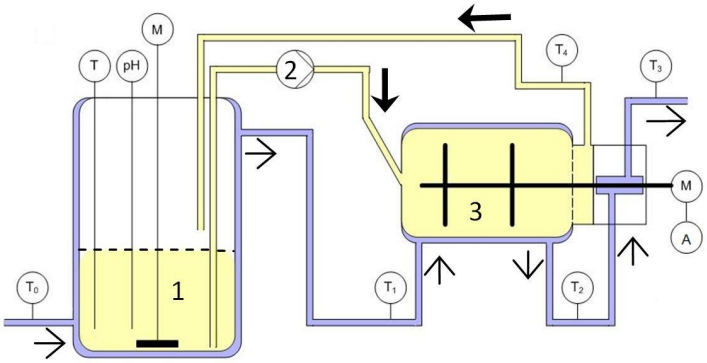

Figure 1 . Grinding set-up and controls, where T is a temperature measurement and pH is a pH control point. Arrows show the circulation of the cooling water (→) and product (➔). The product is pumped from the stirred tank marked as 1 by the pump 2 to the grinding chamber 3. M stands for motor and A for Amp meter.

The product properties required for the particle size measurements are summarized in Table 1. The Mie theory used in light based techniques requires the refractive index and an absorption coefficient of the particles. Determination of these parameters can be difficult, especially the absorption coefficient (also called "imaginary refractive index"). Some researchers determine the absorption coefficient using laser diffraction measurements, but care must be taken with these procedures [6-8].

Table 1 . Product properties of the ground material used as measurement parameters.

Property	Value	Reference and comments
Density	1300 kg.m^{-3}	measured by sucrose gradient centrifugation [9].
Refractive index	1.54-1.698	[10]
Absorption	0	determined using laser diffraction measurements
Solubility in water	30-100ppm	[11-13]

2.2. Detailed description of the techniques used.

2.2.1. Image analysis – SEM, Cryo-TEM

Image analysis techniques consist in making pictures of the particles. Their size is then determined manually or by using software. An overview of image analysis techniques is given by Etzler [14,15], Merkus [16], and Russ [17]. For the analysis of sub-micron particles, optical techniques are not appropriate; the particles being too small, out of the detection range of optical microscopes. Suitable techniques are for example scanning electron microscopy (SEM), transmission electron microscopy (TEM) and atomic force microscopy (AFM). In the present research, SEM and a variant of TEM, Cryo-TEM, have been tested. Cryo TEM stands for cryogenic TEM. The technique

consists of using a classical TEM system to look through cryogenically frozen particle suspensions.

Scanning Electron Microscopy (SEM) and Cryo-TEM (Transmission Electron Microscopy) are well known techniques used to have a visual representation of particles.
The accuracy of the particle size distribution obtained resides in the number of particles analyzed and the representation of the sample prepared. The number of particle to be analyzed is depending on the broadness of the distribution. The more particles analyzed the better the analysis. Computer assisted image analysis could help in measuring a significant amount of particle sizes but has not been used in the present scope.

Principle of the measurement – SEM
SEM images the sample surface by scanning it with a high-energy beam of electrons. The electrons interact with the atoms that make up the sample producing secondary electron. The secondary electrons are detected and transformed into an electrical signal. The intensity of the signal is dependent on the number of secondary electrons emitted. That number of electrons depends on the angle of incidence of the laser beam. By scanning the surface of the sample, a 2D image is made. The very narrow electron beam gives the SEM micrographs a large depth of field. This yields a 3D appearance of the images and is useful for understanding the surface structure of a sample.
The resolution of the SEM used is of few nanometers enabling the size analysis of particles from several nanometers up to a couple of millimeters. The whole range of sizes can not be seen on a single picture. One would need to make images at different magnification to study broad particle size ranges [16].

The size of the particles has been determined by measuring manually and randomly 100 lengths of particles on the SEM picture. The average and standard deviation of the lengths could then be calculated.

Sample preparation – SEM
SEM requires the samples to be dry. The studied suspension is therefore frozen in liquid nitrogen and dried under vacuum for 24 hours. The obtained powder is then placed on the sample holder and gold coated. The gold coating is applied to the particles since the particles do not conduct electricity.
SEM imaging could be carried out at the Delft University of Technology.

Principle of the measurement – Cryo TEM
The TEM technique is based on the transmission of electron through a very thin sample (classically <0.2µm tick). An image is formed from the interaction of the electrons transmitted through the sample. The image is focused onto a CCD camera. In a Cryo TEM system, the thin film is obtained by cryogenic freezing (see Sample Preparation Cryo-TEM section) [16]. The film obtained is made of the vitrificated liquid

phase trapping the particles. The process of cryonization is quick enough (ca 1ms) to freeze the water in a glassy state and to fix the particles as they are in suspension. The particles seen in the frozen matrix are thus expected to be in the same shape and formation as in suspension.
The maximum resolution achieved by Cryo-TEM is of few nanometers. The biggest particles that can be seen are of 3µm, the size of the grid holes used in the sample preparation.

The number of particles seen is very limited. The size of the particles could not be determined with high accuracy. Nevertheless an order of the size could be measured.

Sample preparation – Cryo TEM
Sample preparation for cryo-electron microscopy involves a well defined sequence of steps: application of the particle suspension to a specimen grid, blotting away excess fluid, draining/thinning the film, and finally, vitrification, achieved by plunging the thin sample into a liquid coolant (typically ethane, propane or nitrogen). [18,19]

Cryo-TEM imaging could be performed at the University of Maastricht.

2.2.2. Static Light Scattering

Static light scattering of a particle generates a diffraction pattern function of the particle size shape and the light wavelength. To measure particle size using static light scattering, a diffraction pattern is usually obtained when emitting a Laser light on the sample particles (figure 2). The pattern is measured as the intensity of diffracted light at various angles. The particle size distribution is calculated for spherical particles and assuming that the light has been diffracted only once. The particle size distribution is obtained from the intensity of the diffracted light using a matrix calculation:

$$L = M \cdot Q \tag{1}$$

With L the vector signals of the detector at different scattering angle; Q the normalized quantity of material in the different size classes forming the range of detection of the machine and M the convolution matrix.

The matrix M is based on an optical model. For particles larger than 10µm the Fraunhofer theory is applicable. The intensity at a given diffraction angle is then considered as proportional to the particle size. For smaller particles, close in size to the wavelength of the laser light used, that proportionality is not true anymore. Refraction and absorption of the light are then influencing the resulting diffraction pattern [16]. In those cases the Mie theory will be used. The factors of matrix M are then dependent on the value of the refractive index and the absorption of the material [20,21].

The Particle size distribution can be obtained from the signal of detectors by inversion of the previous equation:

$$Q = M^{-1} \cdot L \qquad (2)$$

With M^{-1} being the deconvolution matrix.

In practice, piece of software uses the least-squares best-fit method or the Phillips-Twomey method [22] to solve the equation. Noise in measured data can influence those calculations and therefore some smoothing of the results might be needed. All values of the particle size distribution (matrix Q) are not allowed to be negative and the maximum in variation between consecutive size classes is limited.
The resolution of the static light scattering technique is thus defined by the number of detectors, the quality of the measured signal and the degree of smoothing of the results.

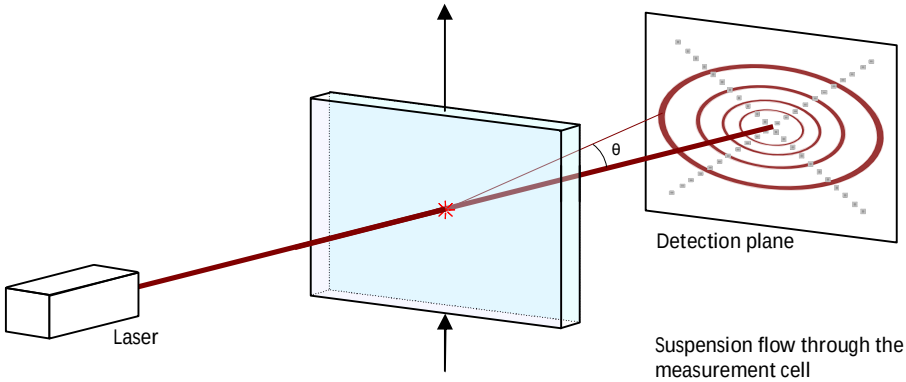

Figure 2 . Principle of classical laser diffraction

The smaller the particle the less intense is the diffraction signal. Classical laser diffraction does not enable the accurate characterization of particles in the submicron range because the diffraction signal of sub-micron particles is very weak and the scattering angles are very broad. The entire signal can not be measured by using a single detector. Different modifications and improvements have been made over the last years to enable sizing of particles in the sub-micron range. Different approaches have been taken to overcome the low scattering intensity of sub-micron particles in comparison to larger particles. An overview is given below:

- Polarization Intensity Differential Scattering (PIDS) uses polarized light to filter out the signal of the coarse particles. This is based on the fact that sub-micron particles scatter light at different intensities for different polarizations; while large particles don't.
- High resolution CCD detectors were introduced to obtain a much higher resolution of the diffraction pattern. This enables the detection of weaker signals such as that of small particles.

- Blue wave technology makes use of a combination of lasers of different wavelengths.[23] The diffraction intensity of the particle is more intense when using shorter wavelength. Therefore measuring with several wavelengths improves the accuracy of the detection of small particle.
- Backscattering detection makes use of extra detectors at angles ranging from 60 to almost 180°. Smaller particles are scattering light to higher angles compared to bigger particles, the extra detectors enables the detection of the small particles.

2.2.2.1. Static light scattering combined with PIDS

Principle of the measurement

The limitation of classical laser diffraction is the poor resolution on the detection of the scattered light of small particles. Devices using static light scattering including PIDS (Polarization Intensity Differential Scattering) use polarized light to filter out the signal of the coarse particles.

PIDS is a technique using 3 different wavelengths (blue, green and red: 450, 600 and 900 nm). One after the other this laser beam is send through the sample. For each wavelength the light is polarized once in a horizontal way and once in a vertical position. When illuminated by polarized light, particles much smaller than the wavelength behave like a dipole. The particles in the sample are thus getting excited by the incident light and start oscillating along the polarization axe. They scatter light in all directions but not that of oscillation. The scattering pattern is roughly a quadratic curve centered at 90 degrees from the oscillating axe. By looking at two different polarization axes, differences are then observed. Bigger particles do not behave like single dipoles but intra-particle interferences occur. The resulting scattering pattern is then more complex and independent on the polarization axes [24]. Therefore, the signal of the smaller particles can be determined at a broader range of angles without being hidden by the signal of larger particles.

The calculations leading to the particle size distribution are based on the resolution of equation 1. The intensity vector L is extended with the values of the intensity at different wavelength and the convolution matrix M is extended to take into consideration the additional data. The corresponding parameters of the convolution matrix are calculated on the base of the Mie theory and the value of the used wavelength.

The limitation of the range of detection of devices based on static light scattering using PIDS comes from the smallest wave length used and the resolution of the detectors. That limit is of about 40nm.

Sample preparation

The particle suspension is introduced in a large amount of fluid in a ratio of 1mL of suspension at 5% (w/w) in 1L of fluid. The concentration of product was in the present work of about 50ppm. That low concentration is required to reach a value of the optical obscuration of the PIDS light of about 50%.

The LS 13320 from Beckman Coulter Inc., USA uses static light scattering combined with the PIDS system. This machine was used in this work.

2.2.2.2. Static light scattering with high resolution detectors

Principle of the measurement

Classical laser diffraction measures the diffraction pattern at a limited number of angles. In most cases 128 or 256 data points are collected. This does not enable to see small variations of the pattern between different angles. Having a better resolution of the detection of the diffraction pattern would enable a better analysis of the signal of both the micron sized particles and the finer particles.

The use of a CCD array that detects the shape of the diffraction pattern with several millions of pixel enables a high resolution in the detection of the scattering pattern. The intensity data could then be processed in the same way as described previously, using the deconvolution matrix. Should all data be used to calculate the particle size distribution using the method from section 2.2.2, a system of millions of equations with the same amount of variables would need to be resolved.

The device tested is the Saturn DigiSizer 5200 from Micromeritics Instrument Corp., USA. It is equipped of high resolution detectors to analyse sub-micron particles. Only a part of the data is used in the matrix calculations because of lack of computational power. This aspect limits the range of sizing allowed on the tested device. The use of high resolution detector enables then to detect particles down to 100nm, and for mono-dispersed reference material to 70 nm. The maximum limit is above 1mm.

Sample preparation

The sample preparation is similar as for the previous unit: the particle suspension is diluted to about 50ppm before being analyzed. The obscuration value of the laser beam should be sufficient enough to reach a good signal to noise ratio but not too high to prevent multiple scattering.

2.2.2.3. Static light scattering combined with blue light technology

Principle of the measurement

The resolution of the detection of the diffraction pattern is linked to the intensity of the diffracted light. As the particles become smaller, they scatter light at higher angles and at lower intensities; thus limiting the detection of very fine particles. The power of the intensity of scattered light has an inverse relationship to the fourth power of the wavelength of the used light source. When using a blue light (wavelength around 400nm) that wavelength is half of that of a red light (wavelength of almost 800nm), the scattering intensity is multiplied by 16. A better noise to ratio can be obtained for the detection of the diffraction signal of submicron particles.

The detection of particle size distribution takes advantages of both red and blue light. As illustrated in figure 3, the red laser light is used for the detection of the scattering pattern at small angles, thus large particles and the blue laser for the detection of the scattering pattern at large angles and very large angles (for the detection of backscattered light). All data are computed using the convolution matrix M (equation

1). The intensity vector L is extended with the values of the intensity at different wavelength and different angles and the convolution matrix M is extended to take into consideration the additional data. The corresponding parameters of the convolution matrix are calculated on the base of the Mie theory and the value of the used wavelength.

The device tested equipped with a blue light technology is the Mastersizer 2000, Malvern Instruments Ltd, UK. The range of the tested device results from the wave length used and the resolution of the detectors. The smallest particles that can be detected are of 10 nm. The upper limit is of a couple of millimeters.

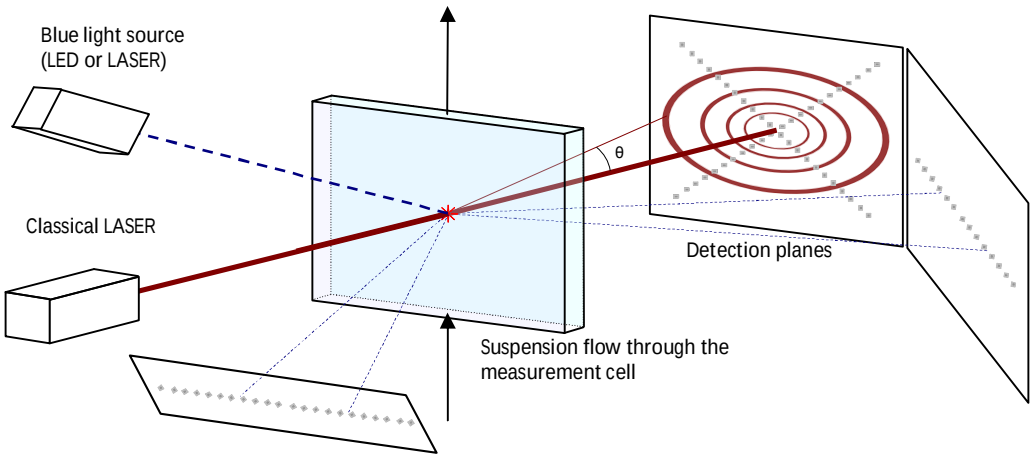

Figure 3 . Laser Diffraction principle improved with a blue LED or Laser and with wide angle and back-scattered light detectors.

Sample preparation
For obscuration requirements as described before, the sample tested needs to be diluted to ca 50ppm.

2.2.2.4. Static light scattering combined with backwards light scattering

Principle of the measurement
The combination of static light scattering with backward light scattering enables a broader range of detection of particle sizes. Static light scattering is detected at angles between 0° and 90°. Light is scattered backward by sub-micron particles only. The angles of diffraction are between 90° and 180°. In measuring the diffraction pattern formed by both the static and backwards light scattering, information is obtained about micron and sub-micron particles.

The Mie theory describing the diffraction at any angle, the particle size distribution can be calculated using the same method as presented in section 2.2.2. The vector L (equation 1) contains then the values of the intensity of diffraction at angles from 0° to 180° and the convolution matrix M is calculated using the MIE theory.

The technique used by the device tested, the LA950 from Horiba, Japan, is based on the detection of the intensity of static and backward scattered light. The range of detection given is of 40nm to a couple of millimeters.

Sample preparation
The sample preparation requires diluting the product particles in the device to about 50ppm. That dilution is required to reach laser obscuration value sufficient for a good signal to noise ratio but not including multiple scattering effects.

2.2.3. Techniques based on Brownian motion

Brownian motion is the movement of particles in a fluid. The distance travelled by particles in a given time is different depending on their mass and thus size. When considering spherical particles from the same material, smaller particles have on average velocity higher as the one of larger particles. The detection of the Brownian motion is therefore a potential method to evaluate the particle size of the moving particles. In this research the particles suspended in water were used; thus the fluid here was water.

2.2.3.1. Photon correlation spectroscopy

Principle of the measurement
The intensity of the scattered light of a particle is measured at a given angle (figure 4). Because of Brownian motion the scattering intensity changes in time. These temporal intensity changes are fitted by a correlation function based on the value of a diffusion coefficient. The diffusion coefficient is related to the particle size by means of the Stokes-Einstein equation [20]:

$$D = \frac{k \cdot T}{3 \cdot \pi \cdot \eta_f \cdot d_p} \tag{3}$$

where k is the Boltzmann constant, d_p the diameter of the particle assuming a spherical particle, η_f the fluid viscosity and T the temperature.

By measuring the signal at several times and multiplying those data, it is possible to measure how correlated the signals are. The interval between two measurements in time is short compared to the time of diffusive motion. In that way there is initially a good correlation which gradually disappears as the time interval becomes longer. By analyzing the shape of the curve, it is possible to extract a diffusion coefficient. The size of the particle is calculated from the diffusion coefficient by the Fick's laws of diffusion in combination with Stokes relation of the friction factor. The hydrodynamic particle diameter is measured, which might be a little bit larger than that of the

particle itself as it contains some liquid shell. The range of detection of the PCS set-up is from about 1nm up to several hundreds of nanometers.

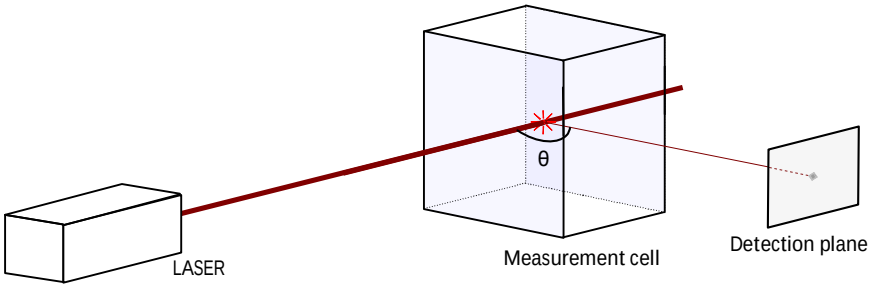

Figure 4 . Principle of a PCS set-up.

Tests have been carried out on a classical DLS set-up available at the Delft University of Technology, Nano Structured Materials Department. It is made of a blue laser entering a temperature controlled glass flask containing the suspension to be analyzed. The diffracted light is detected at a 90° angle from the incident light beam.

Sample preparation

The sample should be free of micron sized particles. The movement of those particles is partly influenced by the gravity forces, causing sedimentation. The velocity of sedimentation interferes in the measurement of the diffusion coefficient. A way to avoid most of the larger particles is to centrifuge of filter them out before the measurement.

The concentration of particle is a critical parameter. Multiple scattering occurs when the concentration of particles is too high. The scattered light from a first particle is then scattered by another particle before reaching the detector. The temporal intensity changes are then not representative of the signal from a single particle anymore, and the measurement will be false [25]. To avoid multiple scattering, measurements are carried out at very low concentration (below 1ppm) [26].

2.2.3.2. Photon cross correlation spectroscopy (PCCS)

Principle of the measurement

As described in the previous section 2.2.3.1, PCS is strongly influenced by the particle concentration in the studied sample and the presence of large particles. Multiple scattering can strongly influence the result quality. Therefore the working concentrations are very low.

When measuring a higher particle concentration, a part of the data should not been used because it comes from multiple scattering. The cross correlation is a technique that enables to use only the single scattered part of the signal.

In stead of a single incident beam as used in classical PCS devices, the PCCS technique uses a splitting of the laser beam in two identical beams focused on the same

measurement point with a different angle. As represented in figure 5, the light of the two beams is scattered in the same condition at the measurement point. Two detectors measure the intensity of the diffracted beams at the same angle (in most cases 90° from the incident beam). The two detected signals are identical.
Should the concentration be high, the diffracted light could be diffracted again by a second particle in the measurement cell. The chance that the two diffracted light rays are multiple scattered in the same way is very small and the signal detected are different in the case of multiple scattering. Two identical detected signals are thus with a high probability the signal of the single scattered light at the measurement point. By filtering out all the data for which the two signals are not identical, the data issued from multiple scattering are not taken into account. The measurement gains in accuracy and working at higher concentrations as for PCS becomes possible.

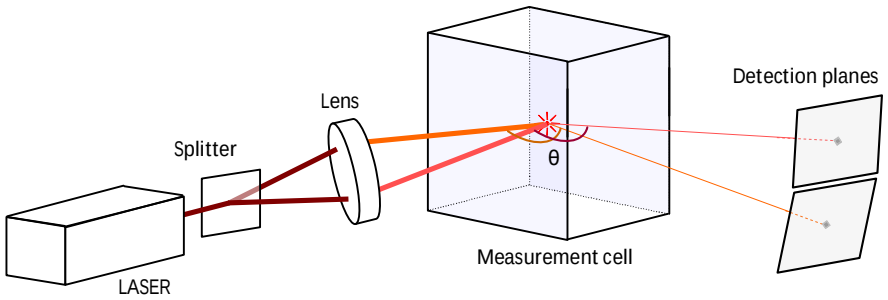

Figure 5 . Principle of the set-up of PCCS.

The Nanophox (Sympatec GmbH, Germany) device tested uses Photon Cross Correlation Spectroscopy (PCCS). This device has been tested in this work. The range of detection of this device is of particle sizes from less than a nanometer to several micrometers (cut off at 10µm).

Sample preparation
The sample did not require any preparation before being measured. The sample could be measured with 5% mass concentration of particles in water.

2.2.3.3. Heterodyne technique

Principle of the measurement
An other technique based on Brownian motion uses the Heterodyne principle. This technique is based on the Brownian motion of the particles but uses another property than PCS. When a ray light is backscattered by a moving particle, the wavelength of the backscattered ray is slightly different from the wavelength of the incident ray. That effect is known as the Doppler Effect. The measurement technique is based on the comparison of the wavelength of the initial beam and the wavelength of the back scattered beam. The two wavelengths are heterodyned (mixed together). The wide spectrum of frequencies resulting is transformed by Fourier Transform to a power spectrum that is inverted to give the particle size distribution. [27]

Practically a sapphire window reflects part of the original signal which heterodynes with the back-scattered light re-entering the sensor as illustrated in figure 6.

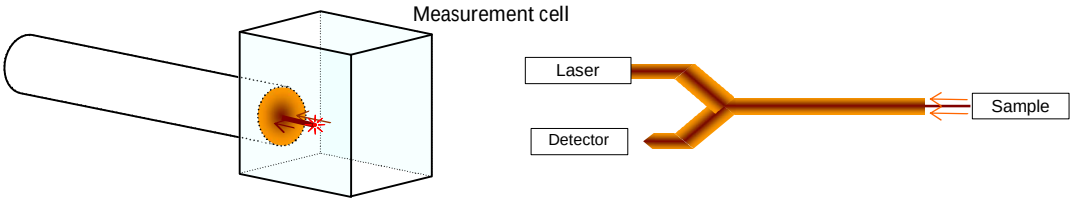

Figure 6 . Schematic representation of the set-up enabling the detection of the backscattered light of moving particles and the formation of the heterodyne with the incident laser light.

The Nanotrack piece of equipment from Microtrac Inc, USA, has been tested to characterize the ground particles. It uses the heterodyne principle. The range of size detectable is from below 1nm in to the micron range.

Sample preparation

The penetration of the light in the suspension is around 100um. Should the concentration be too high, scattering could occur and influence the measurement. Typically in this research the sample was diluted to 0,1% (w/w), since higher concentration give rise to perturbation in the fit of the correlation function.

2.2.3.4. Particle tracking

When looking with an optical microscope to the sample containing sub-micron particles, the particle themselves can not be seen; whereas the diffracted light dots by those particles can be clearly visible. A film of the diffracted light observed under an optical microscope can be made (see figure 7) and using image analysis the speed of the bright dots can be measured. Individual particles are detected and measured using this approach. The velocity of the particles under Brownian motion is linked to the speed of the apparent scattered light as presented in section 2.2.2 by the stokes Einstein equation. The diffusion coefficient is in the case of particle tracking measured as the squared average of the displacement of the particle in time [28]:

$$D = \frac{\overline{(x,y)^2}}{t} = \frac{k \cdot T}{3 \cdot \pi \cdot \eta_f \cdot d_p} \qquad (4)$$

Where x and y are the coordinated of the particles given by the image analysis (2D view) and t the time.

A better image quality is obtained when replacing the normal light source of a microscope by a laser going through the sample, this approach is used by the

NanoSight LM10 developed by Nanosight Ltd, UK. This device has been tested in this research.

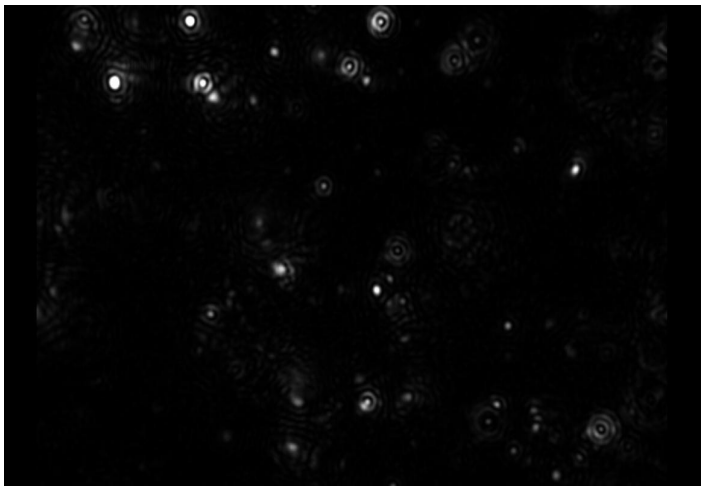

Figure 7 . 2D view of the diffracted light by sub-micron particles.

The technique enables to see particles theoretically from 10nm up to 1um. Brightness and contrast have to be adjusted to have an optimum measurement. In case of a wide size distribution or a bi-modal distribution, the large particles scatter light with much more intensity than smaller ones. The contrast and brightness has then to be fixed in a way that there might be a risk that the small signal might not be detectable anymore. The detection limit is therefore depending on the sample properties.

Sample preparation

Samples need to be diluted a hundred times to ca 500 ppm. The number of particles should be neither too high nor too low. Too many particles will generate particle-particle interaction influencing the Brownian motion. Too few particles will require too long acquisition time for reaching the same result quality.

2.2.4. Disc Centrifugation

Principle of the measurement

Another approach to particle sizing problem could be in first separating the particles depending on their size and analyze separately the amount of particles in each fraction. The separation of particles according to their size can be done using centrifugation. Very small particles can sediment using very high centrifugation forces. [29] When all particles have the same density, the larger particles are centrifuged quicker than smaller particles and are therefore separated. When considering spherical particles, the speed of their sedimentation is directly proportional to their size. In the Stokes regime, the relation between the sedimentation speed and the particle size is expressed by the Stokes law:

$$v_s = \frac{(\rho_p - \rho_f) \cdot d_p^2 \cdot g}{18 \cdot \eta_f} \quad (5)$$

Where v_S is the settling speed, d_P the diameter of the particle, g the gravitational field applied, ρ_p and ρ_f the density of respectively the particle and the fluid and η_f the fluid viscosity.

A device based on this principle is composed of a rotating disk filled with an eluent (figure 8). The eluent presents a gradient of density. This gradient is made by injecting different concentration of eluent at decreasing concentrations of sugar. This gradient enables a more homogeneous sedimentation of the particles. In absence of the density gradient streaming is observed: particles have a tendency to sediment in the bulk. The instability is caused by the effect of the (more dense) suspended particles on the net density of the fluid in which they are suspended. The eluent is covered with a thin paraffin oil layer to prevent evaporation of the eluent. The disc rotates at a constant speed between 600 and 24.000 rpm. A gradient of the rotation speed during the measurement makes it possible to measure broader particle size distribution. The eluent thickness is around 1cm and the detection is made 1mm before the "bottom". The detection is done by a light beam from a LED going through the rotating disc and the suspension; the absorbance is measured. Other detection systems are possible, for example X-Ray absorption for particles that absorb X-Rays.

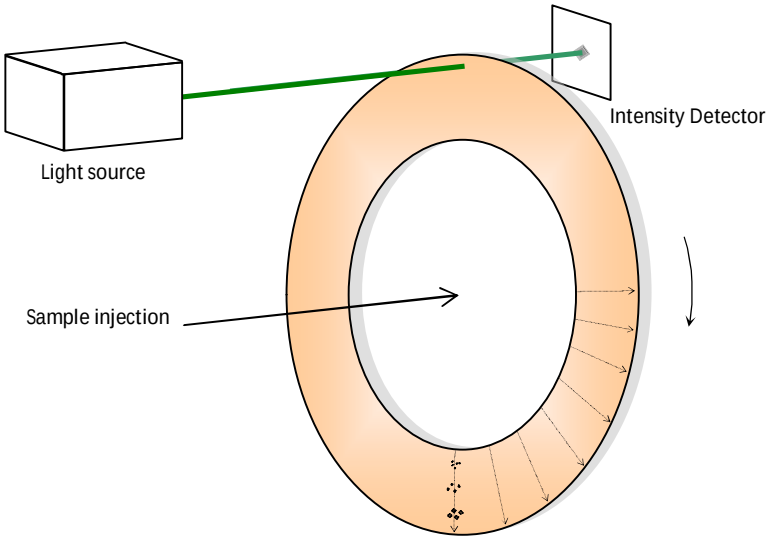

Figure 8 . Schematic of the disc centrifugation process.

Knowing the density and the relative centrifugation time (R_f) from a reference, the program determines the relative amount of particles from each size by looking at the absorption of the beam in time. Thus the particle size distribution can be calculated.

The tested Particle Size Analyzer from CPS Instrument, USA is a disc centrifuge. The range of detection varies from the chosen parameters of the set-up. According to the applied settings, the machine can be used for particles ranging from 5nm up to ca. 100nm or from ca. 100nm to a couple of tens of microns.
The parameters of the setup are tuned in order to analyze a specific range of particles, and the reference material should be chosen in that range, as close as possible to the targeted mean particle size and to the product density. [30]

Sample preparation
The concentration of the product injected should not be too high unless all particles do not start to sediment at the same time. Pre dilution to 1000ppm is therefore needed.
The product might dissolve in the eluent, but several analyses can be done in the same eluent and therefore the eluent will get saturated with the product and no problem of dissolution of the particles appears.

2.2.5. Flow Field Flow Fractionation with UV and light scattering detectors.

Principle of the measurement
The separation of the particles according to their size enables to obtain fractions of very narrow size distribution which facilitate their size analysis.

The separation of the particles according to their size can be done by Flow Field Flow Fractionation. The separation is based on the different in mobility of the particles under a field of forces. The set-up used in this work, Eclipse 2, Wyatt Technology Corp, consists of one inlet for an eluent, an inlet for the sample, and an outlet where fractionated particles come out. Between the inlet and the outlet, a field of forces is applied. In general, theses forces can be from various natures: Gravitational (simple sedimentation or induced sedimentation by a centrifugal force), Thermal, Hydraulic or Electrical. The Eclipse 2 system is for based on hydraulic forces. The set up is composed of two plates; the lower one is porous and covered by a nanomembrane (Figure 9). The flow of eluent is therefore oriented not only to the outlet but also through the membrane. The bigger the particle, the more it is influenced by the flow and the more it will be delayed in the system. In such a system, the fractionation will bring first the smallest particles out and then by order of size the other ones.

The particles exit the Eclipse 2 system in time as single peak with a very narrow size distribution. The concentration of those particles is detected by UV-light (280nm) absorption measurements (1200 Agilent from Wyatt Technology). The particle size is measured on line by using light scattering using the Dawn Heleos system from Wyatt Technology based on 18 angles light scattering detector. The size is calculated in the same way as described in section 2.2.2. The size distribution to be analyzed being very narrow, the scattering pattern is less complex and can fully be used and by only using 18 angles of detection.

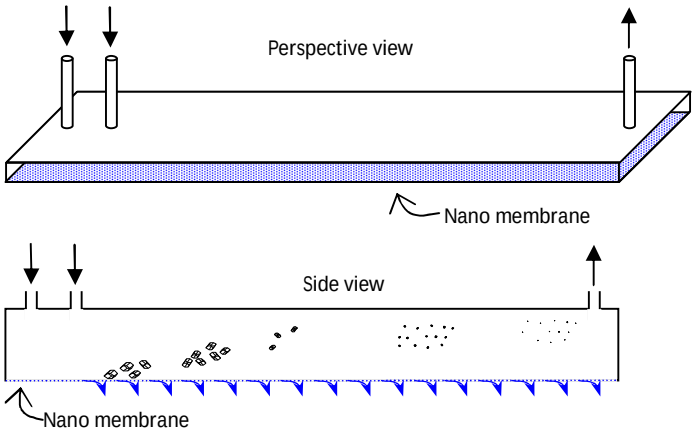

Figure 9 . Principle of Flow Field Flow Fractionation with a membrane.

The system is able to separate particles in the sub-micron size range. The minimum value of detection is at optimum conditions very low and depending on the detection device. In the most accurate cases, macromolecules of 1000 Da are detected, which correspond to sub nanometer “particles”.

Sample preparation
The concentration of the particles in the chamber has to be quite low in order to have a good separation. The sample should be free of large particle. Therefore the sample has to be centrifuged for 2min at 1000 rpm (Mikro 20, Hettich Zentrifugen) and only the supernatant is injected.

The eluent used is water at pH=8 buffered by phosphate (1mM NaH_2PO_4, 200ppm NaN_3).

2.2.6. Other techniques

Other techniques available commercially could not be tested:

- Particle separation by size exclusion chromatography is a technique separating the particles according to their size. The particle size of each out coming sample is analyzed by light scattering techniques. The particles are separated according to their volume. The bigger the particle, the quicker it travels through the column. Particles exit the column as very narrow size distribution and are easily detected by static light scattering. The range of particles that can be fractionated by a column is depending on the structure of the packing. The range is always limited to a narrow size distribution (for example from 5nm to 300nm, from 20nm to 1200nm, from 500nm to 2000nm for the biggest particles analyzable). Bigger particles (>2um) can not be analyzed by such a system, they will not be separated. Large particles could damage the column as well.

The potential presence of aggregates in the studied particles would have induced two problems: First of all, the particle size distribution is then bimodal, the primary particles being ca 10 times smaller than potential aggregates. No column could thus separate primary particles and aggregates. Second, the use of a column for small particles while having at the same time aggregates could block and damage the column. No tests could therefore be done on such a system.

- Acoustics and electro-acoustics are two techniques based on ultrasounds. The first one is a simple method using the properties of the dispersion: attenuation of the signal and speed of sound. Electro-acoustic technique couples the acoustic and electric properties of the dispersion. The tests of this techniques requires large amount of material in high concentration that were not available for the studied product.

Such systems are best for inline measurements or quality control in production plants.

3. RESULTS AND DISCUSSION.

3.1. Image analysis – SEM and Cryo-TEM

Image analysis on single electron microscopy (SEM) and cryogenic transmission electron microscopy (Cryo-TEM) have been performed. Including sample preparation, the average time of measurement is approximately 1 day.

As shown in figure 10, the particles observed with SEM are clusters of smaller particles. The size of the primary particles is determined by measuring manually and 100 particle sizes on the picture. Each particle has been chosen randomly as well as the axe of the particle to be measured. The average value is of 194 ± 20 nm.

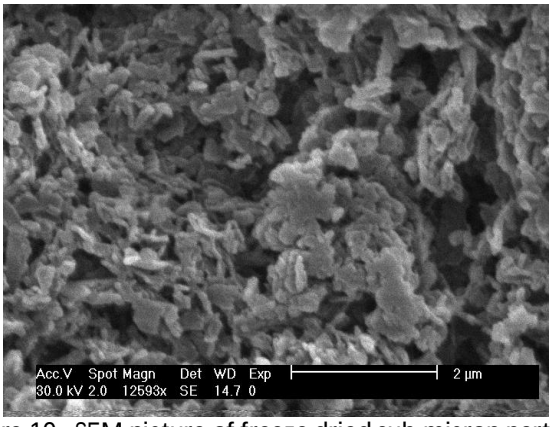

Figure 10 . SEM picture of freeze dried sub-micron particles

The pictures taken using the Cryo TEM imaging are presented in figure 11. Figure 11 shows clearly that the ground particles are aggregated. The size of the primary particles corresponds to the size measured by the SEM (0.18-0.20µm) and the aggregates are in the micrometer range.

A cryo-TEM measurement takes about 20 min including sample preparation.

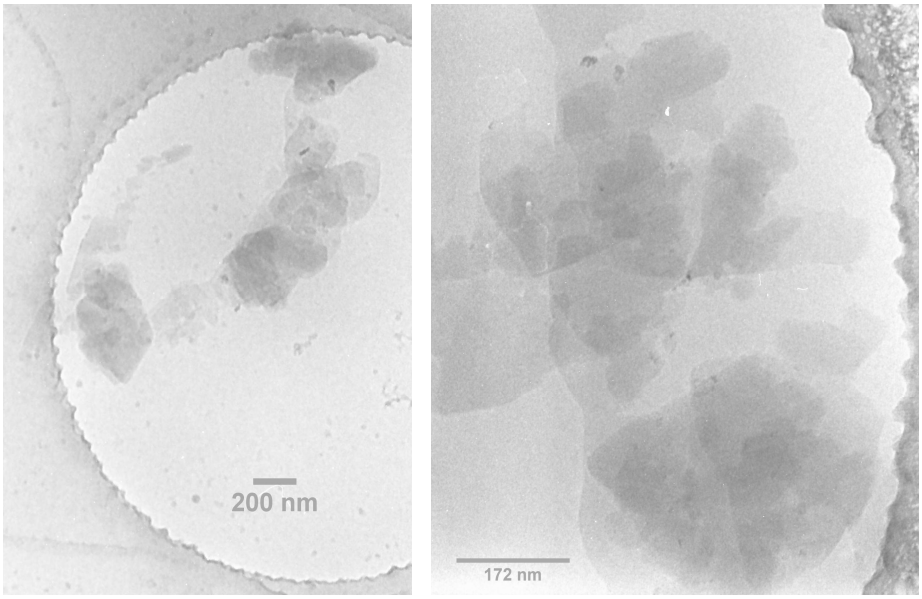

Figure 11 . Cryo TEM Pictures (Univ. Maastricht, Netherlands).

3.2. Techniques based on Static Light Scattering

3.2.1. Static light scattering combined with PIDS – Beckman Coulter LS-13320.

Measurements were carried out on a Beckman Coulter LS 13320 piece of equipment using Static light scattering in combination with PIDS. The measured particle size distribution is shown in figure 12. The mean particle size ($d_{4,3}$) measured is 181nm. That result is very similar to the previous observations by image analysis of the SEM and Cryo-TEM samples.

The particle size distribution measured by the LS 13320 does not show any larger particle that could be of the aggregates. Contrary to the image analysis results, no aggregates are seen.

The average time of measurement is 5 min.

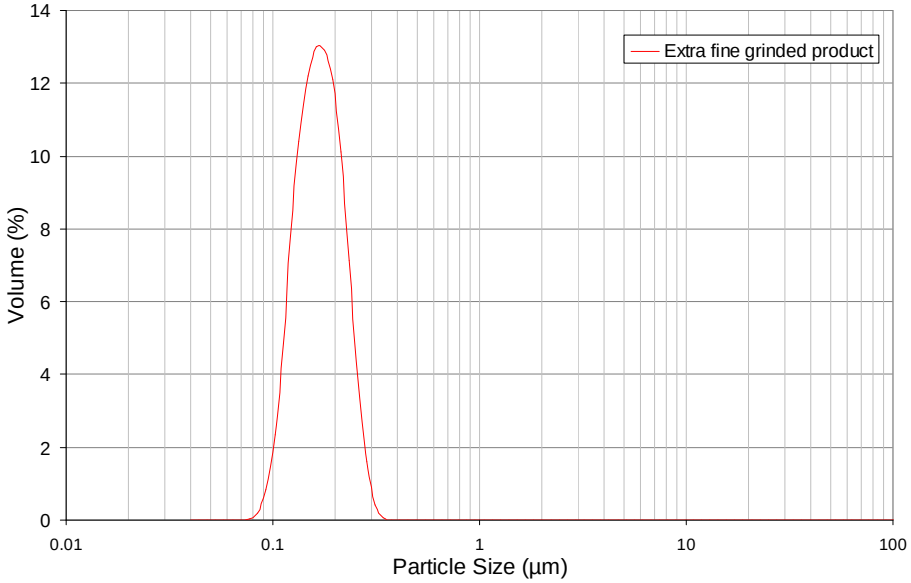

Figure 12 . Particle size distributions ($d_{4,3}$) measured by Beckman Coulter LS 13320.

3.2.2. Static light scattering with high resolution detectors – Micromeritics Saturn DigiSizer 5200

Measurement carried out on the Micromeritics Saturn DigiSizer 5200 is shown in figure 13. The Digisizer 5200 measures the diffraction pattern of the studied particles by using a CCD detector. The mean value ($d_{4,3}$) of the particle size is 354nm.
Larger particles are detected
The presence of larger particles lets us to believe that aggregates are detected by the device. The size of the aggregates corresponds to the observations by image analysis (above 1µm). Some coarser particles are observed as well.
The measurement time is ca 5 min.

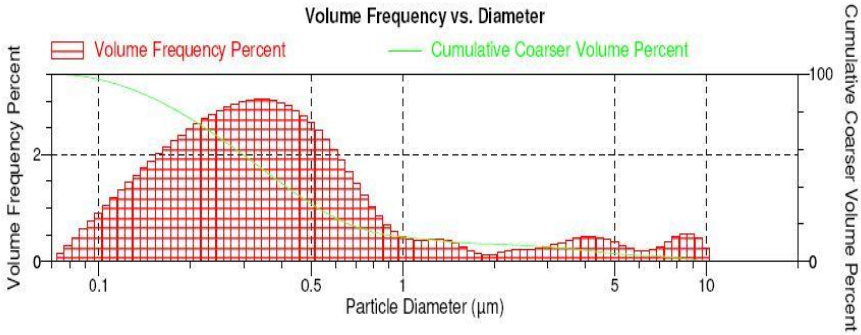

Figure 13 . Particle size distributions ($d_{4,3}$) measured by Micromeritics Saturn DigiSizer 5200.

3.2.3. Static light scattering combined with blue light technology – Malvern Mastersizer 2000

The results of the measurement of the ground particle on the Mastersizer 2000 are shown in figure 14. The main peak detected is at 0,187µm (mean value of the peak $d_{4,3}$). The presence of some larger particles is detected here by the device around 2 and 20µm.

The measurement time in comparable to the Beckman Coulter LS 13320 (ca. 5min).

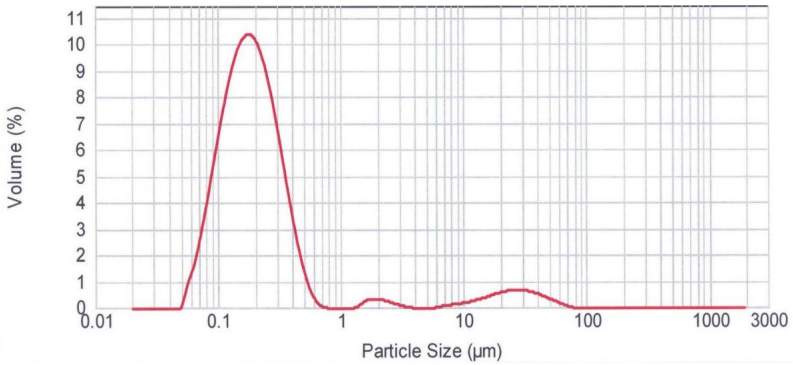

Figure 14 . Particle size distributions ($d_{4,3}$) measured by Malvern Mastersizer 2000.

3.2.4. Static light scattering combined with backwards light scattering – Horiba LA950

The results of measurements done on a Horiba device LA 950 equipped with backscattering detectors are shown in figure 15. The mean particle size measured is 173nm ($d_{4,3}$) and no aggregates are visible.

The measurement time is comparable to all previous static light scattering devices (ca. 5min).

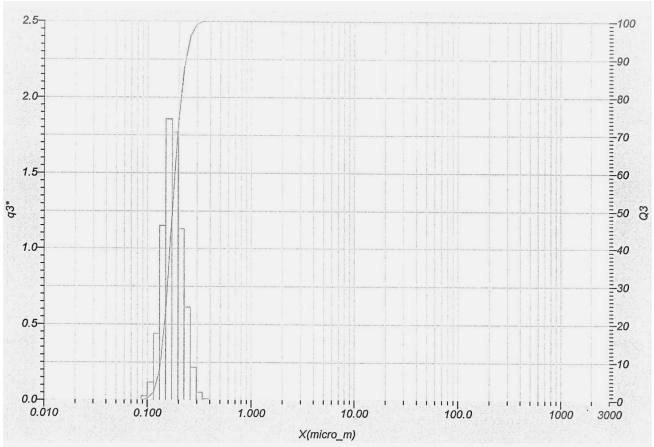

Figure 15 . Particle size distributions ($d_{4,3}$) measured by Horiba LA950.

3.3. Techniques based on Brownian motion

3.3.1. Photon correlation spectroscopy (PCS) – TUDelft equipment

Tests have been carried out on a classical PCS set-up available at the Delft University of Technology, Nano Structured Materials Department.
Measurements were highly influenced by the presence of coarse particles. The coarse particles might be particle aggregates. Several measurements of a single sample of milled product showed that the analysis was not at all reproducible and reliable. Therefore no results are shown.

3.3.2. Photon cross correlation spectroscopy – Sympatec Nanophox

As second attempt was done using a Sympatec Nanophox system (results are given in figure 16). The mean value ($d_{4,3}$) of the small particles peak is 188nm. That value is very similar to the results obtained by most of the light scattering techniques and to the size of the particles on the SEM and Cryo-TEM images.

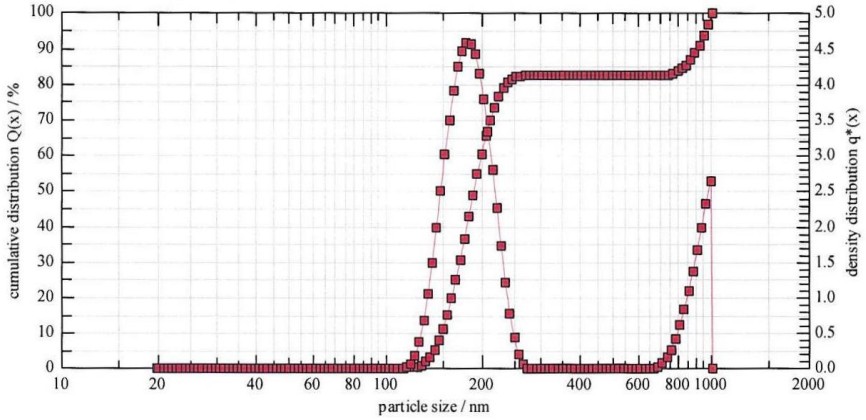

Figure 16 . Particle size distributions ($d_{4,3}$) measured by Sympatec nanophox.

Large particles (above 1µm) were present and visible from the measurement. The aggregates being bigger than the detection limit of the device, no quantification of the size and the amount of aggregates can be calculated.
A typical measurement time is of few minutes.

3.3.3. Heterodyne technique – Microtrac Nanotrac

The measurements given by several tests on the Nanotrac device showed that the presence of aggregates is highly disturbing the measurement (Figure 17). The signal emitted by big particles is influencing the correlation function a lot. The fitting of the correlation function is extremely sensitive and results in huge differences in obtained particle size distributions.
The mean value ($d_{4,3}$) measured for the sample is 853nm, only a few of the small primary particles are actually detected, as if all particles would have flocculate, which has not been the case with identical samples measured by the Nanophox device.

A typical measurement time is of few minutes.

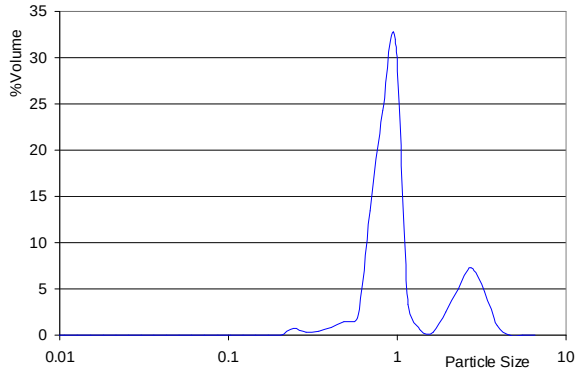

Figure 17 . Particle size distributions ($d_{4,3}$) measured by Microtrac, Nanotrac.

3.3.4. Particle tracking – Nanosight

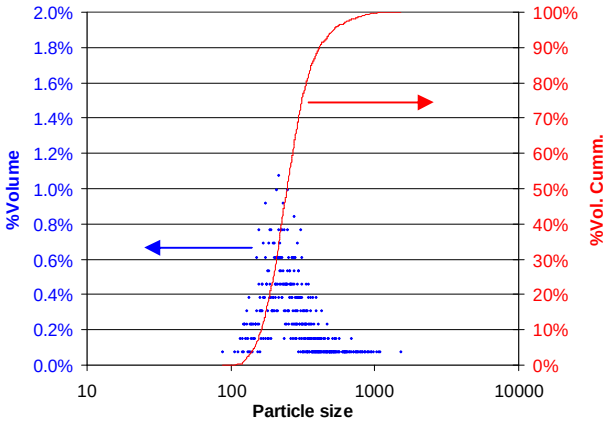

Figure 18 . Characterization of particle size by particle tracking, Nanosight. Particle size distribution ($d_{4,3}$) and cumulative.

The measurements have been carried out on the NanoSight LM10 (results on figure 18). The amount of particles analyzed in the present case is very low (1min acquisition, 540 Mo storage space required, 1305 particles measured). This is mainly due to the high selectivity required on the filmed particle selection. The particles should have a given minimum intensity and remain in the detection for a certain period of time. The resolution of the final data is therefore low, only few particles are taken into consideration.

The shape of the measured distribution can be still seen and no coarse particles have been detected. The mean particle diameter is of 277nm.

A measurement with sample preparation requires few minutes.

3.4. Disc Centrifugation – CPS Particle Size Analyzer

Several trials have been done on the Particle Size Analyzer from CPS Instrument, Newtown, USA (Figure 19). Results showed a mean particle size (381nm). No aggregates could be observed.

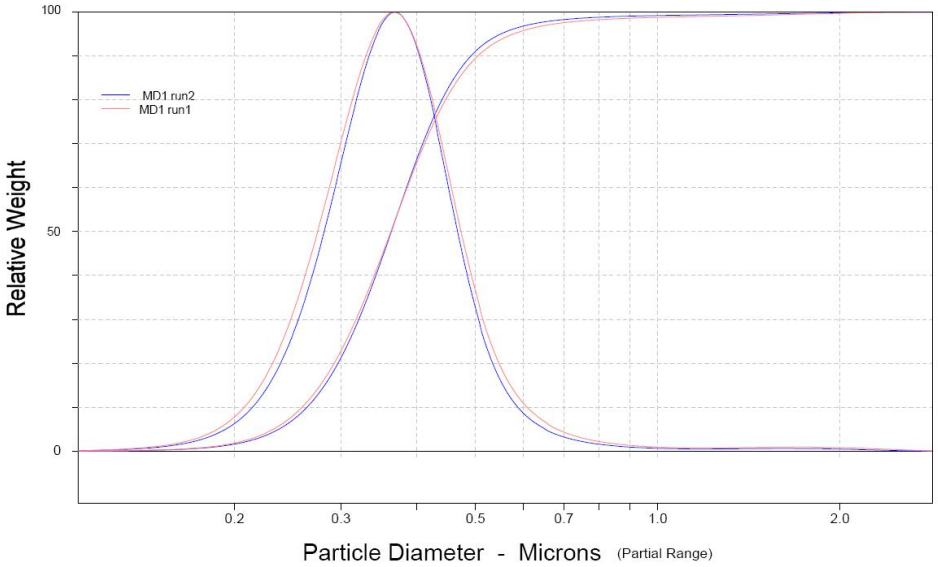

Figure 19 . Analyses by Disc Centrifuge of the grinded particles.

3.5. Flow Field Flow Fractionation with UV and light scattering detectors – Wyatt technology Corp. Dawn Heleos

Measurement of grinded particles in suspension carried out on flow field flow fractionation Eclipse 2 equipment from Wyatt Technology Corp. is presented in figure 20. The sample has been centrifuged before being injected in order to reduce the number of coarse particles that would disturb the measurement. A large peak centered at 26 min analysis time shows particles of a "molar mass" of $2.10^6 g.mol^{-1}$, corresponding to the mass of a mole of particles. A single particle has thus a mass of $3{,}3 \cdot 10^{-18} g$. The studied product has a density of $1300 kg.m^{-3}$, considering particles to be spherical, the median particle size is therefore of 170nm. Larger particles elutes after 60 min analysis. The filtration step did not remove enough of the coarse particles and aggregates or the aggregates formed after filtration. Experiment has been stopped because focus was given on the detection of the smaller particles. The experiment should have been continued for longer time to see the size and proportion of the larger material.

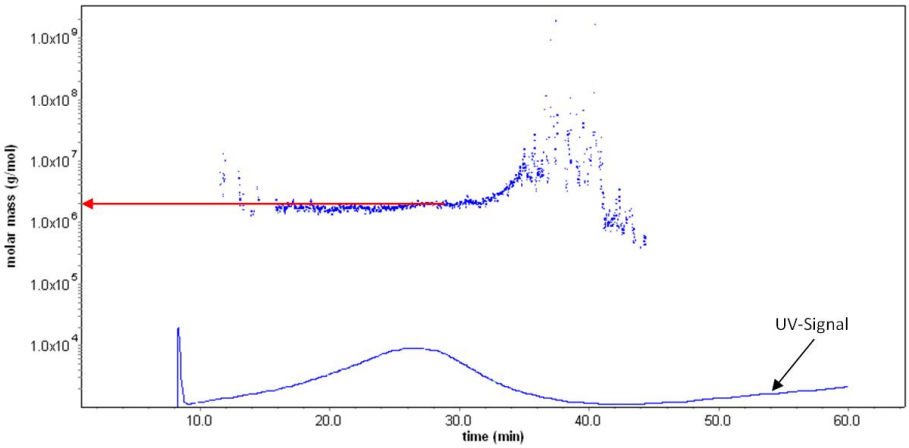

Figure 20 . Plot displays the molar mass measured by DAWN light scattering and as an overlay the UV signal (280 nm, proportional to the concentration) of the Eclipse measurements on the three samples

4. COMPARISON OF PARTICLE SIZE MEASUREMENTS.

The ranges of detection of different technologies available for sub-micron and nano-sized particles are shown in figure 21.

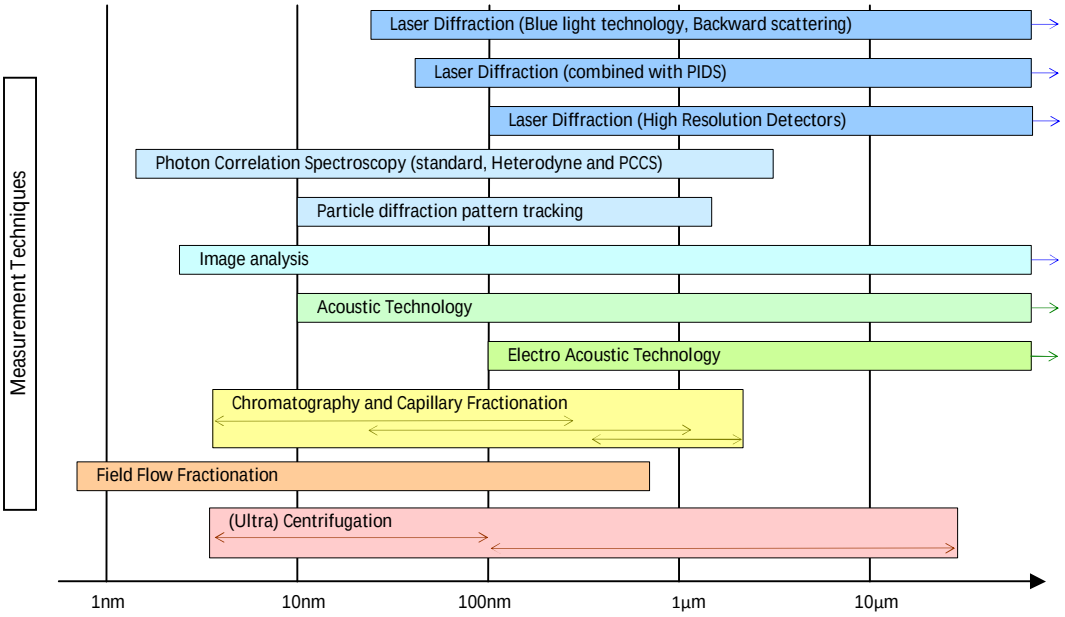

Figure 21 . Overlaps between ranges of detection for different particle size measurement techniques.

Table 2 shows an overview of the results given by the different particle size measurement techniques. Focus is given on the time of measurement the mean particle size measured and the detection of large particles.

Table 2 . Overview of the results given by the different particle size measurement techniques.

Technique		Time of measur-ement	Mean primary particle size $d_{4,3}$ (nm)	Large Particles	Remarks
Imaging techniques	Imaging techniques SEM	1day	194*	Yes	The SEM requires drying and therefore aggregates can not be differentiated from the smaller particles. The technique enables a good evaluation of the shape of the particles.
	Imaging techniques CryoTEM	20min	180-200*	Yes (2-3µm)	Cryo TEM enables an "in solution" look to the particles and enables to see the aggregates and estimate their size as well as the one of the primary particles.
Static Light Scattering	+ PIDS – Beckman Coulter LS13320	~ 5min	181	No	
	High Res. Detect. Saturn DigiSizer 5200	<5min	354	Yes (1-10µm)	
	+ Blue Light Malvern Mastersizer	<5min	187	Yes (1-50µm)	
	+ Back Scattering Horiba LA950	<5min	180	No	
Brownian motion based techniques	PCS	~ 10min	-	"Yes"	No measurement was possible because of the high influence of the concentration and the presence of large particles.
	PCCS	~ 5min	188	Yes (>1µm)	The light aggregates are detected and are above the detection maximum of the machine (1µm)
	Heterodyne	~ 5min	853	Yes	Only the big particles are detected, they most probably disturb the measurement.
	Particle tracking	~ 5min	277	No	The few number of particle actually analyzed in the present case do not enable an accurate quantitative analysis. The coarse particles are not detected; they might have sediment before the measurement.
Disc Centrifugation		20-30 min	381	No	Streaming effects and high Reynolds number might be responsible of the higher values of the particle size measured. High gravity and drag forces might break aggregates.
Flow Field Flow fractionation		60-90 min	170**	Yes	The aggregate particles elute after a very long time. The total distribution could not be therefore detected.

*average length of particle (not $d_{4,3}$)
**median particle size

Image analysis shows primary particles of around 180-200nm. The accuracy of the SEM results depends on how representative the sample on the picture is and how many particles are counted. Measuring 100 particles does not pretend to give an accurate result but is an indication of an order of size.
The product suspension is dried and gold coated before being introduced in the SEM. Therefore the samples are not systematically representative from the original particles in suspension. The aggregated structure could be created during the drying step. An answer to this point is possible using the CryoTEM technology.
The sample preparation for the Cryo TEM imaging includes a process of cryonization that is quick enough (ca 1ms) to freeze the water in a glassy state and to fix the particles as they are in the suspension [18,19]. The particles seen in the frozen matrix are thus expected to be in the same as in the suspension. Figure 11 shows clearly that the ground particles are aggregated. The size of the primary particles corresponds to the size measured by the SEM (0.18-0.20µm) and the aggregates are in the micrometer range. The aggregates are present in suspension. This is concluded from the Cryo-TEM analysis. Similar aggregates are seen in the SEM pictures as well. The aggregated structure observed in the SEM pictures was probably not created during the drying step but are present in the suspension of ground particles.

Cryo TEM also shows presence of larger aggregates. Several techniques do see the small particles of the same size and some larger particles at the same time too. The size of this aggregate could be measured by some techniques. The size of the aggregate ranges mainly between 1 and 50µm.

Some of the static light scattering techniques show both small and larger aggregates but the Beckman coulter LS 13320 and the Horiba LA950 do not see larger particles. There is very little difference between the processing of the particles during the size measurement. They are all measured at similar concentrations and all in demineralized water. All samples are pumped through the measurement windows by using a centrifugal pump. Slight differences are seen in the design of this pump and the shear induced on the product. Should the Horiba La 950 and the Beckman Coulter LS13320 devices induce higher shear on the aggregated particles as the Malvern Mastersizer, those aggregates could break in those first machines and remain intact in the Mastersizer. It could also be a deconvolution difference or a filtering of the data when small amounts of larger particles are detected.
The high resolution detector (Digisizer) shows larger primary particles size as the other techniques based on static light scattering. The device detects large particles. The diffraction signal of the primary particles is therefore included in the signal of the larger particle. The resulting diffraction pattern is therefore very complex. The CCD detectors are capable to detect that diffraction pattern, but as mentioned in section 2.2.2.2 not all acquired data can be processed because of lack of data processing power. That inaccuracy in the calculation might explain the difference in the particle size measured. No quantification of the error made on the value of the particle size could be made to confirm this hypothesis.

Photon correlation techniques are difficult to use because they are strongly influenced by the presence of larger particles. When they settle they give rise to a high motion which results in a shift of the particle size distribution.
Only photon cross correlation spectroscopy shows the primary particle size of the same size as the image analysis but also shows the presence of larger particles. But the size can not be obtained for these, because the upper limit of detection is around 1µm and the particles size distribution shows that larger particles could be present.
The sample being neither stirred nor undergoing any shear, aggregates would not be broken. The large particles observed are thus most probably the aggregates observed on the Cryo-TEM and SEM pictures. No measurement can be done while stirring or applying shear. That would induce a movement of the product particles that is not pure Brownian motion, and the measurement would be wrong.
The measurement is in the case using the heterodyne technique is not reliable enough to clearly determine the aggregate size. Nevertheless, the presence of large particles is clear. Larger particles move because of sedimentation and not only Brownian motion. The signal emitted by big particles is influencing the correlation function a lot. The fitting of the correlation function is extremely sensitive and results in huge differences in obtained particle size distributions.
The mean particle diameter $d_{4,3}$ obtained using particle tracking technique is of 277nm, which is in the order of magnitude as the results given by image analysis and static light scattering techniques.
No coarse particles are detected; what is potentially possible is that the coarse particle sediment out from the focal plane before or during the measurement. They would then not be analyzed.

Centrifugation is capable to see smaller particles but larger particles are expected to sediment that fast that they are not detectable. The mean particle size measured is 381nm; slightly bigger than the one observed by image analysis (180-200nnm) but the results remain in the order of magnitude. Two aspects can be responsible of a larger mean particle size as expected [31]:

At the beginning of the analysis, the entire sample is contained in a thin fluid layer near the surface. A streaming phenomenon enables the particles to sediment faster which leads to a broad initial band. The sedimentation follows then a normal pattern but the calculation of the particle size from the slightly shorter sedimentation time would give slightly bigger results of the particle size.

At very high rotation speed as in the present case (24000 rotations per minute, ca 2900G), the Reynolds number of the particle flow becomes higher and the Stokes law does not describe the sedimentation process accurately. That error could induce a bigger particle size than expected.

Flow field flow fractionation shows the primary particle of 170nm. The results are similar to the results by image analysis. The particle size detected by the multiple angle scattering device is of wide distribution. It is not possible from the data to determine the exact particle size distribution of the tested product. Since the elution was not totally finished, it is not possible to have a quantitative estimation of the

product particles size distribution. For that a reference material should be injected few seconds after the sample to be able to calibrate the results. Larger particles are detected by the UV detector but the time of analysis is then very long.

5. CONCLUSIONS

The above results indicate that the studied milled particles have a primary particle size close to 180nm and strong evidence is there of larger particles which are very likely aggregates. This is clearly seen from the Cryo TEM results.

All the above mentioned techniques should in principle be able to measure samples of dispersion containing particles of ca 190nm but several are disturbed by the presence of large aggregates. It is difficult to estimate the amount of aggregate present, but most of the time; one is interested in what the primary particle size distribution is. Addition of stabilizers, pH optimization or surfactants can reduce the aggregation tendency enormously, but this was not investigated in this research.

It is clear that no single piece of equipment is capable of exactly determining the particle size distribution of our samples, but the static light scattering with low shear on mixing does give a good representation of what is seen with the image analysis by cryo TEM.

6. AKNOWLEDGMENT

The authors want to thank: Leon Bremer from DSM ACES, Geleen in the Netherlands for his kind help with the Malvern Mastersizer; Professor Peter Frederic from the University of Maastricht, The Netherlands; for the sharp Cryo-TEM pictures; and Maria Christina Domingues, from the University of Coimbra and DSM Biotech Center in Delft, The Netherlands, assisting the authors with early stage grinding experiments.

7. REFERENCES.

[1] S.L.A. Hennart, W.J. Wildeboer and G.M.H. Meesters. Identification of the grinding mechanisms and their origin in a stirred ball mill using population balances. Chemical Engineering Science 64 (2009) 4123 – 4130.

[2] S.L.A. Hennart, W.J. Wildeboer and G.M.H. Meesters. Study of The Process of Stirred Ball Milling of Poorly Water Soluble Organic Products using Factorial Design. Submitted to Powder Technology 198(1) (2009) 56–60.

[3] S. Mende, F. Stenger, W. Peukert, J. Schwedes, Mechanical production and stabilization of submicron particles in stirred media mills. Powder Technology 132 (2003) 64–73.

[4] A. Grubenmann, Particle Size Distribution and Aspect Ratio of Organic Pigments. Particle and Particle Systems Characterization 3(4) (1986) 179–186.

[5] H. Lange, Comparative Test of Methods to Determine Particle Size and Particle Size Distribution in the Submicron Range, Particle and Particle Systems Characterization 12(3) (1995) 148–157.

[6] T. Kinoshita, The method to determine the optimum refractive index parameter in the laser diffraction and scattering method, Advanced Powder Technology 12(4) (2001) 589–602.

[7] T. Kinoshita, The influence of refractive index in laser diffraction/scattering particle size measurement, Powder Science and Engineering 25(10) (1993) 56–62.
[8] O. Hayakawa, Y. Yashuda, M. Naitoh and J. Tsubaki, The effect of refractive index input value on particle size distribution measured by the laser diffraction& scattering method, Journal of the Society of Powder Technology 32 (1995) 796–803.
[9] J.T. Lett, Measurement of single strand breaks by sedimentation in alkaline sucrose gradients, in: E.C. Friedberg and P.C. Hanawalt, Editors, DNA repair — A Laboratory Manual of Research Procedures Vol. 1, Marcel Dekker, New York. (1981) 363–378. ISBN 9-9929-2021-1
[10] H. Brik, Analytical profiles of drug substances 10 (1981) 513–561.
[11] J. R. March, P.J. Weiss, Journal - Association of Official Analytical Chemists 50 (1967) 457.
[12] A.P. Struyk, I. Hoette, G. Drost, J.M. Waisvisz, T. van Eek, J.C. Hoogerheide, Antibio. Annual (1957-1958) 878.
[13] W.L. Clark, R.J. shirk, E.F. Kline in N. Molin (ed.), Microbial Inhibitors in Food Stockholm, Sweden (1964) 167–184.
[14] F. M. Etzler, M. S. Sanderson, Particle Size Analysis: a Comparative Study of Various Methods, Particle and Particle Systems Characterization 12 (1995) 217–224.
[15] F. M. Etzler, R. Deanne, Particle size analysis: A comparison of various methods ii, Particle and Particle Systems Characterization 14(6) (1997) 278–282.
[16] H.G. Merkus, Light Scattering Techniques, Particle Size Measurements. Particle Technology Series (2009) Ed. Springer.
[17] J. Russ, The image processing handbook (3rd edition) (1999) CRC Press
[18] P.M. Frederik, D.H.W. Hubert, Cryoelectron Microscopy of Liposomes, Methods in Enzymology 391 (2005) 431–448.
[19] Frederik, P.M., Storms, M.M.H., Automated, Robotic Preparation of Vitrified Samples for 2D and 3D Cryo Electron Microscopy, Microscopy today (2005) 32–38.
[20] R. J. Hunter, Introduction to modern Colloid Science (1994) Oxford Science Publications
[21] W. Witt, S. Röthele, Laser Diffraction - Unlimited?, Particle and Particle Systems Characterization 13(5) (1993) 280–286.
[22] M. Heuer, K. Leschonski, Particle and Particle Systems Characterization 2 (1985) 7–13.
[23] D. M. Scott, Characterizing Particle Characterization, Particle & Particle Systems Characterization 20(5) (2003) 305-310.
[24] I. Ley, Technical notes, Beckman Coulter (2008).
[25] R. Finsy, Advances in Colloid and Interface Science 52 (1994) 79–143.
[26] H.G. Barth (ed), Modern Methods of Particle Size Analysis (1984) Wiley & Sons.
[27] W.M. Farmer, Measurement of Particle Size, Number density, and velocity using Laser interferometer, Applied Optics 11(11) (1972) 2603–2612.
[28] A. Malloy, B. Carr, Particle and Particle Systems Characterization 23 (2006) 197–204.
[29] H. R. Laapas, U.-R. Lahtinen, The Determination of Particle Size Distribution Using Combined gravitational and centrifugal sedimentation analysis, Particle and Particle Systems Characterization 1(1) (1984) 127–131.

[30] T. Detloff, T. Sobisch, D. Lerche, Particle Size Distribution by Space or Time Dependent Extinction Profiles obtained by Analytical Centrifugation, Particle & Particle Systems Characterization 23(2) (2006) 184–187.
[31] I. Laidlaw, M. Steinmetz, Introduction to differential sedimentation. in D. J. Scott, S. E. Harding, & A. J. Rowe (Eds.) (2005), Analytical ultracentrifugation techniques and methods (pp. 270–290). Cambridge: Royal Society of Chemistry.

Chapter 2

Stability of Particle Suspension After Fine Grinding.

This chapter has been published as S.L.A. Hennart, W.J. Wildeboer, P. van Hee, G.M.H. Meesters, Powder Technology 199(3) (2010) 226–231.

Abstract - The objective of this work was to investigate the physical stability of sub-micron particle suspensions of organic crystalline food compounds after grinding. A Dynomill ball mill was used in combination with zirconium oxide grinding beads. The organic product was a poorly water soluble product. During grinding the average particle diameter of the particulate product was reduced to a minimum value in the sub-micron range. Forward light scattering was used to analyze the particle size distribution. Dynamic light scattering measurements, on the other hand, showed that there were aggregates present after grinding. The difference in the obtained particle size distributions using both techniques was related to the shear in the measurement device, i.e. in the laser diffraction measurement the shear was higher than in the dynamic light scattering device. Thus in the laser diffraction measurement the aggregates were broken up by shear, while this was not the case in the dynamic light scattering measurements. The difference in the measurements showed that the particles formed aggregates at low to zero shear.

The aggregation behavior of the particles was studied by measuring the sedimentation behavior of the particles suspension at various pH values. The impact of the pH on the aggregation rate was explained by the zeta potential of the particles. The suspensions were less stable near the iso-electric point of the particles.

1. INTRODUCTION

Particle size reduction of compounds with low solubility can be beneficial in their application. For example, the dissolution rate is dependent on the available surface area [1]. Particle size reduction thus enhances the dissolution rate. Additionally, when used in concentration higher than the solubility, product particle size reduction can improve the distribution of the low soluble compound.

Particle size reduction can amongst others be realized by grinding [2]. After grinding the particles can form aggregates, which is undesirable. This study focuses on the prevention of aggregation after wet grinding of low soluble crystalline organic compounds.

When two colloidal particles approach one another, attractive and repulsive forces come into play. Particle can approach each other because of Brownian motion and

convective transport. The main attraction and repulsion forces are the van der Waals force and the electrostatic interaction force, respectively.

The grinding process used in this research has been tested under different conditions in order to optimize and understand the grinding process and the breakage mechanism [3]. Previous research by Mende et al. [4] on sub-micron grinding of inorganic products showed that the stability of the product and its final particle size are a function of the electrostatic properties of the particles and therefore the pH of the solution.
The detection of aggregates is in practice not always straight forward. Different particle sizing techniques can give different results depending on the measurement conditions. Some techniques such as imaging techniques enable a visual representation of the aggregates in suspension. Sedimentation measurements are another approach to the characterization of the aggregates [5].

In this work the suspension stability was analyzed as function of pH and ionic strength by light scattering and sedimentation measurements. The findings of these measurements are correlated with zeta-potential measurements through the DLVO theory.

2. MATERIAL AND METHODS

2.1. Grinding process

Experiments were carried out using a Dynomill from Bachofen AG (Basel, Switzerland). The ball mill was operated in a recirculation mode. The poorly water soluble organic product was suspended in water. Figure 1 shows the circulation of the product suspension through the grinding chamber (volume of the chamber: 300 mL) that was filled at 80% (bulk volume) with grinding beads (Zirconium oxide, Yttrium stabilized beads from Tosoh, Japan). The product suspension was drawn out through a 0.1 mm gap to prevent the grinding medium to exit the milling chamber. The system was cooled to keep a constant temperature throughout the entire system.

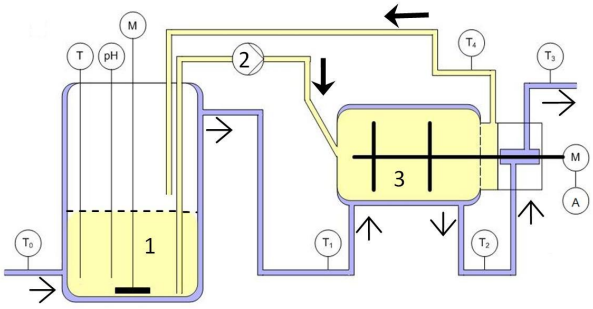

Figure 1 . Grinding set-up and controls, where T is a temperature measurement and pH is a pH control point. Arrows show the circulation of the cooling water (→) and product (➔). The product is pumped from the stirred tank marked as 1 by the pump 2 to the grinding chamber 3. M stands for motor and A for Amp meter.

2.2. Particle size measurement

The particle size distribution was measured two hours after grinding with a forward light scattering (FLS) device (LS13230, Beckman Coulter, USA).

Dynamic Light Scattering (DLS) was carried out with a ZetaSizer (Malvern Instruments, UK) to confirm the results obtained with FLS. DLS analyses particle size on the basis of Brownian motion. The technique is thus limited to analyses of particle sizes below approx. 3 μm. FLS does not have this limitation.

To confirm the results cryo-TEM pictures were taken at the Electron Microscopy Unit of the University of Maastricht, The Netherlands, using the technique as described by Frederik et al. [6,7]. The process of cryonization is quick enough to freeze water to a glassy state and to fix the particles in the suspension.

2.3. Sedimentation measurements

Freshly grinded particle suspensions (1.0% solution with 0.01 mol L^{-1} NaCl) were divided over several bottles. The pH was adjusted to values between 3 and 9 using sodium hydroxide (0.01 mol L^{-1}) and hydrogen chloride (0.01 mol L^{-1}). The ionic strength was thus constant at all pH values. At pH 10, to be able to reach the right pH, the solutions used have ion concentration of 0.05 mol L^{-1}. The amount of acid and base that was required was low compared to the sample volume. The dilution was thus negligible. The pH was set over a period of 48 hours by incremental acid or base dosage until the desired pH was reached. During the process the samples were continuously stirred. After pH adjustment the samples were put in graduated pipettes of 10mL that were closed with a rubber stop to avoid evaporation of liquid. The sedimentation front was recorded over a period of 15 days.

2.4. Zeta potential measurements

The measurements were carried out with freshly prepared suspensions of grinded particles. These suspensions were diluted to 0.1% prior to measurement in the ZetaSizer (Malvern, UK). The ionic strength was fixed to 1 mM using potassium chloride. The zeta potential was as function of pH by automatic titration from pH 3 to 10 using a 4N sodium hydroxide solution.

3. RESULTS AND DISCUSSION

3.1. Characterization by particle size measurements.

Freshly ground product (1.0% solution with 0.01 mol L^{-1} NaCl) had a pH of 5.7. The particle size measurement with FLS indicated the particle size was 180 nm.

In order to confirm these results, DLS measurements were carried out. These measurements showed that the samples contained particles above 1 μm. This finding is contradictory to the FLS measurements. The observed difference is related to the conditions in both measurement devices. In the FLS apparatus the suspension was circulated through the measurement cell, while in the DLS measurement device the suspension did not circulate. The observed difference in particle size is thus related to differences in shear in the two measurement devices. In absence of shear a larger

particle size was measured than at high shear. This indicates that aggregates were formed after grinding, but that these aggregates are weak and break up in a measurement device that exerts shear onto the aggregates, i.e. in the FLS measurements.

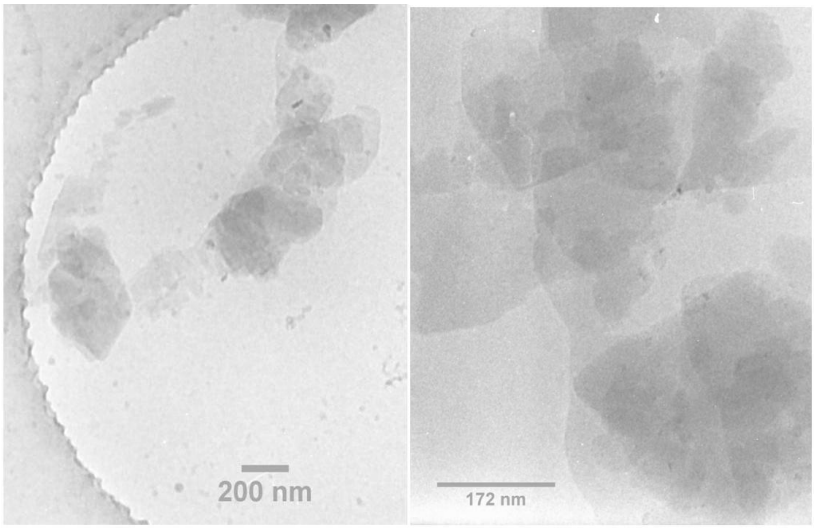

Figure 2 . Cryo-TEM pictures of a ground suspension at pH 5.7 (No buffer)

To confirm this hypothesis cryo-TEM pictures were taken: figure 2 shows aggregates of ground particles. The size of the primary particles corresponds to the size measured by laser diffraction (0.18-0.20 µm). The aggregates were in the micrometer range which corresponds to the DLS measurements. The cryo-TEM pictures thus confirm that aggregates were formed after grinding.

3.2. Sedimentation tests

The sedimentation data are presented in figure 3. The initial sedimentation velocity can be used to determine the aggregate size at t=0, i.e. directly after mixing and setting the pH. Particle sedimentation in these experiments occurred under laminar flow, because the Reynolds number for particle sedimentation was very low in all cases. The suspensions contained 0.76% v/v of organic particles. It is expected that this concentration is low enough to avoid swarm effects in sedimentation. The sedimentation rate of particle swarms is defined by the Richardson-Zaki equation [8,9]:

$$v_{swarm} = v_s \cdot c_V^{\,n} \qquad (1)$$

where v_{swarm} is the sedimentation rate of the swarm, v_s the settling rate of one particle, c_v the volume fraction liquid (c_v = 99.24%), n is a factor dependent on the Reynolds number (Re<0.2 in any case), and can be calculated by:

$$n = 4.6 + 20 \cdot \frac{d_p}{D} \tag{2}$$

where the particle diameter being d_p (d_p = 1.64 µm in the worse case) and the vessel diameter being D (1.0 cm).
For the system that is considered in this work n = 4.60 and the swarm speed is 97% of the settling velocity of the single particles. This confirms that swam effects are negligible in this work. The settling velocity of the particles can thus be expressed by Stokes law:

$$v_s = \frac{(\rho_p - \rho_f) \cdot d_p^2 \cdot g}{18 \cdot \eta_f} \tag{3}$$

with η_f being the fluid viscosity, d_p the stokes particle diameter, ρ_f the fluid density (1000 kg/m^3), ρ_p the particle density and g is the gravitational acceleration. The particle density was measured by sucrose gradient centrifugation [10]. The density of the particles was approx. 1.3 x 10^3 kg m^{-3}.

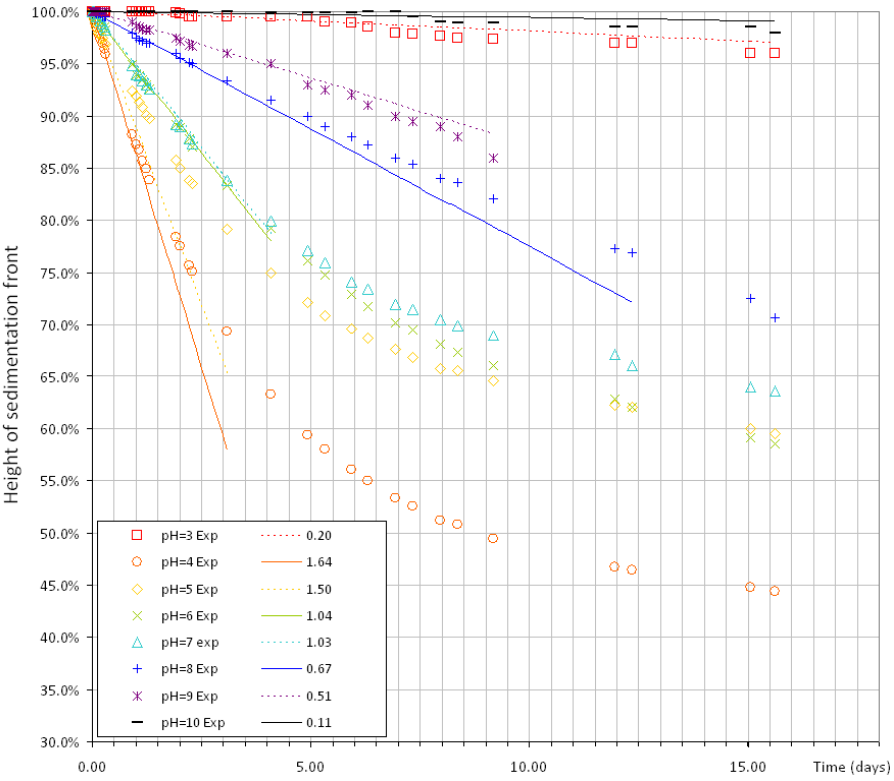

Figure 3 . Sedimentation profile of ground particles as function of pH.
Symbols like O: Experimental Values, lines like –: fitting of Stokes sedimentation theory with indicated aggregate size

Figure 3 depict sedimentation data and fits of the initial sedimentation rates with Stokes law. The graph shows that extreme pH values give higher suspension stability than intermediate pH values. This observation can be explained by the zeta potential measurements that are presented in figure 5. The particle size determined by sedimentation measurements corresponds reasonably well to the cryo-TEM picture in case of unstable suspensions, i.e. highest sedimentation rates. The particle size determined by sedimentation measurements in case of stable suspension, i.e. lowest sedimentation rate, corresponds reasonably well to the forward light scattering measurements.

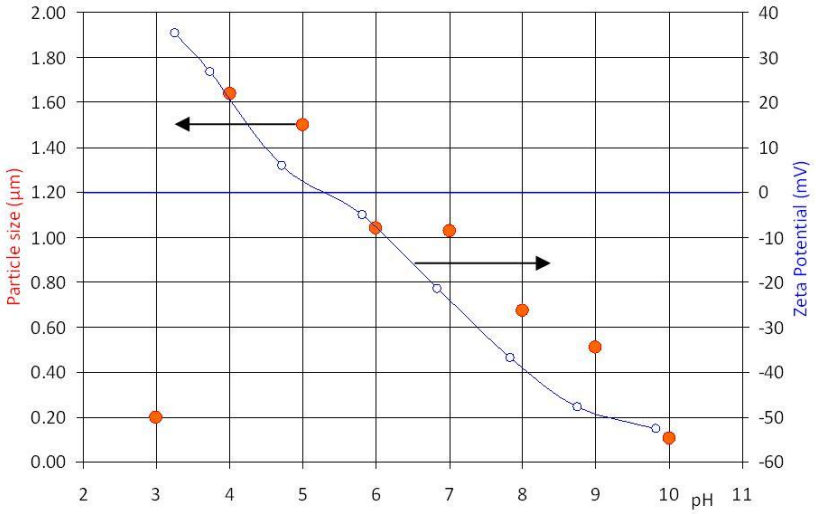

Figure 4 . Zeta-potential (line) and calculated Stokes equivalent particle size (dots) as function of applied pH.

The iso-electric point of the grinded organic product particles is approx. 5.3. The aggregation rate increases when the pH approaches the iso-electric point, which can be explained by the reduction in the electrostatic repulsion between the particles.
At pH 4 the sedimentation seems to be higher than at pH 5 or 6. This is contradictory to the expectations on the basis of the zeta-potential measurements. This contradiction can be explained on the basis of the experimental protocol. The pH of the particle suspensions was set during a period of 48 hour. The pH after grinding was 5.7. The iso-electric point was thus passed for suspensions with a pH below 5.7. The stability during pH control was thus different for samples above pH 5.7 and below pH 5.7. The aggregates that were formed during pH control could be broken up at different rates depending on the zeta-potential and the applied shear. The shear was constant in all cases. It is therefore expected that aggregate break up rate during pH control was higher for more extreme zeta potentials.
An alternative approach would have been to grind the product at the desired pH values instead of setting the pH after grinding in order to avoid passing the iso-electric point for stability testing. Grinding experiment were carried out at various pH values

for the study of the grinding mechanism. It was shown that the grinding kinetics are independent of pH.

4. MODEL INTERPRETATION USING THE DLVO THEORY.

In the described experiments the aggregation rate depended on 1) the Brownian motion of the particles during the sedimentation experiment (perikinetic aggregation) and 2) orthokinetic aggregation during pH change. The latter contributed to the initial sedimentation rate that is considered in this work. The particle interactions are dependent on the shear and the DLVO forces. The DLVO theory describes the forces between charged surfaces interacting through a liquid medium. It combines the effect of the van der Waals attraction and the electrostatic repulsion due to the double layer of counter ions. The electrostatic interaction energy between two spherical particles can be described as follows [11]:

$$V_E = \int F_E = 2 \cdot \pi \cdot \varepsilon_r \cdot \varepsilon_o \cdot d \cdot \zeta^2 \cdot \ln\left(1 + e^{-\kappa \cdot h}\right) \qquad (4)$$

$$\text{if } \frac{d}{2} \rangle\rangle h \text{ and } \kappa \cdot d \rangle\rangle 1$$

where d the diameter of the particles, ε_r the relative permittivity of the fluid (dielectric constant – for water 80), ε_o the permittivity of free space ($8.85 \cdot 10^{-12}$ $F.m^{-1}$), ζ is the zeta potential of the particles, h the distance to the surface, and κ is the reciprocal of the Debye decay length according to Schulze [12]. κ can be calculated by:

$$\kappa = \sqrt{\frac{e^2 \cdot N_{av}}{\varepsilon \cdot k \cdot T} \cdot \sum C_i \cdot z_i^2} \qquad (5)$$

With e the elementary charge ($1.60 \cdot 10^{-19}$ C), N_{av} the Advogadro number ($6.02 \cdot 10^{23}$), ε the actual permittivity of the fluid, k the Boltzmann constant ($1.38 \cdot 10^{-23}$ $m^2.kg.s^{-2}.K^{-1}$), T the temperature in Kelvin, C_i the concentration of ion i and z_i its charge. For samples at pH 6 to 9 the ion concentration was 10.0 mmol/L, while for the sample at pH 10 it was 50.0 mmol/L.

The Van der Waals interaction energy between two particles can be described with the following equation [12,13]:

$$V_{vdW} = -\frac{A_{123}}{24 \cdot h} \cdot d \qquad (6)$$

where A_{123} is the Hamaker constant. The constant depends on the material properties of both the interacting bodies and the intervening medium. The Hamaker constants can be calculated on the basis of the dielectric and optical properties of the interacting materials. This information was not available for the product that is considered in this work.

Various values for the Hamaker constant were therefore evaluated in a range that is typical for biological material, i.e. $1{,}0.10^{-19}$ J to $1{,}0.10^{-18}$ J, as suggested by Sasahara et al.[14].

The sum of the electrostatic and Van der Waals interaction energies is presented in figure 5.

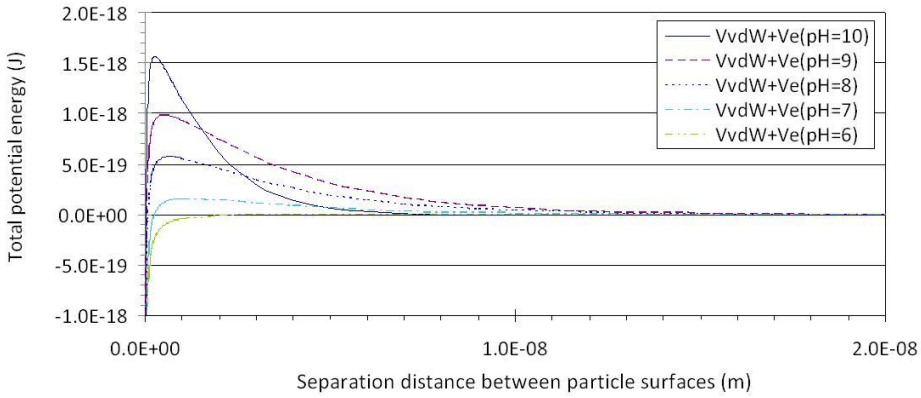

Figure 5 . Interaction energy as function of the separation distance between the particles and the pH of the surrounding fluid (Hamaker constant 10^{-19} J).

The energy barrier that counter acts the formation of aggregates between the particles can be approximated using the energy maximum in figure 5. In all cases the maximum potential energy (figure 5) is reached for distances below 2.10^{-9} m, which is much smaller than the radius of the particles (90.10^{-9}m). The product κ.d (ratio between the particle diameter and the Debye length) is 1800 and thus much higher than 1. Since equation 4 can only be used if d/2 >> h and k.d >> 1, this is proven to be a valid assumption. Equation 4 can thus be used for calculation of the maximum potential energy.
Figure 6 shows the relation between the initial rate of sedimentation and the maximum in the potential energy-distance curve, i.e. the energy barrier.

Verwey and Overbeek [15] showed that particle suspensions with energy barriers of approx. 20 kT are stable for several months in case of perikinetic aggregation. For the system that is considered in this work the initial rate of sedimentation is only affected by orthokinetic aggregation. The energy barrier that is required for obtaining a stable particle suspension can thus differ from the values for perikinetic aggregation. This limit value is higher in case of stirring since additional energy is provided to the particles to interact.

As shown in figure 6 Hamaker values below $5 . 10^{-19}$ J clearly show that with increasing energy barrier the suspensions become more stable. For higher Hamaker constants

this trend is much less clear. It is thus expected that the Hamaker constant is below 5 . 10^{-19} J. The stability of ground particles thus shows a correlation with the energy barrier between the particles.

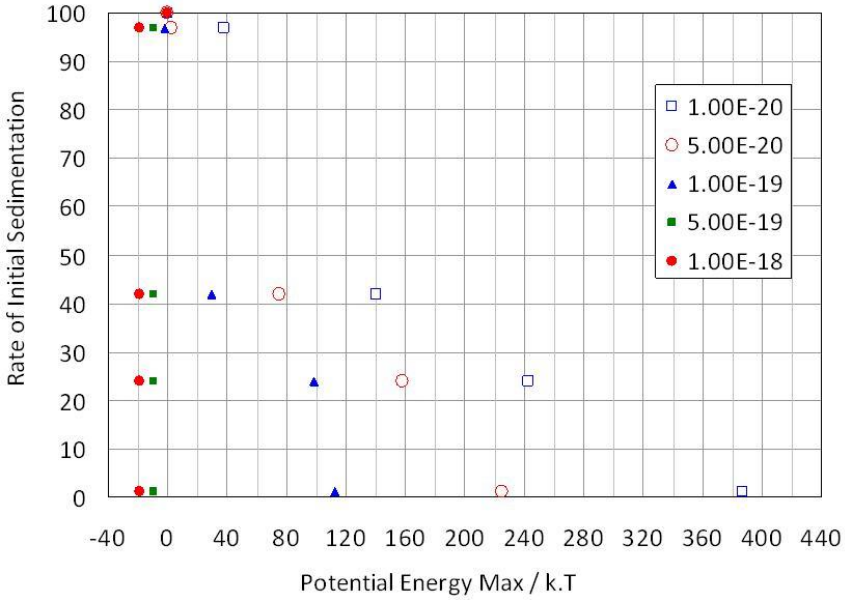

Figure 6 . Experimental determined initial rate of sedimentation versus calculations of the energy barrier at Hamaker constants of 10^{-20}, 5.10^{-20}, 10^{-19}, 5.10^{-19}, and 10^{-18} J.

5. CONCLUSION

In this work the stability of ground organic particles has been studied. Laser diffraction measurement showed that the particle size after grinding was in the sub-micron range. Dynamic light scattering measurements, on the other hand, showed that there were larger particles present after grinding. Cryo-TEM analysis showed that these larger particles were actually aggregates. The difference in the particle size analyses with both techniques was related to the shear in the measurement device, i.e. in the laser diffraction measurement the shear was higher than in the dynamic light scattering device. Thus in the laser diffraction measurement the aggregates were broken up by shear, while this was not the case in the dynamic light scattering measurements.

The stability of the particle suspension was determined by measuring the initial sedimentation rate. This measurement technique shows differences in the aggregate size for different pH values. The zeta-potential of the particles for different pH conditions has been measured. The stability showed good correlation with the zeta-potential measurements via the DLVO theory. The stability of ground particles thus shows a good correlation with the energy barrier between the particles. The higher the energy barrier the less aggregation could occur and the smaller the aggregates

are. The energy barrier increases with an increase of the electrostatic repulsion, i.e. the zeta-potential. The particle suspension becomes more stable when driving away the pH from the iso-electric point.

6. ACKNOWLEDGEMENTS
The authors want to thank: Leon Bremer from DSM ACES, Geleen in the Netherlands for his kind help with the Malvern Zetasizer; Professor Peter Frederic from the University of Maastricht, The Netherlands for the sharp Cryo-TEM pictures; and Maria Christina Domingues, from the University of Coimbra and DSM Biotech Center in Delft, The Netherlands, assisting the authors for early stage grinding experiments.

7. REFERENCES
[1] M. Barzegar-Jalali, H. Valizadeha, M.-R. S. Shadbada, K. Adibkiaa, G. Mohammadia, A. Farahania, Z. Arasha, A. Nokhodchi, Cogrinding as an approach to enhance dissolution rate of a poorly water soluble drug (gliclazide), Powder Technology 197(3) (2010) 150–158.
[2] L. G. Austin, R. S. C. Rogers, Powder technology in industrial size reduction, Powder Technology 42 (1985) 91–109.
[3] S.L.A. Hennart, W.J. Wildeboer, P. van Hee, G.M.H. Meesters, Identification of The Grinding Mechanisms And Their Origin in a Stirred Ball Mill Using Population Balances, Chem. Eng. Sci. 64 (2009) 4123–4130.
[4] S. Mende, F. Stenger, W. Peukert, J. Schwedes, Mechanical production and stabilization of submicron particles in stirred media mills, Powder Technology 132 (2003) 64–73.
[5] L.-S. H. Lum, S. G. Malghan, S. B. Schiller, Standard reference materials for particle size analysis of ceramic powders by gravity sedimentation, Powder Technology 87 (1996) 233–238.
[6] P.M. Frederik, D.H.W. Hubert, Cryoelectron Microscopy of Liposomes, Methods in Enzymology 391 (2005) 431–448.
[7] P.M. Frederik, M.M.H. Storms, Automated, Robotic Preparation of Vitrified Samples for 2D and 3D Cryo Electron Microscopy, Microscopy today (2005) 32–38.
[8] L. Janssen, M. Warmoeskerken, Transport Phenomena Data Companion. Edward Arnold Ltd, London, UK (1987) ISBN 0-7131-3618-9
[9] L. Davies, D. Dollimore, J. H. Sharp, Sedimentation of supsensions: implications of theories of hindered settling, Powder Technology 13 (1975) 123–132.
[0] J.T. Lett, Measurement of single strand breaks by sedimentation in alkaline sucrose gradients. In: E.C. Friedberg and P.C. Hanawalt, Editors, DNA repair — A Laboratory Manual of Research Procedures Vol. 1, Marcel Dekker, New York. (1981) 363–378. ISBN 9-9929-2021-1
[1] D. J. Shaw Introduction to colloid and Surface Chemistry, 3rd edition. Butterworths (1980) 186-202. ISBN 0-19-855386-2
[2] H. J. Schulze, Physico Chemical elementary process in flotation. Developments in mineral processing, Elsevier, Amsterdam (1984). ISBN 0-4449-9643-5.

[3] P.A. Hartley, G.D. Parfitt, L.B. Pollack, The role of the van der Waals force in the agglomeration of powders containing submicron particles, Powder Technology 42 (1985) 35–46.
[4] A. Sasahara, H. Uetsuka, T. Ishibashi, H. Onishi, A needle-like organic molecule imaged by noncontact atomic force microscopy, Applied Surface Science 188 (2002) 265–271.
[5] E.J.W. Verwey, J.Th.G. Overbeek, Theory of stability of lyophobic colloids. Elsevier, Amsterdam (1948) 58-59. ISBN 0-4864-0929-5

Part III

Application of Ground Particles

Distribution of Poorly Soluble Particles in Films and Coatings.

This chapter has been submitted as S.L.A. Hennart, P. van Hee, F. Destaing, A.J. Vis, J. van der Lee, E. Mendes, W.J. Wildeboer, G.M.H. Meesters, Powder Technology (2011)

Abstract – The present work studies the distribution of a poorly water soluble preservative in a coating that is applied on food surfaces. The preservative is present in the coating at concentrations above the saturation concentration. Preservative particles are thus dispersed in the coating. The study focuses on the influence of the preservative particle size on the shelf life of the coated food stuff. The shelf life of the coated food stuff was studied as a function of diffusion, degradation, solubilization, and distribution of the preservative particles in the coating. Model calculations using Fick's law on diffusion including degradation of the preservative were used to determine the distribution of dissolved and particulate preservative throughout the coating as function of time. The maximum shelf life of the coated food stuff was obtained when the preservative concentration reached a level below the minimum inhibitory concentration (MIC) at any location in the coating.
Challenge tests were performed on cheeses using a coating that contained an antifungal compound to verify the model. The challenge tests and the model calculations showed that small preservative particles are more efficient than larger particles when the same concentration of preservative is used in the coating. This is mainly due to the improved distribution of preservative particles in the coating and the fact that diffusion of the preservative is in many cases the limiting factor for optimal distribution of the dissolved preservative. The shelf life of the coated food stuff can thus be enhanced by reduction of the preservative particles in the food coating.

Keywords: Distribution, Diffusion, Sub-micron particles, Food coating, Degradation, Solubility, Characteristic times.

1. INTRODUCTION

Several research groups in the food industry have been studying antimicrobial agents in food and on food surfaces (among others: Teerakarn et al.[1], Gill et al.[2], Vojdani et al.[3], Ouattara et al.[4], Warin et al.[5], Ozdemir and Floros[6,7]). The aim of these studies was to obtain optimal antimicrobial protection of the food stuff. In all the cited papers it is highlighted that the shelf life is systematically dependent on an equilibrium between 1) the molecular diffusivity of the product, 2) the consumption or degradation rate of antimicrobial ingredient, 3) the dissolution behavior and 4) the distribution homogeneity of the particles of the antimicrobial compound. A fifth parameter is the minimum inhibitory concentration (MIC) of the antimicrobial compound. Microorganisms are able to grow in or on the food stuff when the concentration of the antimicrobial compound in solution is below the MIC. The microbial shelf life of the food stuff is thus limited by the time the dissolved preservative concentration remains above the MIC.

Optimization of the microbial shelf life of the coated food stuff requires a study on the interaction between all five parameters that were mentioned above. Diffusivity depends amongst others on the nature of the matrix, temperature, and the size of the antimicrobial compound. Increasing the diffusivity enables a better coverage of the food stuff and may thus lead to an increase of the microbial shelf life of the food stuff when diffusion of the preservative is limiting [8-12]. Consumption and/or degradation of the preservative are dependent on the chemical stability and the presence of microorganisms that are attacked by the antimicrobial compound. Dissolution of the preservative particles depends on the properties of the particles and the surrounding medium and the available surface area for dissolution. The preservative particle distribution is dependent on the preservative dosage and particle size. The critical dissolved concentration of the preservative is given by the MIC for the microorganisms from which the food stuff needs to be protected.

The present work studies the distribution of a poorly water soluble preservative in a coating on a food stuff (see figure 1). The objective is to determine the influence of the preservative particle size on the shelf life of the coated food stuff. In the first part of the work a model is used to evaluate the impact of the above mentioned parameters. Each aspects of the model (diffusion, degradation, dissolution and distribution) are presented before a theoretical model is calculated. In a second part the experimental method for the determination of each aspect is presented. In a third part of the paper the experimental results are given and an accelerated shelf life test is used to experimentally verify the model calculations.
Different sizes of the preservative particles were obtained by wet grinding. Particle sizes of 15 μm and approx. 0.2 μm were tested. The grinding process to obtain these particle sizes has been described elsewhere [13,14].

2. MODELING

The thickness of antimicrobial films or coatings on food stuffs is in the range of 1 to 100 μm. The distance between the preservative particles is often in the same order. In this work coating films with a thickness of 10-30 μm are studied in combination with preservative particles of 0.2 – 15 μm at concentrations where the distance between the preservative particles is in the order of 10 μm. The coating system can thus be regarded as a two dimensional system when diffusion of the dissolved preservative is concerned. This is schematically shown in figure 1.

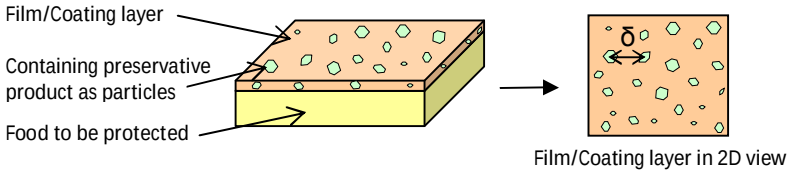

Figure 1 – Schematic representation of the distribution of preservative particles in a coating.

In the two dimensional approach the dissolved preservative concentration C(x,y,t) is a function of time t and the position (x,y) in the coating. The system can be further simplified by zooming in on two preservative particles and describing the dissolved preservative concentration as function of the distance between two preservative particles. This simplification leads to the description in equation 1, where x is the position between two preservative particles that runs from 0 to δ. The equation includes Fick's second law of diffusion [15,16] and a degradation term B(x,t).

$$\frac{\partial C(x,t)}{\partial t} = D \cdot \frac{\partial^2 C(x,t)}{\partial x^2} + B(x,t) \tag{1}$$

Where C is the dissolved preservative concentration (ppm), x the position between two preservative particles (m), t the time (s), D the diffusion coefficient ($m^2.s^{-1}$).

Two approaches are taken for modeling of the coating system. One approach makes use of numerical calculations for determining when the dissolved preservative concentration reaches a concentration below the MIC. A second approach makes use of characteristic times for each of the sub-processes, i.e. dissolution, diffusion and degradation of the (dissolved) preservative, to evaluate the rate limiting steps for preservative action of the coating.

2.1. Diffusion of the preservative

The diffusion coefficient D can be described by equation 2.

$$D = \frac{k \cdot T}{3 \cdot \pi \cdot \eta_f \cdot d_m} \tag{2}$$

where k is the Boltzmann constant, d_m the diameter of the molecule assuming a spherical molecule, η_f the fluid (or matrix) viscosity and T the temperature. The apparent diffusivity will be lower when the molecule is not spherical [21]. The characteristic time for diffusion (τ_{diff}) is defined as the time required for a molecule to diffuse over the distance δ (equation 3). The determination of the distance δ and the diffusion coefficient is explained in the experimental protocols section (paragraph 3.4) and experimental results section (paragraph 4.1, 4.4).

$$\tau_{diff} = \frac{\delta^2}{D} \tag{3}$$

2.2. Degradation of the preservative

The degradation rate of the dissolved preservative is described as a first order chemical degradation reaction:

$$B(x,t) = \frac{dC(t)}{dt} = -k_d \cdot C(t) \tag{4}$$

Where C(t) is the concentration of product at time t (ppm) and k_d the degradation rate constant (s^{-1}). The determination of constant k_d is discussed in the experimental protocols section (paragraph 3.1) and experimental results section (paragraph 4.2).

The characteristic time for degradation (τ_{deg}) is defined as the inverse of the first order degradation rate constant:

$$\tau_{deg} = \frac{1}{k_d} \tag{5}$$

2.3. Dissolution and solubility of the preservative

The dissolved preservative concentration directly after application of the coating to the food stuff is assumed to be equal to the solubility (C_s) of the preservative. This is the starting point for the model calculations, i.e. $C(x,0) = C_s$. The second assumption for the model calculations is that the concentration of dissolved preservative at the preservative particle surface is equal to the solubility of the preservative, i.e. the dissolution rate is much faster than the diffusion and degradation rates. The boundary condition for the model calculations thus is: $C(0,t) = C_s$ and $C(\delta,t) = C_s$. The validity of these assumptions will be proven further on in this paper (paragraph 4.3).
The dissolution rate constant (k_{diss}) for the preservative is defined from Noyes and Whitney [17] as:

$$\frac{dC(t)}{dt} = k_{diss} \cdot (C_S - C(t)) \tag{6}$$

With C(t) the concentration of the preservative in time and C_S the product solubility.
The determination of k_{diss} is presented in the experimental protocols section (paragraph 3.2) and experimental results section (paragraph 4.3).

The characteristic time for the preservative dissolution process (τ_{diss}) is inversely proportional to the dissolution rate constant k_{diss}.

$$\tau_{diss} = \frac{1}{k_{diss}} \tag{7}$$

2.4. Distribution of the preservative and the distance **δ** between two particles.

The shelf life of the coated food stuff is assumed to be equal to the time that is required to reach the MIC for the dissolved preservative at any position in the coating. The most critical point in this respect is the position in the coating where the distance between the preservative particles is the largest. At this position the distance that needs to be traveled by the dissolved preservative molecules from the preservative particle surface, where dissolution takes place, to a position in the middle between two preservative particles is the largest. The biggest gaps in the coating with regard to preservative particle coverage are thus most critical for the shelf life of the coated food stuff.

The determination of this critical gap size in the preservative particle coverage is discussed in paragraph 3.4, results are given in paragraph 4.4.

2.5. Modeling of the coating system

The differential equation describing the system is given by combining equations 1 and 4 (equation 8). The model depends of five parameters: 1) dissolution rate constant, 2) degradation rate constant, 3) diffusivity of dissolved preservative, 4) inter particle distance, and 5) preservative particle size.

$$\frac{\partial C(x,t)}{\partial t} = D \cdot \frac{\partial^2 C(x,t)}{\partial x^2} - k_d \cdot C(x,t) \tag{8}$$

The initial (IC) and boundary (BC) conditions as described in paragraph 2.3 are:

$$\begin{cases} IC: C(x,0) = C_S \\ BC: C(0,t) = C(\delta,t) = C_S \end{cases} \tag{9}$$

With C_S being the solubility of the product in the matrix.

The model has been analytically solved using a Fourier series (see Appendix). Equation 10 shows the solution of equation 8 using the initial and boundary conditions:

$$C(x,t) = C_S + \sum_{n=0}^{\infty} \frac{4 \cdot k_d \cdot \delta^2 \cdot C_S}{D \cdot \left((2 \cdot n+1) \cdot \pi\right)^3 + (2 \cdot n+1) \cdot \pi \cdot k_d \cdot \delta^2} \cdot \left(e^{-\left(D\left(\frac{(2n+1)\pi}{\delta}\right)^2 + k_d\right) \cdot t} - 1 \right) \cdot \sin\left(\frac{(2 \cdot n+1) \cdot \pi \cdot x}{\delta}\right) \tag{10}$$

Equation 10 is valid until the preservative particles are fully dissolved in the coating matrix. At the time noted $t_{ø}$ the preservative particles are fully dissolved and the boundary conditions change into $BC_{ø}$:

$$BC_{ø}: \left.\frac{\partial C(x,t)}{\partial x}\right|_{x=0} = \left.\frac{\partial C(x,t)}{\partial x}\right|_{x=\delta} = -k_d \cdot C(x,t) \tag{11}$$

The time $t_{ø}$ at which the preservative particles are fully dissolved is given by equation 12:

$$m_{part}\Big|_{t=0} = D \cdot S_{part} \cdot \int_{t=0}^{t_{ø}} \left.\frac{\partial C(x,t)}{\partial x}\right|_{x=0} \cdot dt \tag{12}$$

With $\left.\frac{\partial C(x,t)}{\partial x}\right|_{x=0}$ being the flux of product from the particle surface into solution, m_{part} being the mass of the particle and S_{part} the surface of the product particle.

The surface area through which the flux is calculated is considered to be constant in time and equal to the surface area of the preservative particles at t=0. This assumption is acceptable when the distance δ between the preservative particles is much larger than the preservative particle size (d_p). When this is not the case, inaccuracies may be introduced in the calculations. This assumption is reasonable for $\delta/d_p > 10$ but may give inaccuracies for $\delta/d_p < 10$. This approach was chosen to keep the calculation times at acceptable levels. The model is expected to give a reasonable approximation of the order of magnitude of the shelf life and the inaccuracies that are introduced by this assumption are expected to have little influence on the conclusions that are drawn in this work.

The MIC for the microorganisms is assumed to be constant at one third of the solubility of the preservative, C_s. The shelf life of the coated food stuff is thus resembled by equation 13:

$$C\left(\frac{\delta}{2}, t_C\right) = \frac{C_S}{3} \tag{13}$$

Numerical calculations were performed in Matlab in two steps. The first step from t=0 to $t=t_ø$ was calculated using the 500.000 first sum elements from equation 10. The second step was a numerical solution using equation 8, $BC_ø$ from equation 11, and the solution of equation 10 at $t=t_ø$ as starting condition. The number of sum elements used for the Matlab calculation was 5 times the minimum required iteration number to obtain accurate numerical results.

The critical time was determined for a range of values of the characteristic times of diffusion (τ_{diff}) and degradation (τ_{deg}). The characteristic time for dissolution was assumed to be much lower than the characteristic times for degradation and diffusion.

An example of the concentration profiles of the preservative at δ/2 is given in figure 2 for conditions when diffusion is faster than degradation and vice versa. As illustrated, the initial concentration at t=0 is the product solubility C_S. The concentration decreases in time because of the degradation process that is partly compensated by the diffusion from the product particle. The graph shows that when the particles are completely dissolved, at $t=t_ø$, only degradation takes place and a second drop in concentration is observed. The critical time (the shelf life t_C) is reached when the concentration at δ/2 is of one third of the product solubility C_S. When the characteristic diffusion time for degradation is higher than the characteristic time for diffusion ($\tau_{deg} > \tau_{diff}$) then $t_C > t_ø$, and vice versa.

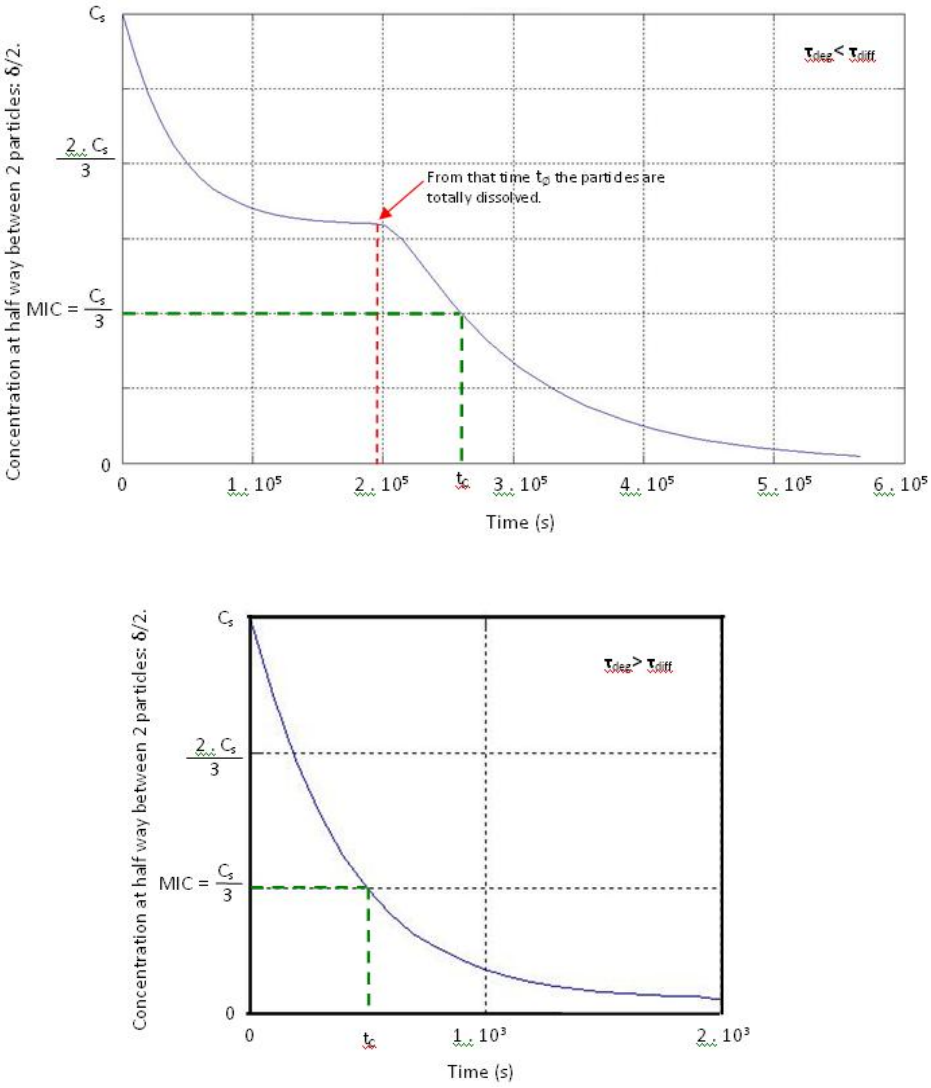

Figure 2 . Concentration profile of active product at equal distance between two particles: C (δ/2, t)

Top: The shelf life is reached after the preservative particles are fully dissolved ($t_C > t_Ø$). Bottom: The shelf life is reached before the preservative particles are fully dissolved ($t_C < t_Ø$).

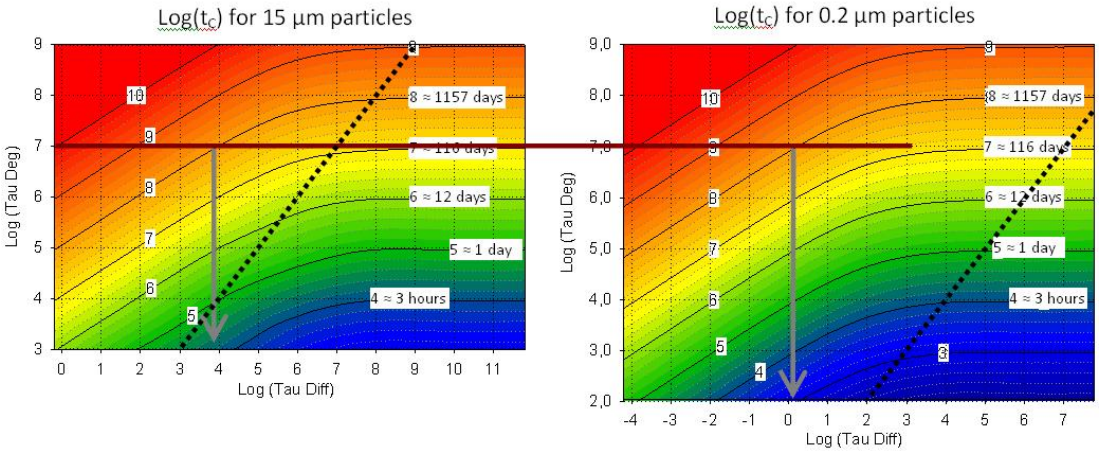

Figure 3 – Contour plots of the characteristic times for diffusion (τ_{diff}) and degradation (τ_{deg}) calculated with a diffusion constant D of 6.16 . 10^{-14} $m^2.s^{-1}$ (cf. paragraph 4.1). The critical times, i.e. the shelf life of the coated food stuff, was calculated with the numerical model that has been described in section 2. The values in the contour plots represent time in 10^x seconds.
The short dotted line represents the limit for which $\tau_{diff} = \tau_{deg}$.

Results of the shelf life calculations are presented in Figure 3. The numerical model takes into account the diffusion rate constant, the degradation rate constant, preservative particle size, and the inter-particle distance for the preservative particles. The model is used to calculate the shelf life of the coated food stuff, t_C. The shelf life is depicted in figure 3 as function of the characteristic degradation time τ_{deg} and the characteristic diffusion time τ_{diff}. The characteristic time for degradation is dependent on the stability of the product in the coating and is thus not influenced by the particle concentration or particle distribution. The characteristic time for diffusion is dependent on the inter-particle distance and thus on the particle number concentration and the particle distribution. $t_ø$ is a function of the flux of product from the particle surface into solution and thus from the diffusion coefficient, the inter-particle distance and the degradation rate (equation 10). The calculations in figure 3 are only valid for the specific diffusion coefficient that was used. If a different diffusion coefficient is used differences can be expected.

The impact of particle size is determined by comparing data from the left and the right graphs in figure 3 at constant preservative dosage. An increase in preservative particle size at constant preservative concentration causes the number concentration of preservative particles in the coating to decrease, and thus gives an increase in inter-particle distance. In this fashion the particle size has an effect on the distribution of preservative particles and thus on τ_{diff}. In addition, particle size affects the time for complete dissolution of the preservative particles, $t_ø$, which in most cases has an

impact on the shelf life of the coated food stuff. The choice has been made to represent the shelf life, t_C, as function of the characteristic degradation time τ_{deg} and the characteristic diffusion time τ_{diff}. Different plots are thus required to represent different preservative particle sizes, i.e. 15 µm and 0.2 µm.

The numerical calculations show that a small characteristic diffusion time and a high characteristic degradation time are the best for a long shelf life, which is logical because under these conditions diffusion of dissolved preservative molecules is much faster than degradation of dissolved preservative molecules. Under these conditions the diffusion process is fast enough to supply preservative throughout the coating without degradation causing local dips in the dissolved preservative concentration. The opposite, a short characteristic degradation time and a long characteristic diffusion time, gives a short shelf life because the diffusion process is not fast enough to allow for rapid replacement of degraded preservative in the coating.

The effect of preservative particle size is clearly shown by comparison of the two graphs in figure 3. An example is plotted in figure 3: at a given characteristic degradation time ($\tau_{deg} = 10^7$ s) and a required shelf life ($t_C = 10^8$ s) the characteristic diffusion time is significantly lower when using smaller preservative particles (15 µm particles: $\tau_{diff} = 10^{3.8}$s; 0.2 µm particles: $\tau_{diff} = 10^0$ s).

Should the diffusion constant for the preservative is a given. A lower characteristic time for diffusion thus implies a shorter inter-particle distance. This implies that in order to get the same shelf life a shorter inter-particle distance is required when working with smaller particles. It will be shown in a later section that the required shorter inter-particle distance can be reached with the smaller particles even at lower product concentration than that of the larger particles.

The calculations showed in Figure 3 are done using the diffusion coefficient D fixed (value discussed in paragraph 4.1). The contour plot is obtained by variation of the inter-particle distance δ. When referring to the equation 3 and 10, the concentration profile of the product c(x,t) is a function of the τ_{diff} and becomes independent of D and δ (Equation 14).

$$C(x,t) = C_S + \sum_{n=0}^{\infty} \frac{4 \cdot k_d \cdot \tau_{diff} \cdot C_S}{((2 \cdot n+1) \cdot \pi)^3 + (2 \cdot n+1) \cdot \pi \cdot k_d \cdot \tau_{diff}} \cdot \left(e^{-\left(\frac{1}{\tau_{diff}} \cdot ((2 \cdot n+1) \cdot \pi)^2 + k_d\right) \cdot t} - 1 \right) \cdot \sin\left(\frac{(2 \cdot n+1) \cdot \pi \cdot x}{\delta}\right) \qquad (14)$$

The time at which the preservative particles are fully dissolved $t_ø$ is a function of the flux of product from the particle surface into solution and the diffusion coefficient (equation 12). In the case that the critical time is larger as the time at which particles

are fully dissolved ($t_C > t_\varnothing$), two identical characteristic diffusion times but from different diffusion coefficient will lead to two different values of the critical time.

The calculations in figure 3 being done assuming a fix diffusion coefficient are only valid for any diffusion coefficient when the critical time is shorter as the time at which the preservative particles are fully dissolved ($t_C < t_\varnothing$). In the case that the critical time is longer as the time at which the preservative particles are fully dissolved ($t_C > t_\varnothing$), the calculation are only valid for the diffusion coefficient of the studied product ($D = 6.16 . 10^{-14}\ m^2.s^{-1}$).
The critical time is longer as the time at which the preservative particles are fully dissolved ($t_C > t_\varnothing$) when the characteristic diffusion time for degradation is longer as the characteristic time for diffusion ($\tau_{deg} > \tau_{diff}$). Inversely, the critical time is shorter as the time at which the preservative particles are fully dissolved ($t_C < t_\varnothing$) when the characteristic diffusion time for degradation is shorter as the characteristic time for diffusion ($\tau_{deg} < \tau_{diff}$).

The flattening of the curve in figure 3 for high characteristic diffusion time (on the right hand side of the dotted lines) is related to the balance between the degradation rate and the diffusion rate. The contribution of the preservative particles (i.e. preservative particle concentration, distribution and size) is diminished when the degradation rate is much higher than the diffusion rate. Under these conditions the molecules that dissolve from the particle surface will be degraded before they can distribute over the coating. This causes the shelf life to be mainly dependent on the dissolved preservative concentration at t=0 and the degradation rate.

3. EXPERIMENTAL METHODS.

3.1. Measurement of the degradation rate constant.

The degradation rate constant was determined in the coating prior to application at room temperature in absence of light. The preservative concentration was measured as function of the storage time. The initial preservative concentration was 6.5 times the value of the solubility C_S. First order degradation reaction kinetics (Equation 4 with n=1) were fitted to the experimental data.

In application the preservative-containing coating will be exposed to another environment. The preservative will undergo more potential degradation mechanisms such as oxidation due to contact with air and higher microbial contamination which may give enhanced consumption of the preservative. The degradation rate constant that has been measured in this work is thus expected to be an underestimation of the degradation rate constant that can be encountered in application.

3.2. Measurement of the dissolution rate.

Preservative particles of 15 and 0.2 μm were dispersed in a phosphate buffer (0.01 M, pH=6.2) at various concentrations. The mixtures were stirred at ambient conditions and samples were taken in time. The preservative particles were removed from the

samples by filtration using a 0.02 µm syringe filter. The preservative concentration in the filtrate was determined using UV-VIS spectrophotometry.

In the actual coating system dissolved polymer is present. The dissolution measurements thus deviate from the real life application. The introduction of polymers makes the measurement much more complex. The filter used in the filtration would block due to these polymers. Centrifugal separation of the particles from the liquid phase would not be possible because of the high viscosity of the liquid phase and the small particle size of the preservative particles. Nevertheless, it is expected that the dissolved polymers do not have a significant impact on the solubility of the preservative.

3.3. Characterization of the distribution of the particles in the matrix

Inhomogeneities in the preservative particle distribution are unfavorable for the shelf life of the coated food stuff because inhomogeneities result in larger inter-particle distances locally in the coating matrix. An increase in inter-particle distance gives an increase in the diffusion distance and thus shifts the balance between the diffusion rate and the degradation rate in favor of the degradation rate. The process of dispersing the particles in the matrix should thus be optimized to achieve a homogeneous preservative particle distribution. In the present case study the particles were well mixed throughout the coating matrix. The coating was applied by dipping the food stuff into the coating. The applied coating was dried at ambient conditions. This procedure is expected to give a random distribution of the preservative particles in the applied coating.

3.4. Calculation of the inter-particle distance distribution

As represented in figure 1, the preservative particles are projected onto a 2D surface. Assuming a random particle distribution in the coating matrix, the distribution of squares that do not contain any preservative particles can be calculated analytically using the Bose-Einstein statistics. The number of empty squares M_{empty} is calculated as function of the total number of squares M and the number of particles N according to the following equation:

$$M_{empty} = \frac{M \cdot (M-1)}{M+N-1} \tag{14}$$

The probability P that a square surface area is empty is equal to the fraction of empty squares:

$$P = \frac{M_{empty}}{M} = \frac{(M-1)}{M+N-1} \tag{15}$$

Equation 15 gives the probability distribution for the empty square size. Given a confidence interval (probability P) and a concentration (number of particles N), the

value of the number of cells (M) can be calculated (equation 15). The surface area of a cell is calculated as the ratio between the surface area of coating and the corresponding number of cells (M) (Equation 16).

$$\text{Surface area of 1 cell} = \frac{1}{M} = \frac{1}{\frac{P}{1-P} \cdot N_{part} + 1} \quad (16)$$

The inter-particle distance distribution δ_p is taken as the diagonal size of the empty squares and can be calculated for a given confidence interval P equation 17.

$$\delta_P = \sqrt{2} \cdot \sqrt{\frac{1}{\frac{P}{1-P} \cdot N_{part} + 1}} \quad (17)$$

With P being the confidence interval (P=0.90 corresponds to δ_{90}, which indicates that 90% of the empty squares are smaller than the given value) and N_{part} being the number of product particles per unit surface area. The number of particles per unit surface area is calculated from the preservative concentration, the coating thickness and the preservative particle size.

3.5. Accelerated shelf life test; determination of antimicrobial activity of the coating.

Freshly brined Gouda cheeses were challenged with Penicillium discolor and coated with various coating formulations to determine the relation between shelf life and coating formulation. Coatings with various preservative particle sizes were applied. The methods that were used to obtain these preservative particle sizes are reported by Van Hee et al [18]. The number of mould spores that was able to germinate on the treated cheese surfaces is indicative for the anti-fungal activity of the preservative in the coating. The cheeses (10 per coating type) were considered to be no longer protected by the product when 50% of the cheeses analyzed had at least one growing colony on their surface.

Plasticoat (DSM Food Specialties, The Netherlands) was used as a coating. Several preservative concentrations with various particle sizes were added to this coating. The cheeses were contaminated with Penicillium discolor PED1, CR1A and Penicillium discolor PED74, L1 spores at a concentration of 1.1×10^3 cm^2 after application of the coating. The cheeses were visually checked for fungal growth on a daily basis for three weeks. The experiment was carried out with two different preservative particle sizes ($d_{4,3}$), i.e. 15 µm and 0.2 µm.

4. EXPERIMENTAL RESULTS AND DISCUSSION

4.1. Determination of the diffusion coefficient.

Over the last decades several methods have been developed to measure diffusion coefficients in liquid systems [19-21]. One example is the measurement of the

diffusivity of preservatives in whey protein films by Franssen et al. [22] Pieces of films were placed between 2 mesh screens and immersed into a large amount of water/glycerol mixture. The concentration profile in time into the liquid phase could be determined. The diffusion coefficient were determined from the data obtained using the Fick's law for plane sheets defined by Crank [23].

The preservative that is used in this case study has a diffusion coefficient ranging from 6.16×10^{-14} to 37.8×10^{-14} m^2s^{-1} at 24°C in whey protein edible films [21]. The matrix used in the present application contains is composed of Plasticoat (DSM Food Specialties, Delft). The diffusion coefficient is dependent on the nature of the matrix. Franssen et al. [21] showed that the increase of plasticizer decreases the diffusion coefficient of the active product in the matrix. When used in protein films with up to 50% (w/w) plasticizer (glycerin), the diffusivity increases up to 6 times. This is probably due to the change in viscosity. No specific measurements have been carried out with the coating that is investigated in this work, i.e. Plasticoat. The diffusivity that is used in this research is assumed to be $D= 6.16 \times 10^{-14}$ m^2s^{-1}, which is the lowest value that was reported for the whey protein films [21].
Givne a molecule size of 1nm, the value of the diffusivity would correspond to a viscosity of 7.10^{23} Pa.s. This is in the order of magnitude of viscosity between hard resins to glass.

4.2. Measurement of the degradation rate constant

The degradation rate constant was determined according to the method that is described in paragraph 3.1. Figure 3 depicts the measurement results. The degradation rate constant that was obtained from the fit of the data using equation (4) is 8.13×10^{-8} s^{-1}. R^2 of the fit was 0.94, which indicates that the assumption of first order degradation kinetics seems appropriate.

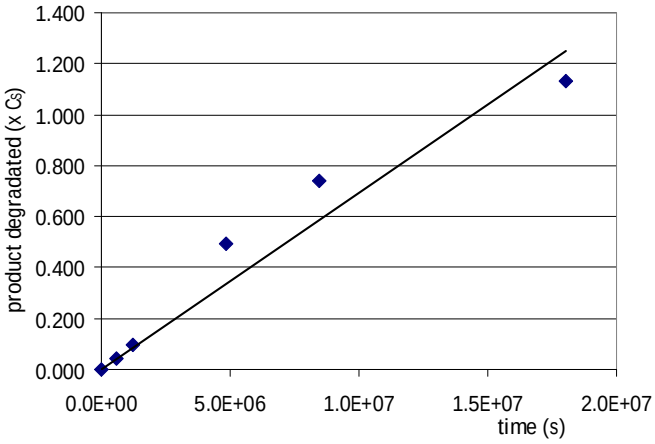

Figure 3 – Degradation of preservative as function of time.

4.3. Measurement of the dissolution rate constant of the preservative

The dissolution profile of the preservative in water has been measured experimentally. For both ground and not ground particles the same total quantity of preservative has been added to the same volume of buffered solution. As shown in Figure 4 ground particles dissolve much faster than larger particles.

k_{diss} that was obtained for 0.2 μm particles from the fit of the experimental data is 0,95 s^{-1}. For the 15 μm particles this was 0.05 s^{-1}.

The characteristic time for dissolution is:

For 15μm particles, $\tau_{diss,15\mu m} = 10^{1.3}$ s

For 0.2μm particles, $\tau_{diss,0.2\mu m} = 10^{0.02}$ s

As set in paragraph 2.3, the model is valid for values of τ_{diff} and τ_{deg} higher than 10 times the τ_{diss}:

For 15μm particles, τ_{diff}, $\tau_{deg} > 10^{2.3}$ s

For 0.2μm particles, τ_{diff}, $\tau_{deg} > 10^{1.0}$ s

The rate of dissolution is an important aspect part of the model. As mentioned in paragraph 2.3, the model will only be valid if the characteristic dissolution time (τ_{diss}) is much smaller than the characteristic diffusion time (τ_{diff}) and the characteristic degradation time (τ_{deg}).

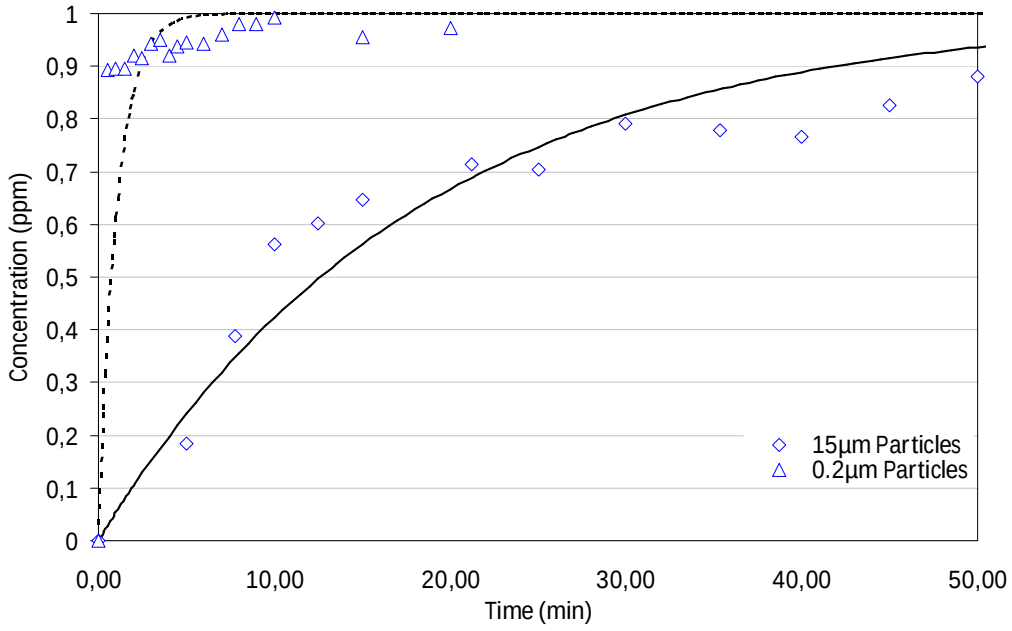

Figure 4 . Concentration of dissolved preservative in water as function of time.

(data points represent measurement data and lines are fits)

4.4. Inter-particle distance distribution

The inter-particle distance δ is calculated from equation (16) for two confidence intervals, 50% and 90%. These confidence intervals show the percentage of gap sizes smaller than the value that is indicated in figure 5. The figure shows that the average inter-particle distance for 0.2 μm particles is much smaller than for 15 μm particles at constant preservative dosage. This is logical because a reduction in particle size at constant preservative concentration results in an increase in the particle number concentration and therefore a reduction of the inter particle distance.

As mentioned in section 2.5 the model is accurate if the inter-particle distance is at least 10 times larger than the particle size x_i. Figure 5 can be used to determine when this is the case:

For 15 μm particle $\delta_{50} > 150$ μm → $C_T/C_S < 70$
For 15 μm particle $\delta_{90} > 150$ μm → $C_T/C_S < 700$
For 0.2 μm particle $\delta_{50} > 2$ μm → $C_T/C_S < 2$
For 0.2 μm particle $\delta_{90} > 2$ μm → $C_T/C_S < 9$

The model as plotted in figure 6 will be valid in case the concentrations considered are above the limits calculated. The corresponding τ_{diff} can be read from the figure.

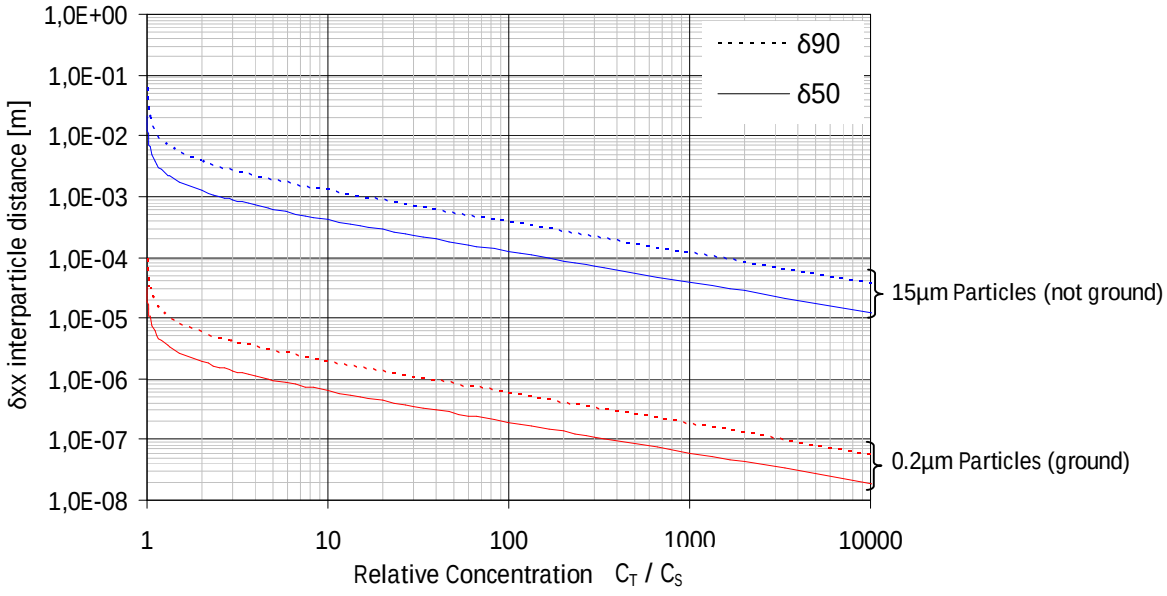

Figure 5 – The inter-particle distance distribution (δ_{50} and δ_{90}) for random distributed particles in a matrix as function of the total particle concentration C_T (coating thickness 10^{-4} m).

4.5. Experimental results of the Accelerated shelf life test

10 cheeses were tested per preservative particle size. As a reference a coating without preservative was tested. The results are presented in Table 2.

Table 2 – Microbial shelf life of coated cheese (the time indicates when 50% of the cheeses had at least 1 mould colony; the standard deviation indicates the measurement variation for each set of 10 cheeses).
Letters correspond to experimental data points in Figure 6.

	Product Relative Concentration (C_T/C_S)			
Particle Size	0.0	3.0	5.0	8.3
15 µm	4 days	-	10.7 ± 2.1 days (B)	11.3 ± 3.0 days (D)
0.2 µm		19.6 ± 4.5 days (A)	20.1 ± 9.6 days (C)	-

The results show that the protection against fungal growth increases when the preservative concentration is increased and/or smaller preservative particles are used.

4.6. Experimental results versus model forecasts.

Figure 6 shows a comparison between the challenge tests from table 1 and the model calculations from section 2.

τ_{diff} was calculated using the diffusion coefficient discussed in section 4.1 and the inter-particle distance δ that was calculated in section 4.4. The preservative concentration corresponding to the inter-particle distance is plotted on parallel axes. One axis indicates the value of the concentration of preservative when defining the inter-particle distance as the value of δ_{50}. The other axis indicates the value of the concentration of preservative when defining the inter-particle distance as the value of δ_{90}. The domain of inaccuracy of the model is indicated by the diagonal patterned areas. The upward diagonal zone indicates the area where characteristic dissolution time approaches characteristic time of diffusion and degradation ($\tau_{diff} < 10\ \tau_{diss}$ and $\tau_{deg} < 10\ \tau_{diss}$). The downward diagonal zone indicates where the inter-particle distance approaches 10 times the particle size.

The challenge test results are summarized in figure 6. All challenge tests were performed under the same conditions, which implies that τ_{deg} should be the same for all data challenge test data. The experimental data have been plotted for different definitions of the inter-particle distance. The inter-particle distance for the challenge tests was calculated on the basis of the particle concentrations that were applied. .

The measured characteristic degradation time (cf section 4.2 - dash dotted line in figure 6) is higher than of the value that is indicated by the challenge tests. This is probably due to the fact that in the challenge test the coating dries after application. The degradation rate is dependent on the water content in the coating, because the

water content determines the amount of preservative that can be dissolved. Less preservative is dissolved when the water content is low and thus less preservative is susceptible to degradation in a dry coating.

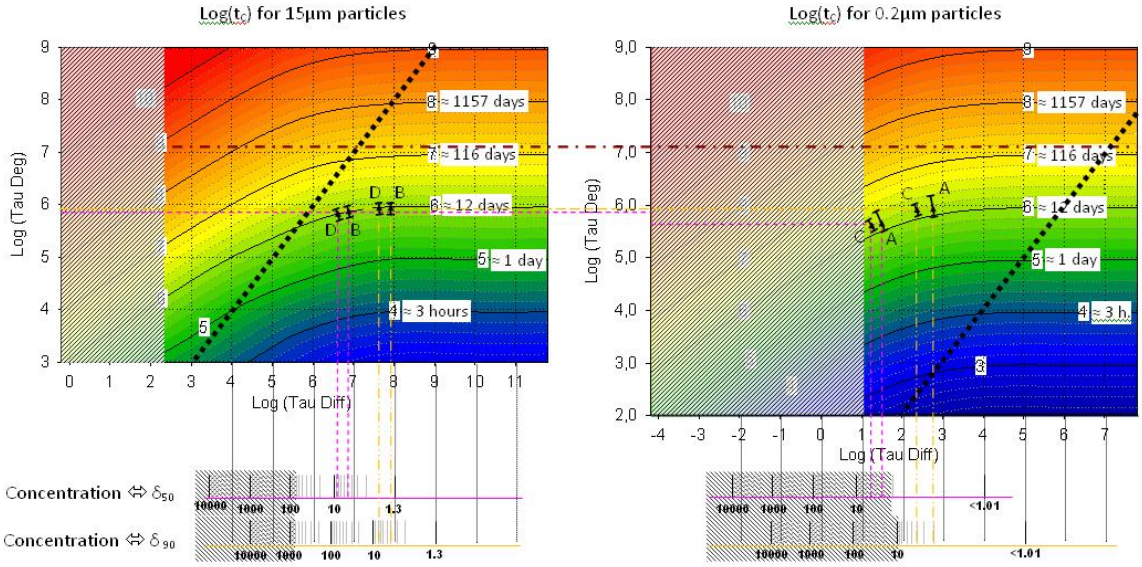

Figure 6 – Critical time (in seconds) as function of the characteristic times to diffusion (τ_{diff}) and degradation (τ_{deg}).

- *Relative concentration scales (C_T/C_S) are plotted at the corresponding values of the τ_{diff} depending on the definition of the parameter δ (δ_{50} and δ_{90} from the distribution of distance between particles).*
- *Thick short dotted line represents the limit for which $\tau_{diff} = \tau_{deg}$.*
- *Dash dotted line: Characteristic degradation time of preservative in the wet coating.*
- *Short Dashed line: Characteristic degradation time and characteristic diffusion time for the accelerated shelf life test considering δ_{50} as the interparticle distance. Letters correspond to the experiment results in Table 1.*
- *Long double dashed line: Characteristic degradation time and characteristic diffusion time for the accelerated shelf life test considering δ_{90} definition of parameter δ. Letters correspond to the experiment results in Table 1.*
- *Upward diagonal patterned zone: Characteristic dissolution time approaches characteristic time of diffusion (=less than one order of magnitude difference). The model will thus be inaccurate in this range, because the dissolution rate is not taken into account in the model (cf section 4.3).*
- *Downward diagonal patterned zone: The interparticle distance approaches the particle size. The model will thus be inaccurate in this range (cf section 4.4).*

When using the δ_{50} definition of the distance distribution a difference between the measured and the predicted τ_{deg} can be observed (short dashed lines in figure 6). The

difference in τ_{deg} for 0.2 μm ($\tau_{deg} = 10^{5.90}$) and 15 μm particles ($\tau_{deg} = 10^{5.65}$) is rather large. Most probably, the definition of δ is then not appropriate. A better fit is obtained taking the definition of δ as the δ_{90} from the distribution of inter-particle distances (double dashed lines in figure 6). The measurement of the shelf life considers the first growing colony on a cheese. In the challenge test spores are spread over the cheese in a homogeneous fashion. The biggest inter-particle distance is thus expected to be most appropriate for determination of the shelf life. The δ_{90} definition is thus preferred and gives a good correlation between the model calculations and the challenge test.

Figure 6 shows that smaller particles offer a better protection of the coating at constant preservative dosage. The impact of preservative concentration on the shelf life is limited compared to the change in preservative particle size, at least within the tested ranges.
The objective of this work is to obtain the desired shelf life with a minimum preservative dosage. The optimal preservative particle formulation is dependent on the properties of the system, such as the characteristic time to degradation (τ_{deg}) and the diffusion coefficient. A characteristic time of diffusion much higher than of the characteristic time of degradation ($\tau_{diff} > 10 \cdot \tau_{deg}$) implies that the particles will not dissolve completely before the shelf life is reached. Under these conditions diffusion is then the limiting factor. Inversely, a characteristic time of diffusion much smaller than that of degradation will increase the coating shelf life. The preservative degradation process will then determine the shelf life. In this case all preservative particles will be dissolved before the shelf life is reached.

5. CONCLUSION

Model calculations on the distribution of a preservative in a coating were used to determine the microbial shelf life of a coated food product. A case study was performed with a cheese coating containing an anti-fungal compound with low solubility. The preservative was dosed to the coating at concentrations above its saturation concentration. Preservative particles were thus dispersed in the coating. The anti-fungal compound is active only in dissolved state. The dissolution, diffusion and degradation behavior of the anti-fungal compound thus affect the anti-microbial protection that is given by the coating. In addition, the inter-particle distance is of importance. The weakest points in the coating are in the middle between the preservative particles.

The model has shown that an optimum shelf life can be obtained when the characteristic time for diffusion is much shorter than the characteristic time for degradation. The characteristic time for diffusion can be controlled by optimizing the inter-particle distance, i.e. a reduction of the inter-particle distance gives a reduction of the characteristic time for diffusion. At constant preservative concentration the inter-particle distance can be reduced by reduction of the preservative particle size.

The impact of the preservative concentration decreases dramatically when the characteristic time for diffusion is much larger than the characteristic time for degradation. This is due to the fact that the diffusion process is too slow to replenish the degraded preservative in between the preservative particles. Under these conditions the shelf life is mainly determined by the dissolved preservative concentration at t=0 and preservative particles will be present in the coating when the shelf life is reached. This implies that the preservative is not used very efficiently, because not all the preservative that is present in the coating is used for the anti-microbial action of the coating.

Experimental results show that the microbial shelf life of coated cheeses increases with an increase in preservative concentration and/or with a reduction in preservative particle size at constant preservative dosage. These findings correspond to the model calculations. The model gave a reasonable prediction of the accelerated shelf life test. The model shows that the distribution of the preservative particles throughout the coating is of great importance. Such a model can be used to find the optimum formulation for food coatings including the optimum particle size and concentration of active ingredient.

6. ACKNOWLDEGEMENTS
The authors want to thank Henk Schuttelaars from the Delft Institute of Applied Mathematics/Mathematical Physics, at the Delft University of Technology in the Netherlands for his kind help with the analytical solution for the differential equations. Kees van Hee should be thanked for helping in the calculation of the inter-particle distance.

7. NOMENCLATURE

$B(x,t)$: birth/death term [$ppm.s^{-1}$]
$C(x,t)$: concentration of product [ppm]
C_S : solubility [ppm]
d_m : diameter of a molecule [m]
D : diffusion coefficient or diffusivity [$m^2.s^{-1}$]
k : Boltzmann constant [$m^2.kg.s^{-2}.K^{-1}$]
k_d : constant of degradation [first order: s^{-1}]
k_{diss} : constant of dissolution [first order: s^{-1}]
m_{part} : mass of one particles [kg]
$N_{particles}$: number of particles [-]
S_{part} : surface area of a particle [m^2]
t : time [s]
t_C : microbial shelf life of coated food stuff [s]
$t_ø$: time at which particles are dissolved [s]
T : temperature [K]
$V_{suspen.}$: volume of suspension in the system [m^3]
x : position [m]
x_i : particle size [m]

α : proportionality factor [$m.s^{-1}$]
δ : distance between two particles [m]
η_f : viscosity [Pa.s]
τ_{diff} : characteristic time of diffusion [s]
τ_{deg} : characteristic time of degradation [s]
τ_{diss} : characteristic time of dissolution [s]

8. APPENDIX

Resolution of the differential equation:

$$\frac{\partial C(x,t)}{\partial t} = D \cdot \frac{\partial^2 C(x,t)}{\partial x^2} - k_d \cdot C(x,t)$$

$$\text{with } \begin{cases} C(x,0) = C_S \\ C(0,t) = C(\delta,t) = C_S \end{cases}$$

The resolution of the equation is done by change of variable:

$$V(x,t) = C(x,t) - C_S$$

The equation becomes:

$$\frac{\partial V(x,t)}{\partial t} = D \cdot \frac{\partial^2 V(x,t)}{\partial x^2} - k_d \cdot V(x,t) - k_d \cdot C_S$$

When using the Fourier series approach, the Eigen functions are assumed to be like

$$V(x,t) = \sum_{n=1}^{\infty} a_n(t) \cdot \sin\left(\frac{n \cdot \pi \cdot x}{\delta}\right)$$

Writing

$$C_S = \sum_{n=1}^{\infty} a_n \cdot \sin\left(\frac{n \cdot \pi \cdot x}{\delta}\right)$$

leads to

$$a_n = \frac{2}{\delta} \int_0^{\delta} C_S \cdot \sin\left(\frac{n \cdot \pi \cdot x}{\delta}\right) \cdot dx$$

Thus

$a_n = 0$ if n even;

$$a_n = \frac{4 \cdot C_S}{n \cdot \pi} \text{ if n odd.}$$

And the equation (2) becomes:

$$\sum_n \frac{\partial a_n}{\partial t} \cdot \sin\left(\frac{n \cdot \pi \cdot x}{\delta}\right) = \sum_n \left(-a_n \cdot \left(\frac{n \cdot \pi \cdot x}{\delta}\right)^2 - k_d \cdot a_n - \frac{4 \cdot k_d \cdot C_S}{n \cdot \pi} \right) \cdot \sin\left(\frac{n \cdot \pi \cdot x}{\delta}\right)$$

Using the border conditions before particle is totally dissolved:

$$\frac{\partial a_n}{\partial t} = -\left(D \cdot \left(\frac{n \cdot \pi}{\delta}\right)^2 + k_d \right) \cdot a_n - \frac{4 \cdot k_d \cdot C_S}{n \cdot \pi}$$

By integration:

$$a_n = a_n(0) \cdot e^{-\left(D \cdot \left(\frac{n \cdot \pi}{\delta}\right)^2 + k_d\right) \cdot t} - \frac{4 \cdot k_d \cdot \delta^2 \cdot C_S}{D \cdot (n \cdot \pi)^3 + n \cdot \pi \cdot k_d \cdot \delta^2}$$

The initial conditions describes that $a_n(0) = 0$ and thus :

$$a_n(t) = \frac{4 \cdot k_d \cdot \delta^2 \cdot C_S}{D \cdot (n \cdot \pi)^3 + n \cdot \pi \cdot k_d \cdot \delta^2} \cdot \left(e^{-\left(D \cdot \left(\frac{n \cdot \pi}{\delta}\right)^2 + k_d\right) \cdot t} - 1 \right)$$

This leads to the full solution (equation 10 in section 2.5):

$$C(x,t) = C_S + \sum_{n=0}^{\infty} \frac{4 \cdot k_d \cdot \delta^2 \cdot C_S}{D \cdot ((2n+1) \cdot \pi)^3 + (2n+1) \cdot \pi \cdot k_d \cdot \delta^2} \cdot \left(e^{-\left(D \cdot \left(\frac{(2n+1) \cdot \pi}{\delta}\right)^2 + k_d\right) \cdot t} - 1 \right) \cdot \sin\left(\frac{(2n+1) \cdot \pi \cdot x}{\delta}\right)$$

9. REFERENCES

[1] A. Teerakarn, D.E. Hirt, J.C. Action, J.R. Rieck, P.L. Dawson, Nisin Diffusion in Protein Films: Effect of Film Type and Temperature, J Food Sci 67(8) (2002) 3019–25.

[2] C.O. Gill, A review. Intrinsic bacteria in meat, J Appl Bact. 47 (1979) 367–78.

[3] F. Vojdani, J.A. Torres, Potassium Sorbate Permeability of Methylcellulose and hydroxypropyl methylcellulose coatings: Effect of fatty acids. J Food Sci 55 (1990) 841–46.

[4] B. Ouattara, R.E. Simard, G. Piette, A. Begin, R.A. Holley, Diffusion of acetic and propionic acids from chitosan-based antimicrobial packaging films. J Food Sci 65 (2000) 768–73.

[5] F. Warin, V. Gekas, A. Voirin, P. Dejmek, Sugar diffusivity in agar gel/milk bilayer systems. J Food Sci 62 (1997) 454–456.

[6] M. Ozdemir, J.D. Floros, Film composition effect on diffusion of potassium sorbate through whey protein films, J Food Eng 68 (2003) 511–516.

[7] M. Ozdemir, J.D. Floros, Analysis and modeling of potassium sorbate diffusion through edible whey protein films, J Food Sci 65 (2001) 149–155.

[8] J. Kärger, F. Grinberg, P. Heitjans, Diffusion Fundamentals. ISBN: 3-86583-073-0. Leipziger Universitätsverlag, Leipzig (2005) Paperback.
[9] J.B. Fox, Diffusion of chloride, nitrite, and nitrate in beef and pork. J Food Sci 45 (1980) 1740–1744.
[10] M.B. Perez-Gago, J.M. Krochta, Water vapor permeability of whey protein emulsion films as affected by pH, J Food Sci 64 (1999) 695–698.
[11] A. Gennadios, C.L. Weller, R.F. Testin, Temperature effect on oxygen permeability of edible protein-based film, J Food Sci 58 (1993) 212–219.
[12] N. Gontard, S. Guilbert, J. Cuq, Edible wheat gluten film: Influence of the main process variables on film properties using response surface methodology, J Food Sci 57 (1992) 190-199.
[13] S.L.A. Hennart, W.J. Wildeboer, G.M.H. Meesters, Identification of the grinding mechanisms and their origin in a stirred ball mill using population balances, Chem Eng Sci 64 (2009) 4123-4130.
[14] S.L.A. Hennart, W.J. Wildeboer, G.M.H. Meesters, Study of The Process of Stirred Ball Milling of Poorly Water Soluble Organic Products using Factorial Design. Powder Technology 198(1) (2010) 56-60.
[15] A. Fick, Poggendorff's Annel Physik 94 (1855) 59.
[16] A. Fick, Phil Mag 10 (1855) 30.
[17] A.A. Noyes, W.R. Whitney, The rate of solution of solid substances in their own solutions, J. Am. Chem. Soc. 19 (1897) 930–936.
[18] P. Van Hee, G.M.H. Meesters, W.J. Wildeboer, S.L.A. Hennart, A.J. Vis. Stabilized micronized particles. WO Patent # 2008/110626.
[19] W.A. Wakeham, Measurement of the transport properties of fluids. Oxford, Blackwell Scientific Ed (1991).
[20] W. Naesens, G. Bresseleers, P. Tobback P, A method for the determination of diffusion coefficients of food components in low- and intermediate moisture systems, J Food Sci 46 (1981) 1446–1449.
[21] A. Redl, N. Gontard, S. Guilbert, Determination of sorbic acid diffusivity in edible wheat gluten and lipid based films, J Food Sci 61 (1996) 116–120.
[22] L.R. Franssen, T.R. Rumsey, J.M. Krochta, Whey Protein Film Composition Effects on Potassium Sorbate Diffusion, J Food Sci 69(3) (2004) C347–C350.
[23] J. Crank, The mathematics of diffusion. 2nd edition (1975) New York: Oxford University Press.

General Conclusions and Outlook

In general this thesis increases the knowledge on grinding micron sized organic particles into sub-micron particles using stirred media mills.

The current model from Kwade and Schwedes on grinding in stirred media mills could not characterize fully the grinding process of any product in any mill. This model is generalized to a model characterizing the milling of a given powder in any mill.

Analysis of the obtained particle sizes shows to be quite difficult, but consensus is found on establishing the final particle sizes that can be reached. Why the particle size can not be reduced to much lower levels than the one found at 180nm is partly due to the re-agglomeration of smaller particles but remains difficult to explain. Grinding of inorganic product shows a much further size reduction than for our organic particles even when using surfactants.

From application trials, it is shown that the product quality increases with respect to mould protection with decreasing particle size. A model simulating the mould protection activity of the particles in coatings is developed. This model is validated by the application trials.

1. CONCLUSIONS AND DISCUSSION ON THE MILLING PROCESS

1.1. Conclusions on the milling process

The first part focuses on the milling process of the antifungal product down to sub-micron scale.

The conclusions of the first chapter of part I are that the process parameter do not have an influence on the final particle size but on the time of grinding the final particle size and the contamination level. The particle size reduction process follows specific breakage mechanisms depending on the size of the product particles. The breakage rate of coarse particles is influenced mainly by the rotation speed. Fine particles have a breaking rate influenced mainly by the size of the grinding media.
The rotational speed has a somewhat higher impact on the heavy metal contamination level than grinding medium bead size. Higher rotational speeds and/or larger grinding medium particles give more heavy metal contamination when the grinding time is kept constant. The heavy metals originate from the wear of the grinding chamber and the grinding media.

The second chapter explains that the origins of the forces leading to breakage are dependent on the particle size to be broken. Coarse particles break under high intensity forces leading to cleavage and fracture. Fine particles are produced by abrasion. Cleavage and abrasion of particles are typical from compression forces and long shear that are present in the centrifuged packed bed of grinding beads.

The third chapter enables prediction of the grinding time using a population balance model. The grinding process is in equilibrium with an agglomeration process. The population balance model is defined by four critical parameters; two of them describing the breakage of particles and the other two, the re-agglomeration of the fines. The grinding is defined by a frequency factor depending on the mill characteristic and an efficiency factor depending on the product milled. The agglomeration of fines is defined by the agglomeration efficiency factor and the equilibrium size between the grinding and the agglomeration process.

The product milled is very brittle and according to the approach from Kwade [1], Stadler and Schwedes [2], the shear induced by the translation movements of the beads is enough to break the particles.
The grinding profile is defined as the median particle size of the broken particles (x_{50}) plotted as function of the number of stress events (SN) in the mill. This number of stress events is calculated for one initial product particle. SN represents the number of stresses that an initial particle needs to undergo during the grinding process to reach the desired fine particle size. SN is proportional to the total surface of the grinding media. It is also proportional to a frequency of stress events.
The approach from Kwade, Stadler and Schwedes of the characterization of a given product in a given mill is in the third chapter generalized to the grinding profile of a given product in any mill by considering that the frequency of collision is defined as the angular rotation speed (ω) of the mill corrected by a mill efficiency factor (γ_F). That mill efficiency factor describes how good the impellor transfers its energy to the grinding media. The mill efficiency factor is shown proportional to the contact area ot the impellors with the centrifuged bed of grinding media. The stress number is thus purely a characteristic of the product ground.

The last chapter of the first part of this thesis presents the use of population balance model and the grinding profile to the comparison of two mills (Dispermat SL unit form Getzmann GmbH, Germany and Dynomill KDL unit from Bachofen AG, Switzerland).

The frequency factor ("a") of the population balance model is a linear function of the ratio tip speed over grinding media size. Factor "a" is dependent on the mill characteristics. It is slightly lower for the Dispermat SL unit compared to the Dynomill KDL. The designs of the impellor and the grinding chamber of the Dispermat Mill generate most probably higher density zones generating slightly less specific breakage events than in the Dynomill KDL.

The second factor "b" of the population balance model is grinding efficiency factor, which is a linear function of the stress energy up to a point where the efficiency is at its maximum. Factor "b" was expected to be function only of the material properties. Indeed, factor "b" could be considered constant on both the Dynomill KDl and the Dispermat SL.

The generalized approach from Kwade, Stadler and Schwedes leads to the representation of the stress number (SN) necessary to reach a target particle size of the milled particles. That representation of the grinding profile is product specific. No significant differences could be observed between the grinding profiles measured in the tested mills. Any similar stirred media mill is therefore expected to present the same grinding profile. Further studies could show that the process parameters of up-scaled or down scaled mills or mills with other design of their impellors can be predicted using the stress number corresponding to the desired particle size.

1.2. Discussion on the milling process

From the first part of the thesis it can be highlighted that the antifungal product can be ground in stirred media mills. The shear induced by the translation movements of the beads breaks the particles (part I chapter 3). This matches the observations that the particles undergo cleavage and abrasion (part I chapter 2). Those breakage mechanisms are typical from compression forces and long shear that are induced by the translation movements of the beads.
The adapted stress number defined as in part I chapter 3 describes the breakability of the milled product (part I chapter 3 and 4).

$$SN \propto \frac{m_{total,GM}}{\frac{1}{6} \cdot d_{GM} \cdot \rho_{GM}} \cdot \frac{(\gamma_F \cdot \omega) \cdot t}{N_P} \quad (1)$$

With $m_{total,GM}$ the total mass of grinding media in the chamber, ω the angular rotation speed of the stirrer, t the time of grinding, d_{GM} the diameter of a grinding medium, ρ_{GM} the density of the grinding media, N_P the number of product particles in the grinding chamber and γ_F the surface area of the impellor in contact with the grinding media.

The stress number is function of the grinding time, the rotation speed (ω) and the invert of the grinding media size (d_{GM}^{-1}). That corresponds to the observation of the factorial design study (part I chapter 1). The higher the rotation speed and the smaller the grinding media, the shorter the grinding time is to reach the required stress number.
The stress number is as well a function of the surface area of the impellor in contact with the grinding media. From Equation 1, increasing that surface enables to reduce the time of grinding.

The Stress number as defined in this thesis, function of the process parameters, is expected to be product dependent. Future research could investigate the grinding profile of different products and determine how the product properties influence the stress number. Further investigation on the material properties would investigate the influence of the crystal strength on the grinding profile. Product with different crystal

structures are expected to break following different grinding profiles. That would lead to a general description of grinding any product in any stirred media mill.

Further research is required to completely optimize and validate the present approach. Different filling ratios of grinding media in the grinding chamber should influence the factor γ_F which is expected to remain then proportional to the surface of the impellor in contact with the grinding media.

DEM simulation including particle, grinding media and fluid flow in the grinding chamber would enable the finest optimization of the design of grinding mills.

2. CONCLUSIONS AND DISCUSSION ON THE CHARACTERIZATION OF THE GROUND PARTICLES

2.1. Conclusions and discussions on particle size characterization.

The second part of the thesis focuses on the characterization of the size and the physical stability of the particles.
The size distribution of the ground particles is measured on different devices. The results indicate that the primary average particle size is close to 180nm and that there are larger particles.
There is strong evidence that the primary particle size is close to 180nm and that the larger particles are very likely aggregates. This is clearly seen from the Cryo TEM results.
All the tested techniques should in principle be able to measure samples of dispersion containing particles of ca 180nm but several are disturbed by the presence of large aggregates. It is difficult to estimate the amount of aggregate present, but most of the time, one is interested in what the primary particle size distribution is. Addition of stabilizers, pH optimization or surfactants can reduce the aggregation tendency enormously, but this is not investigated in this research.
It is clear that no single piece of equipment is capable of exactly determining the particle size distribution of our samples, but the static light scattering with low shear on mixing does give a good representation of what is seen with the image analysis by cryo TEM.

The physical stability of the ground particles is already highlighted in the first chapter: measured in water, the particles are present in the form of primary particles and agglomerates. The agglomeration behavior of the particles has been studied in the second chapter.

Further developments are needed to be capable to characterize the size, shape and behavior of sub-micron particles. Imaging techniques require still complicated sample preparations. Other sizing techniques are influenced by the particle environment or are not capable to measure broad range of particle sizes.

2.2. Conclusion and discussion on the sub-micron particle stability.

The stability of the particle suspension is determined by measuring the initial sedimentation rate. This measurement technique shows differences in the aggregate size for different pH values. Changing the pH values influences the zeta-potential of the particle surface. Using the DLVO theory, the stability of ground particles shows a good correlation with the energy barrier between the particles. The higher the energy barrier the less aggregation can occur and the smaller the aggregates are. The energy barrier increases with an increase of the electrostatic repulsion, i.e. the zeta-potential. The particle suspension becomes more stable when driving away the pH from the iso-electric point.

The product could be milled further by the addition of different surfactants. Changing the crystalline structure in combination with the additions of surfactants, polymers or other additives changing the apparent zeta potential of the particle might allow reaching smaller and more stable particles.

3. CONCLUSIONS AND DISCUSSION ON THE APPLICATION OF THE GROUND PARTICLES TO PRESERVATION OF FILMS AND COATINGS.

The last part of the thesis tests the sub-micron particles in their application and compares their efficiency versus non-ground product. The experimental results clearly show that protection against fungal growth increases when higher product concentrations are used (ground and not ground). Also micronized product particles provide the longest protection against mould growth. It is clear that a decrease in product particle size increases protection against fungal growth in time.

A model is designed and the different aspects regulating the concentration of the product in the coating are included: the product diffusion, the product dilution, the particle distribution, the product degradation and the limit of sensitivity of the microbe to the product.

The weakest point in a coating is the point where the concentration reaches at first the limit of sensitivity of the microbe to the product. That point is the position in the middle of two particles.

From the model is seen that the distribution of the particles in the coating is of great importance. Reducing the particle size or increasing the concentration enables the increase of the specific number of particles. Thus the distribution of particles in the matrix changes and the distances between the particles reduces. The diffusing molecules in the coating reach faster the position in middle of two particles; this increases the shelf life of the food product.

The model developed for the analysis of concentration of active product in the coating could benefit from further research. The impact of the environment (light, air, spores concentration) on the degradation rate needs to be investigated. The optimum model would from simple measurement of the environment determine the optimal coating formulation in terms of particle size and concentration of active product required to reach the target shelf life.

REFERENCES:

[1] A. Kwade, L. Blecher, J. Schwedes, Motion and stress intensity of grinding beads in a stirred media mill. Part 2: Stress intensity and its effect on comminution, Powder Technology 86(1) (1996) 69–76.

[2] R. Stadler, R. Polke, J. Schwedes, F. Vock, Naßmahluing in Rührwerksmühlen, Chem Ing Tech 62(11) (1990) 907–915.

Acknowledgments

Many people companies and institutions have been implicated in this project. To all of them I would like to express my great gratitude and thanks for believing in our project and in young researchers!

Un grand merci à vous… A great thank to you…

all the students who contributed to the development of this research:

Maria Christina Domingues from the University of Coimbra, Portugal, and DSM Biotech Center in Delft, The Netherlands, assisting for early stage grinding experiments.

Vincent Drouet from the Ecole supérieure de Chimie Physique et Electronique (CPE Lyon), Lyon, France, assisiting with the design of the population balance model.

Fanny Destaing from the Université Claude Bernard in Lyon, France assisting with the study of the distribution of particles in coatings.

Ida Kölmann from the Technical University of Delft, assisting with the X-Ray diffraction measurements

all the researchers and experts of great help and support:

Prof. Arno Kwade from the Technical University in Braunschweig, Germany for the helpful discussions.

Pieter Vonk and Leon Bremer from DSM ACES, Geleen in the Netherlands for all interesting discussions regarding population balance modeling and particle sizing.

Prof. Henk Schuttelaars from the Delft Institute of Applied Mathematics / Mathematical Physics, at the Delft University of Technology, Delft in the Netherlands for his kind help with the analytical resolution of differential equations.

Prof. Peter Frederic from the University of Maastricht, The Netherlands; for the sharp Cryo-TEM pictures

My colleagues, from the DSM BioTechnology Center and from the Enzymes and Dairy Industry unit: Albert-Jon Vis, Jan van der Lee, Ferry van Rijn, Daan Verkoeijen, Marco van Haastert, Albert Schaap, Tony van den Burg, Roelof Kooman, Frank Waaijer, Henk Bijl, Arthur Janse, John Visser, Ibo Ozkan, Pieter Kerkhof, Sandjai Sardjoepersad, Sebastiaan Peeters, Jeroen Vermunt, Jeroen den Hollander, Dilip Raghoenath, Fred Eswilder, Jos Webbers, Richard Zamolo, John Mokveld, Martin Zegwaard, Andre Groenendaal, Jacque Stark, Ben de Haan, Klaas Osinga.

A special thank to Monique Parisius and Ria Lemmers for helping in getting integrated in the company and in filling in all administrative requirements.

My colleagues, from the Delft University of Technology: Giacomo Perfetti, Bas van Laarhoven, Jan van Erven, Valérie Butselaar-Orthlieb, Henk Merkus, Henk Nugteren, Andreas Schmidt-Ott, the technical assistants and a special thank to Wil Stolwijk and Karin Wilhelm for helping me with the administration of the TU Delft.

Florent, Robin and Ella, Aurora and Frank, Michael, Coby and Arie for helping me to answer technical questions and translate the summary and propositions in Dutch.

all the institutions and companies without which this work would not have been possible:

The European Union through the Marie Curie 6th Framework Program and the Research Training Network "Biopowders"

DSM Food Specialties, The Netherlands, hosting and co financing this project

Delft University of Technology, The Netherlands, Faculty of Chemical Engineering, NanoStructured Material group.

Hosokawa Alpine GmbH, Germany for early grinding tests

Getzmann GmbH, Germany for believing in young researchers and helping in the comparison of different mills

All companies providing particle characterization solutions that could be tested in the framework of this project: Beckmann Coulter, Malvern, Sympatec, CPS Instruments, Wyatt Technologies, Microtrac, Nanosight, Horiba, Micromeritics.

A special thanks to my supervisors helping me to manage a PhD project and develop skills:

Hans W.J. Wildeboer, Line Manager Downstream Processing Department. Thanks a lot for making me feeling home from my very first day in the Netherlands and in your department. Thanks for all the input for my personal development. Thanks a lot for your pieces of advice.

Gabrie M.H. Meesters, Senior Scientist and associated Professor. Thanks a lot for offering me that great opportunity to carry out a PhD within DSM Food Specialties. Thank you for keeping my PhD on the right tracks. Thanks for helping me to do the "helicopter" – to keep a global overview on my work.

Pim van Hee, Downstream Processing Scientist. Thank you very much for showing me how dimensionless or characteristic numbers can be so handy. Thank you also for introducing me to those complex theories; those were, thanks to you, easy to understand. Thanks a lot for helping me to reach a high level of scientific thinking.

Curriculum Vitae

Personal information

	Stéphen HENNART
Address	Hammarskjoldlaan 693, 2286HT Rijswijk, NL
Telephones	0031 152 79 2263 Mobile: 0031 6 30 47 60 23
E-mail	Stephen.hennart@dsm.com
Nationality	French
Date & Place of birth	14 September 1982, Rouen, France
Gender	Male

Current Position: Product Application Expert at DSM

Work experience

Since January 2010 — DSM Food Specialties, Delft, The Netherlands.

As Product Application Expert, I have the responsibility to coordinate product development with the project manager and the R&D, to define with the product manager and communication department the value proposition and product strategy and to participate to conferences and Expert Groups.

The work focuses in the field of detection of (antibiotic) residues in dairy food products.

February 2006 – December 2009 — DSM Food Specialties, Delft, The Netherlands.

Officially as Assistant Scientist, I did my PhD within the Recovery and Formulation department of DSM Food Specialties R&D. (Graduation August 2011)

The objectives were to grind poorly water soluble compounds to extreme small scale to improve product efficiency in different applications.

July-August 2003 — Degussa AG, Rheinfelden, Germany.

This two month internship consisted in the design of a distillation plant for extra high quality product production. I could see and participate there the application of chemical engineering in a large industry. The design being finished and contacts with constructors taken, the project has been followed and the installation built within the following quarter.

July-August 2001 — Cognis, Düsseldorf, The Netherlands.

The two month placement at Cognis was my first experience within an industrial R&D group. By using rheological studies, we improved the texture and flow properties of soap based products such as shampoos.

Education & training

2000 - 2005	MSc Program at the INSA in Rouen, Normandy, France INSA is the National Institute for Applied Sciences, a public school of engineering in France. Diploma obtained in Chemical Engineering with speciality in Fine Chemistry
2005	MSc Program at the University in Rouen, Normandy, France I added to my last year of engineering program at the INSA a series of courses from the Rouen University – Fine Organic Chemistry Institute (IRCOF). Diploma obtained as Master in Fine Organic Chemistry
1997 - 2000	Secondary Program: Lycée Flaubert, Rouen, Normandy, France. European and Scientific section. Diploma Bac S *"European" mention "Bien"*
Languages	French and German – Mother tongues English and Dutch – Fluent Portuguese – Working knowledge Spanish - Basics
Social skills and Organisational competences	Recently, organized several social events within DSM (DBC Department integration, Department social events, etc) Educational background in management and Project management. Supervision of many students and trainee within DSM and the Delft Technical University.
Technical skills & competences	Chemical Engineering, Food and Pharma Processing, Educational Background in Biochemistry and Nuclear Chemistry, Analytical Techniques, Inorganic Chemistry.
Other skills & competences	Good adaptability to new environments. I am currently travelling >50% of my working time. I had the pleasure and opportunity to travel around South Africa, Brasil, Argentina, USA and Europe sometimes on my own, sometimes with friends or family, but each time I adapted fast to the local culture and way of life. So did I when I arrived 5 years ago in the Netherlands.
Driving licence(s)	Private car.

Additional Information

Articles

- Stability of particle suspensions after fine grinding - Hennart, S.L.A., Wildeboer, W.J., van Hee, P., Meesters, G.M.H. 2010 Powder Technology 199 (3), pp. 226-231

- Study of the process of stirred ball milling of poorly water soluble organic products using factorial design - Hennart, S.L.A., Domingues, M.C., Wildeboer, W.J., van Hee, P., Meesters, G.M.H. 2010 Powder Technology 198 (1), pp. 56-60

- Identification of the grinding mechanisms and their origin in a stirred ball mill using population balances - Hennart, S.L.A., Wildeboer, W.J., van Hee, P., Meesters, G.M.H. 2009 Chemical Engineering Science 64 (19), pp. 4123-4130

- Characterization and Modeling of a Sub-Micron Milling Process Limited by Agglomeration Phenomena - Hennart, S.L.A., van Hee, P., Drouet, V., Domingues, M.C., Wildeboer, W.J., Meesters, G.M.H. 2009 Chemical Engineering Science - *accepted*

- The Validation of the Delvotest SP NT for AOAC Research Institute Performance Tested MethodsSM Certification (Certificate #011102) - Hennart, S.L.A., Faragher, J. 2011 J AOAC Int - *accepted*

- The Validation of the Delvotest SP NT DA for AOAC Research Institute Performance Tested MethodsSM Certification (Certificate #011101) - Hennart, S.L.A., Faragher, J. 2011 J AOAC Int - *accepted*

- Comparison of Stirred Media Mills for Sub-Micron Grinding - Hennart, S.L.A., Wildeboer, W.J., van Hee, P., Meesters, G.M.H. 2009 Chemical Engineering Science - *submitted*

- Particle Size Characterization of Extra Fine milled Product - Hennart, S.L.A., van Hee, P., Wildeboer, W.J., Meesters, G.M.H. 2010 Part. Part. Char.– *submitted*

- Distribution of Poorly Soluble Particles in Films and Coatings - Hennart, S.L.A., van Hee, P., Destaing, F., Vis, A.J., van der Lee, J., Mendes, E., Wildeboer, W.J., Meesters, G.M.H. 2011 Powder Technology - *submitted*

Patent

- Stabilized micronized particles. van Hee, P., Meesters, G.M.H., Wildeboer, W.J., Hennart, S.L.A., Vis. A.J. WO Patent # 2008/110626.